Reply to Referee #1

We would like to thank the reviewer for comments and questions which helped us to improve the manuscript. The reviewer comments are given below together with our responses and changes made to the manuscript.

1.1 Comments: *Interferences in the OH detection, OH chemical modulation tests: Was the propane concentration varied in the field? From lines 265 – 267 it is unclear if the variable titration efficiency is a laboratory result or field observation. If it was the latter, how was titration efficiency determined in the field?*

Response: The amount of propane and corresponding titration efficiency (changed to removal efficiency according to Referee #3) was optimized and determined in the field before each titration test. More detail information is provided in the revised manuscript.

Change: We added on Page9 L269: "The knowledge of ε is essential for an accurate quantification of potential interferences. The removal efficiency was tested and optimized in the field using the OH calibration device as a radical source. The value of ε was found to depend on the flow rates of the added gases (propane and nitrogen). Propane was added as a 5% mixture in nitrogen with a flow rate between 0.02 and 0.2lpm (Liter per minute) which was further diluted in a carrier flow of pure nitrogen (0.04 to 0.5lpm). The dependence of ε on the flow rates showed that mixing of the injected propane into the high flow of ambient air was inhomogeneous similar to results reported in Novelli et al. (2014). Because of technical difficulties with the flow regulation, the removal efficiency was re-determined before each ambient titration test. The values obtained for ε ranged between 80% and 97% with an accuracy of 10% (1 σ) at fixed nominal propane and nitrogen flows."

1.2 Comments: *Were laboratory tests conducted to ensure no internal removal of OH in the cell (line 273)?*

Answer: We did kinetic calculation to estimate the impact of propane addition on internal removal of OH in the cell, which show only minor impact as long as the removal efficiency is less than 100%.

Change: We revised the text from Page 10 Line 273 to Line 275: "Kinetic calculations show that the added propane removes less than 0.3% of internally produced OH. The calculation assumes that the added propane is homogeneously mixed in the sampled air, yielding an expected OH lifetime which is larger than 0.1s and therefore much longer than the residence time (3ms) in the low-pressure detection cell. Therefore, the propane concentrations used in the chemical-modulation tests are not expected to influence possible OH interference signals."

1.3 Comments: Figure 2: What do the dashed lines correspond to? It is difficult to assess from this figure if there is any diurnal variation in the magnitude of the interference signal? Could the authors comment on any variation observed, e.g. as a function of atmospheric composition? Is this possible unknown interference signal of sufficient magnitude to account for the modelled measured OH discrepancy at [NO] < 300pptv (line 479)?

Answer: In Figure 2, the dashed lines separate one set of test from the other. To assess the possible variation of the interference signals, we summarized the conditions during the 6 titration experiments in a new table. We found no evidence that the unaccounted interference correlates with other measured species. The signal appears to be similar with values within the range of 1×10^6 cm^{-3} in quite different chemical conditions during the campaign. For a large range of NO concentrations, the residual OH determined in the titration tests was similar. If an accounted signal of 1×10^6 cm^{-3} was subtracted from the measured OH concentration, the observed-to-modelled ratio of OH would be reduced from 1.4 to 1.2 for NO<300ppt and from 1.9 to 1.5 for NO<100ppt.

Change: We added a discussion about the averaged unaccounted signal and model-measurement discrepancy comparison and revised the text from Line 522 to Line 524: "The median diurnal profiles of the measured and modelled OH concentrations agree within their errors of 10% (1σ) and 40%, respectively, from sunrise to midafternoon. When the median NO mixing ratio (cf. Fig. 6) drops gradually from 0.3ppbv to 0.1ppbv in the afternoon, a systematic difference evolves, with measured OH concentrations being approximately $1\times10^6 cm^{-3}$ higher than the model calculations. The discrepancy is of similar magnitude as the averaged unexplained OH determined in the chemical modulation experiments (Table 2). Thus, the overall agreement for

OH would improve, if the unaccounted signal was fully considered as an OH measurement interference. However, the underestimation of OH would persist for low NO conditions if a potential unaccounted signal was subtracted. When NO concentrations are less than 100pptv, the observed-to-modelled OH ratio would be reduced from 1.9 to 1.5, indicating that an OH source would still be missing for low NO conditions."

2. ***Comments:*** *Possible RO_2 interference: Fuchs et al. (Review of Scientific Instruments, 2008) report a possible interference in the RO_2 instrument from pernitric acid and methyl peroxy nitrate which have the potential to thermally decompose in ROx system and be detected as HO_2 and CH_3O_2. Could the authors comment on the impact this interference may have for these field conditions, particularly under the high NOx conditions experienced in the morning? Could this interference explain the model measured discrepancy in RO_2 at this time? What is the impact of this interference on the ozone production rate calculated from the measured HO_2 and RO_2 concentrations?*

Answer: We calculated the thermal decomposition of the peroxy nitric acid (HO_2NO_2), methyl peroxy nitrate ($CH_3O_2NO_2$) and PAN as Fuchs et al. (2008) did. Although these species could cause interference and help to explain the underestimation of HO_2 and RO_2, the impact is so small that have only minor impact on our measurements for high NO condition.

Change: We added on Page 11 L338: 'A bias in the measurement of RO_2 may be caused in polluted air by peroxy radicals, which are produced in the low-pressure converter of the RO_2 instrument by thermal decomposition of peroxy nitric acid (HO_2NO_2), methyl peroxy nitrate ($CH_3O_2NO_2$) and PAN (Fuchs et al., 2008). In the atmosphere, HO_2NO_2 and $CH_3O_2NO_2$ are in a fast thermal equilibrium with HO_2 and CH_3O_2, respectively, together with NO_2. The possible interference scales with NO_2, which was highest during the Wangdu campaign in the morning (median value of 15 ppbv; cf. Fig. 6). For this condition, according to model calculations by Fuchs et al. (2008), HO_2NO_2 and $CH_3O_2NO_2$ are expected to produce interferences of +2.6 % and +9 % for the detected HO_2 and CH_3O_2 radicals, respectively. Since HO_2 and CH_3O_2 contributed about 50 %

(measured) and 10 % (modelled) to the total ROx in the morning, the estimated interference for measured RO_2 is only +2 %. The interference from PAN decomposition in the instrument was calculated by Fuchs et al. (2008) to be 0.1 pptv per ppbv of PAN. Since PAN concentrations modelled for the Wangdu campaign are less than 1 ppbv, also from this compound no significant interference is expected. Another bias may be due to the perturbation of the reactor chemistry from high ambient NO concentrations (Fuchs et al., 2008). For the measurements in the ROx and HO_2^* mode, the corresponding interferences are estimated to be less than +1 % and +3 %, respectively, at 15 ppbv NO.'

3. **Comments:** *Model measurement comparison of RO_2: The manuscript focusses on the differences observed between measured and modelled RO_2 in the morning, but in figure 5 the model under-predicts RO_2 and $RO_2^\#$ until 16:00. Some comments should be provided on this under-prediction; the under-prediction in OH reactivity cannot account for this under-prediction beyond 10am. Please extend this commentary to lines 849 in the Conclusion also. Owing to the strong coupling between RO_2, HO_2 and OH (highlighted in figure 11), how does the model under-prediction of total RO_2 impact the model's ability to predict OH and HO_2? Could the model be scaled to reproduce [RO_2] and then the performance of the model to predict OH and HO_2 re-assessed? There are inconsistencies in the modelled and measured radical ratios (and OH reactivity) that warrant further investigation. Section 3.6 would benefit from a more detailed discussion of the modelled RO_2 species – what are the other $RO_2^\#$ species in figure 8? Please define 'MO_2' in this figure caption.*

Answer: Considering the uncertainties, RO_2 and $RO_2^\#$ were significantly underestimated only during the morning (06:00—10:00) hours. To resolve the issue of the model under-estimation of the RO_2 and $RO_2^\#$, three sensitivity studies were done to investigate the possible impact of a faster recycling (S1), a primary source (S2) and a slower removal rate (S3) of RO_2. In the revised manuscript, we added the results from two sensitivity tests to the Figure 5 (see following).

Change: In the revised manuscript, we added the sensitivity run with scaled VOCs (S1) and additional primary source (S2) in Figure 5.

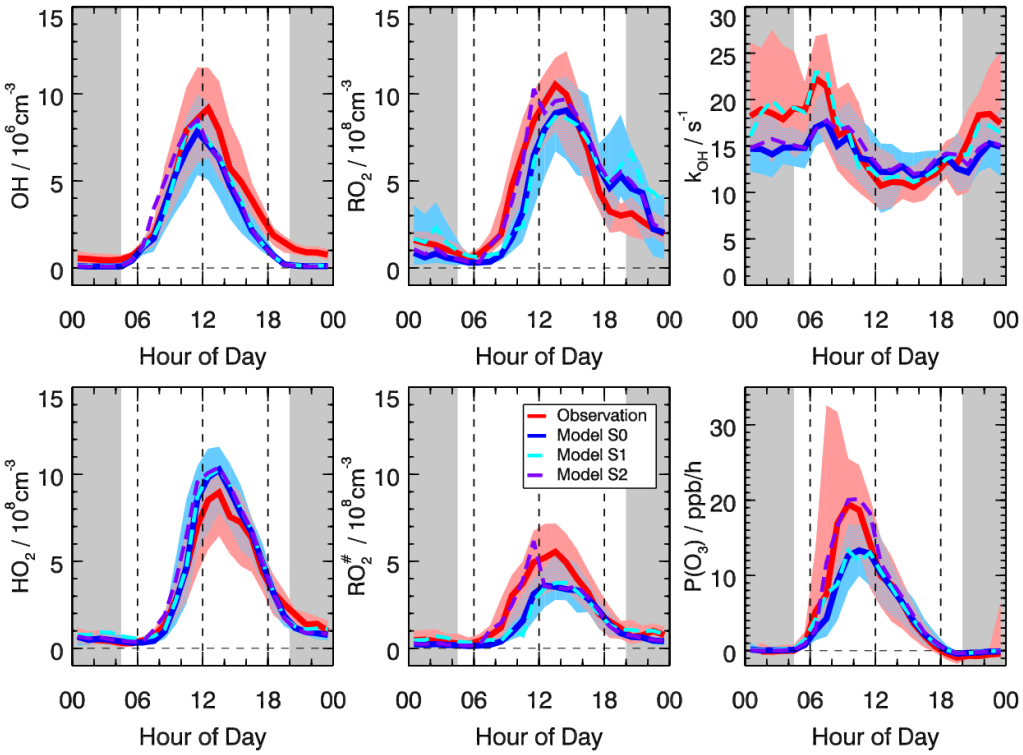

Figure 5 Comparison of hourly median diurnal profiles of OH, HO_2, RO_2, $RO_2^{\#}$ concentrations and k_{OH} and the ozone production rate $P(O_3)$ (thick lines give median values, colored areas give 25% and 75% percentiles). S0 (blue line) denotes results from the base model run. S1 (cyan, dashed line) shows results, when the VOC concentrations in the model are increased to match the observed OH reactivity. S2 (violet, dashed line) shows results, when an additional primary RO_2 source ($2 ppbv h^{-1}$) is added in the model for the time between 6:00 and 12:00. Grey areas indicate nighttime.

We added a sentence at the end of Section 2.4 Page 13 Line 408: "The uncertainty of measurements and modelling needs to be taken into account in the comparison. The uncertainty of radical measurements is mainly determined by the measurement accuracies (OH: ±11%, HO_2: ±16%, RO_2: ±18%). A series of tests based on Monte Carlo simulations show that the uncertainty of the model calculations is approximately 40%."

We revised the text in Page 17 Line 528 "RO_2 and $RO_2^{\#}$ were significantly underestimated during the morning (06:00—10:00) hours with an observed-to-

modelled ratio of 3 to 5, which is larger than the combined uncertainty (a factor of 2). Reasons for discrepancies between measured and modelled RO_2 are further analyzed in Section 3.6."

Page 18 from Line 569 to Line 596, we revised the text "The strong underprediction of the observed RO_2 by more than a factor of 4 in the morning cannot be explained by the measurement errors and interferences discussed in Sections 2.3.4 and 2.3.5. In order to explore potential reasons for this underprediction, several sensitivity tests were performed. First, the impact of a faster OH to RO_2 conversion by an increased amount of VOC was tested (model sensitivity run S1). Second, an additional primary source of RO_2 was introduced into the chemical mechanism (S2). Third, the possibility of a slower removal rate of RO_2 was tested (S3).

The first possibility (S1) is supported by the observation that the modelled OH reactivity in the base run (S0) is smaller than the measured OH reactivity in the morning until about 09:00. If this missing reactivity is caused by unmeasured VOCs, the true RO_2 production from reactions of VOCs with OH would be larger than the modelled one. To fill this gap, the total concentration of the measured VOCs was increased to match the measured kOH in the time window from 06:00 to 09:00. The relative partitioning of the VOCs was not changed. The model run (S1) with the upscaled VOC reactivity resolves part of the RO_2 discrepancy until 09:00 (Fig. 5). The observed-to-modelled RO_2 ratio is improved from 2.8 to 1.7 without affecting the good model-measurement agreement for OH and HO_2. Further sensitivity tests showed that the modelled RO_2 is not sensitive to the speciation of the additional VOC reactivity, since the required change of k_{OH} is relatively small (< 20%). Because no missing OH reactivity was found after 09:00 h in the morning, the gap between measured and observed RO_2 cannot be explained by unmeasured VOCs later in the morning.

In sensitivity test S2, an additional primary source of RO_2 (OLTP) from terminal alkenes was introduced into the model. A source strength of 2 ppbv h-1 from 06:00 h to 12:00 would be required to achieve a good model-measurement agreement (within 20 %) for both RO_2 and $RO_2^{\#}$. The modelled OH and HO2concentrations also increase and are slightly overpredicted by about 10% and 20%, respectively. This can still be considered as agreement within the error of measurements and model calculations. After 12:00 the difference between modelled and measured RO_2 becomes smaller than 15%, within the range of the accuracy of RO_2 measurements.

A candidate for an additional primary RO_2 source would be reactions of VOCs with chlorine atoms, which are produced by photolysis of nitryl chloride ($ClNO_2$) (Osthoff et al., 2008). $ClNO_2$ is formed from the heterogeneous reactions of Cl^- ions with nitrogen pentoxide (N_2O_5) and accumulates during nighttime. After sunrise, $ClNO_2$ is expected to be completely photolysed within a few hours. The resulting Cl atoms can abstract H-atoms from saturated hydrocarbons or can add to alkenes. The alkyl radicals produce RO_2 which in case of alkene-derived peroxy radicals carry a chlorine atom. $ClNO_2$ was measured by a CIMS instrument at the Wangdu field site from 20 June to 8 July (Tham et al., 2016). The concentrations increased during night and reached on average high values of 0.5 ppbv at 08:00 h, followed by a decay to zero until 11:00 h. In their study, Tham et al. (2016) investigated the role of $ClNO_2$ photolysis on the photochemical formation of RO_2 and ozone during the Wangdu campaign. They used the MCM v3.3 with an additional chlorine chemistry module by Xue et al. (2015). We repeated the study by adding the same chlorine chemistry to our modified RACM2 mechanism and found the same additional formation rates of RO_2 and O_3 as reported by Tham et al. (2016). In our model run, a $ClNO_2$ source is assumed that leads to a linear increase of $ClNO_2$ during nighttime to a maximum value of 0.5 ppbv at 08:00 h on every day. After 08:00 h, the modelled source is turned off. $ClNO_2$ starts to photolyze after 06:00 h with a photolysis frequency that was calculated from the measured actinic flux. A maximum Cl production rate of 0.2 ppbv h-1 is obtained at 08:00 h, yielding an additional RO_2 production with a similar rate. Compared to the additional RO_2 production rate required for model run S2, this is an order of magnitude too small. The mechanism is also not capable to sustain the additional RO_2 production during the whole morning, because $ClNO_2$ is photolytically depleted within 2 - 3 hours. Even if the modelled source strength is increased to match the highest $ClNO_2$ mixing ratio of 2 ppbv observed on 21 June (Tham et al., 2016), the additional primary RO_2 production of 0.5 ppbv h-1 is still not sufficient. Thus, although $ClNO_2$ photolysis was a relevant radical source, it alone cannot explain the missing source of RO_2 radicals in the morning.

A further model test (S3) was performed, in which the rate of RO_2 removal was artificially reduced by decreasing the reaction rate constants between RO_2 and NO. Such a reduction would be justified, if the rate constant for RO_2+NO would be systematically too large in the model. Another reason could be a systematic measurement error of the NO concentration, or a segregation effect between RO_2 and NO due to inhomogeneous mixing in case of local NO emissions. In order to account

for the discrepancy between modelled and measured RO_2 in the morning, the loss rate would have to be changed by a factor of 4, which seems unrealistically high for each of the above mentioned possibilities. Also, there is no plausible reason why a systematically wrong rate constant or NO measurement error would appear only during morning hours."

A more detailed discussion of the modelled RO_2 species is added in Sect. 3.6 as suggested. In Line 563 Page 18, we added: "In the group of modelled $RO_2^{\#}$ species, isoprene peroxy radicals (ISOP) make the largest contribution during daytime. Other modelled $RO_2^{\#}$ include peroxy radicals from alkenes, aromatics, long-chain (> C_4) hydrocarbons, and MVK and MACR. Among the RO_2 radicals which do not belong into the RO_2# group, peroxy radicals of short-chain (<C_5) alkanes are dominating: methyl peroxy radicals (MO2), ethyl peroxy radicals (ETHP), and peroxy radicals HC_3P from HC_3 (e.g., propane). Acetyl peroxy radicals (ACO_3+RCO_3) are also a substantial fraction of RO_2."

Minor comments:

Comments: *Line 331: Do the $RO_2^{\#}$ concentrations determined in the HO_2 and RO_2 cell agree?*

Answer: $RO_2^{\#}$ is only measured in the RO_2 cell. The HO_2 cell measured HO_2 with a minimum contribution from $RO_2^{\#}$ (see section 2.2.3).

Comments: *Line 358: Please give the typical solar background at noon. Was it necessary to shade the cells?*

Answer: We revised the text in 358: 'The typical solar background was about 40 cts/s which is a factor of 20 higher than the typical background signals obtained at night. Therefore, the detection limit was reduced by a factor of 5. A shade-ring was installed during the campaigns to shield the cell from direct solar radiation.'

Comments: *Line 527: 'HO_2 concentrations are well reproduced by the model during the daytime'. From figure 5 it looks like the model has a tendency to over-predict*

[HO_2] in the afternoon. Could this over-prediction be masking the full magnitude of the model underprediction of OH at this time (as HO_2 is a strong recycling of OH)?

Answer: In a sensitivity model run, we constrained the HO_2 concentration to the observed values and found the underprediction of OH would be more significant, because the original model predicted slightly higher concentrations of HO_2. The observed-to-modelled ratio of OH would increase to 1.8 in this case. An analysis of the OH budget using only measurements is done in our accompanying paper by Fuchs et al. 2016. This study shows that the OH destruction cannot fully be explained by known production rates in the late afternoon, when NO concentrations are lowest. We revised the text in line 527:"In general, HO_2 concentrations are reproduced by the model during daytime within the combined uncertainties of measurements and model calculations. Nevertheless, the model has a tendency to over-predict HO_2 in the afternoon. If we constrain the model to the observed HO_2 concentrations, the observed-to-modelled OH ratio increases from 1.6 to 1.8 for daytime averaged conditions (04:30–20:00)."

Comments: *Line 593-594: 'scaling VOC concentrations to match measurements.' which VOC species were scaled? Does the VOC species chosen influence the modelled [RO_2]?*

Answer: All input VOCs are scaled (see in table 2) to remain the same ratio between different VOC species. Sensitivity tests showed that the modelled RO_2 is not very sensitive to different specific VOC species since the required change of modeled k_{OH} is relatively small (< 20%). The detailed explanation described above was added in the discussion of the RO_2 underprediction (refer to question 3).

Comments: *Line 595 'can be partly closed.' and also, line 701 'rate better agrees..' please provide the percentage change.*

Answer: More detail information is provided in the text as: "The observed-to-modelled RO_2 ratio is improved from 2.8 to 1.7"

Comments: *Line 720 – 723: This statement seems to be at odds with the model-*

measurement comparison presented in this manuscript which shows good agreement between modelled and measured HO_2 in the morning but a modelled measurement discrepancy for RO_2. Calculating ozone production from an RO_2 concentration estimated from HO_2 could mask a high morning ozone production rate.

Answer: The statement is changed to: 'Total photochemical ozone production rates were directly measured in a sunlit environmental chamber during the SHARP campaign in Houston (Texas) 2009 (Cazorla et al., 2012; Ren et al., 2013). The comparison with ozone production rates determined from measured HO_2 and from modelled HO_2 and RO_2 suggests that the model underestimated both HO_2 and RO_2 at high NOx in the morning.'

Comments: *Line 769: There is no experimental evidence that HONO formed from the reaction of HO_2.H2O + NO_2, as postulated by Li et al., (2014), occurs and so shouldn't be speculated on here.*

Answer: We canceled the statement as suggested.

Comments: *Line 770: Could an example of OH+hydrocarbon which does not form HO_2 or RO_2 be provided here.*

Answer: We modified the text in line 770 as "Further radical terminating OH losses include reactions with unsaturated dicarbonyls (DCB1, DCB 2, DCB 3) and acetyl nitrate species (PAN, MPAN, etc) in RACM2."

Comments: *Line 848: Please provide the equivalent NO required in the previous campaigns for comparison.*

Answer: The equivalent NO required in the previous campaign is 0.8ppbv for PRIDE-PRD2006 and 0.4ppbv for CAREBEIJING2006. We rephrased the text: "…This behaviour is qualitatively in agreement with previous results from two field campaigns in China, in the Pearl River Delta and in the North China Plain, where the required equivalent NO is 800pptv and 400pptv (Lu et al., 2012, 2013)."

Reply to Referee #2

We would like to thank the reviewer for comments and questions which helped us to improve the manuscript. The reviewer comments are given below together with our responses and changes made to the manuscript.

1) **Comments:** *The authors performed several Interference measurements using an external chemical titration technique. Unfortunately it appears that these interference measurements were not done continuously but were done only on four specific days. However, it is not clear exactly when the tests were done and what the ambient conditions were during each test. Were any tests done when NO was less than 300 pptv, the conditions when the model-measurement discrepancies were the greatest, or was the measured interference similar for all ambient levels of NO? This should be clarified. Adding the times when these tests were done to Figure 3 would provide more information on whether these tests were done under typical ambient conditions for the campaign. Was this interference subtracted from all of the OH measurements?*

Answers: Because the titration device was a prototype, the chemical modulation tests were only performed on four days. The time period and chemical conditions are summarized and showed in a new figure in the revised manuscript. The unexplained residual signal are constant in the range of $1\times10^{6}cm^{-3}$, independent on the ambient NO concentrations.

Referee #1 also had similar questions about the titration experiments. Therefore, we would like to refer to our answer to question 1 of Referee #1 for more detail information.

Change: We added a sentence in Line 431: "Because the test results are not sufficiently accurate to draw firm conclusions about an unknown interference, the OH data in this work was not corrected for a potential interference. Instead, the differences found in Fig. 2 are treated as an additional uncertainty of the OH measurements presented in this paper."

2) **Comments:** *On page 17 the authors state that the measured OH concentrations are approximately 1×10^{6} cm^{-3}greater than model predictions during the afternoon*

when the mixing ratios of NO decrease from 0.3 to 0.1 ppb. This discrepancy appears to be consistent with the average measured interference of $1\times10^6 cm^{-3}$ described on page 14, suggesting that the observed discrepancy with the model could be due to the interference. This possibility should be discussed in more detail.

Answers: If an accounted signal of 1×10^6 cm^{-3} was subtracted from the measured OH concentration, the observed-to-modelled ratio of OH would be reduced from 1.4 to 1.2 for NO < 300ppt and from 1.9 to 1.5 for NO < 100ppt.

Change: We added a discussion about the averaged unaccounted signal and model-measurement discrepancy comparison and revised the text from Line 522 to Line 524: "The median diurnal profiles of the measured and modelled OH concentrations agree within their errors of 10% (1σ) and 40%, respectively, from sunrise to midafternoon. When the median NO mixing ratio (cf. Fig. 6) drops gradually from 0.3ppbv to 0.1ppbv in the afternoon, a systematic difference evolves, with measured OH concentrations being approximately $1\times10^6 cm^{-3}$ higher than the model calculations. The discrepancy is of similar magnitude as the averaged unexplained OH determined in the chemical modulation experiments (Table 2). Thus, the overall agreement for OH would improve, if the unaccounted signal was fully considered as an OH measurement interference. However, the underestimation of OH would persist for low NO conditions if a potential unaccounted signal was subtracted. When NO concentrations are less than 100pptv, the observed-to-modelled OH ratio would be reduced from 1.9 to 1.5, indicating that an OH source would still be missing for low NO conditions."

3) Comments: *In their measurements of HO_2, the authors varied the added NO to determine the interference from alkene and aromatic peroxy radicals. However, it is unclear to me how the authors determined the RO_2 conversion efficiencies described on page 11 unless the absolute conversion efficiency for one of the NO flows was determined through calibrations with known concentrations of peroxy radicals. Did the authors perform RO_2 conversion efficiency calibrations similar to that described in Fuchs et al., 2011? This should be clarified.*

Answers: The NO concentration was in all cases lowered to values, at which no significant interferences from RO_2 in the HO_2 detection are expected (p10 l296-299).

The NO concentration was varied between two values, in order to check, if this was the case, because a systematic difference between measurements at the two NO concentrations is expected, if RO_2 was detected together with HO_2. For the majority of measurements, the difference was only a few percent, which means that essentially no RO_2 interferences were present. Nevertheless, a small correction was applied, for which was assumed that the interference from RO_2 was the same at all times. The correction factor was derived from a regression analysis between measurements at different NO concentrations.

Change: We revised the text from Line 307 to Line 311: "The HO_2^* ratios were used to derive correction factors for the determination of interference-free HO_2 concentrations. For small NO concentrations as used in this work, we assume that the interference from $RO_2^\#$ is directly proportional to the applied NO concentration. Based on this assumption, we derived HO_2^*/HO_2 ratios of 1.02, 1.05, and 1.2 for the addition of 2.5, 5, and 20ppmv NO, respectively. These ratios were then used as correction factors to generate a consistent data set of interference-free HO_2 concentrations from the HO_2^* measurements. After all, the correction was small enough that deviations from this assumption would not significantly affect our results."

4) Comments: *It is not clear how the authors derive the $RO_2^\#$ concentrations and compare it to the model. The measured HO_2^* in the ROx channel reflects the conversion of alkene, aromatic, and other RO_2 radicals to HO_2 in the detection cell with a conversion efficiency dependent on the RO_2 radical as described in Fuchs et al. (2011). Subtracting the HO_2 measured in the HO_2 axis gives $RO_2^\#$. Ideally, the authors should compare this measured value which is the result of various conversion efficiencies to the modeled $RO_2^\#$, where the individual modeled RO_2 concentrations are scaled by their expected conversion efficiencies, which are not necessarily all 0.8. However, it appears that the authors are scaling the measured $RO_2^\#$ by an average conversion efficiency of 0.8 and comparing this value to the modeled concentration of the sum of the interfering RO_2 concentrations. This should be clarified. Have the authors measured the individual RO_2 conversion efficiencies for their instrument?*

Answers: In the current setup, the $RO_2^\#$ concentrations is derived from the HO_2 concentrations detected in the HO_2 cell and the HO_2^* concentrations detected in the

RO_2 cell applying the expression $RO_2^{\#} = (HO_2^{*} - HO_2)/0.8$. An averaged relative detection sensitivity for the $RO_2^{\#}$ in the RO_2 cell is estimated to be 0.8 according to previous publications (Fuchs et al., 2011; Lu et al., 2012) and dominant VOCs reactivity groups (mainly alkenes and isoprene) in Wangdu. We have performed tests on the RO_2 conversion efficiency for simple alkene, e.g. ethene, propene, for this new instrument and observed similar conversion efficiencies as Fuchs et al. (2011) reported for low NO concentrations in the detection cell. The other RO_2 conversion efficiencies are then extrapolated as done in Lu et al. (2012).

Change: We modified the text in Line 331 as "The concentration measurements of HO_2 (from the HO_2 cell) and of HO_2^{*} (from the ROx system) allow to estimate the total concentration of $RO_2^{\#}$ (Whalley et al., 2013)：$RO_2^{\#} = ([HO_2*] – [HO_2])/\alpha RO_2^{\#}$"

5) Comments: *The authors state that the underestimation of the RO_2 concentrations by the model during the high NO conditions in the morning is improved when the OH reactivity of the model is increased, but few details are provided. Similar results were found during CalNex by Griffith et al. (JGR, 2016). How much did the modeled RO_2 increase in this scenario? Perhaps the results of this model run could be added to Figures 5 and 9.*

Answers: We have performed sensitivity test to upscale the VOC reactivity, which is shown in the revised Figure 5 as following (S1). In this sensitivity test, the input VOC concentrations are scaled up so that the modelled OH reactivity agree to measurements. The observed-to-modelled RO_2 ratio is improved from 2.8 to 1.7 on average from 06:00 to 09:00. More detail information is given in the revised manuscript as following.

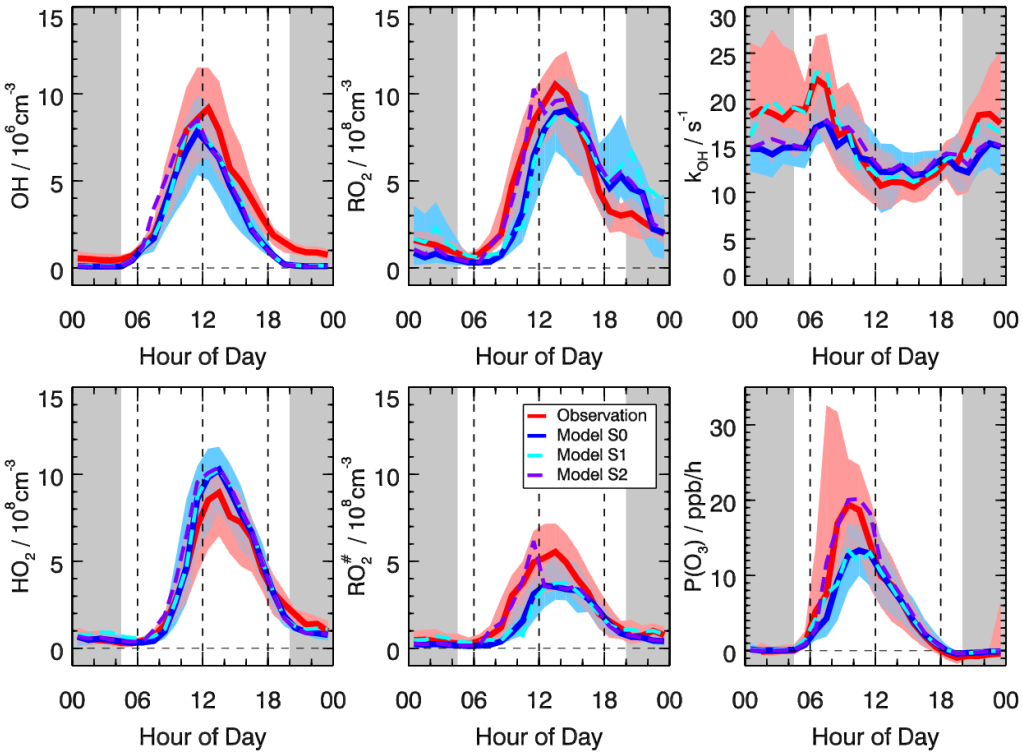

Figure 5 Comparison of hourly median diurnal profiles of OH, HO_2, RO_2, $RO_2^{\#}$ concentrations and k_{OH} and the ozone production rate $P(O_3)$ (thick lines give median values, colored areas give 25% and 75% percentiles). S0 (blue line) denotes results from the base model run. S1 (cyan, dashed line) shows results, when the VOC concentrations in the model are increased to match the observed OH reactivity. S2 (violet, dashed line) shows results, when an additional primary RO_2 source ($2ppbvh^{-1}$) is added in the model for the time between 6:00 and 12:00. Grey areas indicate nighttime.

Change: We revised Page 18 from Line 569 to Line 596: "The strong underprediction of the observed RO_2 by more than a factor of 4 in the morning cannot be explained by the measurement errors and interferences discussed in Sections 2.3.4 and 2.3.5. In order to explore potential reasons for this underprediction, several sensitivity tests were performed. First, the impact of a faster OH to RO_2 conversion by an increased amount of VOC was tested (model sensitivity run S1). Second, an additional primary source of RO_2 was introduced into the chemical mechanism (S2). Third, the possibility of a slower removal rate of RO_2 was tested (S3).

The first possibility (S1) is supported by the observation that the modelled OH reactivity in the base run (S0) is smaller than the measured OH reactivity in the morning

until about 09:00. If this missing reactivity is caused by unmeasured VOCs, the true RO_2 production from reactions of VOCs with OH would be larger than the modelled one. To fill this gap, the total concentration of the measured VOCs was increased to match the measured kOH in the time window from 06:00 to 09:00. The relative partitioning of the VOCs was not changed. The model run (S1) with the upscaled VOC reactivity resolves part of the RO_2 discrepancy until 09:00 (Fig. 5). The observed-to-modelled RO_2 ratio is improved from 2.8 to 1.7 without affecting the good model-measurement agreement for OH and HO_2. Further sensitivity tests showed that the modelled RO_2 is not sensitive to the speciation of the additional VOC reactivity, since the required change of k_{OH} is relatively small (< 20%). Because no missing OH reactivity was found after 09:00 h in the morning, the gap between measured and observed RO_2 cannot be explained by unmeasured VOCs later in the morning.

…"

6) Comments: *Similarly, the authors find that the model underestimates the rate of ozone production under high NO conditions due to the underestimation of RO_2 radicals by the model. Similar results were found during CalNex (Brune et al., Faraday Discuss., 2016, 189, 169; Griffith et al., JGR, 2016). Does the underestimation of RO_2 (and therefore P_{O3}) depend on the measured OH reactivity? Griffith et al. (2016) found that the underestimation of P_{O3} by the model was higher when the OH reactivity from VOCs was the greatest.*

Answers: In the sensitivity run, in which we scaled VOCs to match measured OH reactivity, also the discrepancy between modelled and calculated ozone production rate is reduced (see revised figure 5).

We tested, if there is a correlation between the underestimation of RO_2 by the model and VOC reactivity. However, no clear relation is observed for this campaign.

Change: We added discussion on ozone production underprediction found in other field campaigns, including CalNex, to show the common feature of model inability to reproduce peroxy radical concentration for high NOx condition. The text is added to the end of Section 3.8: "Other HOx field studies have also found that models underpredict the observed ozone production rate in urban atmospheres (Martinez et al., 2003; Ren et al., 2003; Kanaya et al., 2008; Mao et al., 2010; Kanaya et al., 2012; Ren

et al., 2013; Brune et al., 2016; Griffith et al., 2016). In these studies, the observed production rates were determined from measured HO_2 concentrations only, without the contribution of RO_2 for which measurements were not available. In general, the ozone production from HO_2 was underpredicted by chemical models at NO mixing ratios greater than 1 ppbv, reaching a factor of about 10 between 10 ppbv and 100 ppbv NO. In campaigns before 2011, unrecognized interferences from RO_2# species may have contributed to the deviation between measurement and model results. The interference, however, is expected to account for less than a factor of 2, because HO_2 and RO_2 concentrations are approximately equal (Cantrell et al., 2003; Mihelcic et al., 2003) and $RO_2^{\#}$ is only a fraction of the total RO_2 (e.g., Fig. 5). This expectation has been confirmed in recent studies, where the interference was taken into account and the significant underprediction of the ozone production from HO_2 still persists (Ren et al., 2013; Brune et al., 2016; Griffith et al., 2016). During the CalNex-LA 2010 campaign in Pasadena (California), part of the discrepancy could be explained by unmeasured VOCs, which were recognized as missing OH reactivity (Griffith et al., 2016). Another major reason for the HO_2 underprediction could be an incomplete understanding of the HO_2 chemistry at high NOx concentrations (Ren et al., 2013; Brune et al., 2016; Griffith et al., 2016). ”

Reply to Referee #3

We would like to thank the reviewer for comments and questions which helped us to improve the manuscript. The reviewer comments are given below together with our responses and changes made to the manuscript.

Note: All the comments to change grammar and wordings suggested by the reviewer were changed accordingly. We appreciate the detail correction.

Comments: *Line 14. It is a bit confusing to say the RO_2 is in good agreement, but then to say that RO_2 is underestimated by a large amount in the morning. Suggest changing this text to make the points clearer.*

Answers: We changed the text Line 11:"…If additional OH recycling equivalent to 100 pptv NO is assumed, the model is capable of reproducing the observed OH, HO_2 and RO_2 concentrations for conditions of high VOC and low NOx concentrations. For HO_2, good agreement is found between modelled and observed concentrations at day and night. In case of RO_2, the agreement between model calculations and measurements is good in the late afternoon when NO concentrations are below 0.3ppbv. A significant model underprediction of RO_2 by a factor 3 to 5 is found in the morning at NO concentrations higher than 1ppbv, which can be explained by a missing RO_2 source of 2 ppbv h^{-1}."

Comments: *Line 45. Do the values of 0.8 and 0.4 ppbv refer to average or median values required? If so, state this.*

Answers: We changed the text Line 45: "An equivalent of 0.8 ppbv and 0.4 ppbv of NO was required in PRD and Beijing on average, respectively."

Comments: *Line 109. Note that peroxy radicals will also shift the NO to NO_2 ratio as the air travels down the sample line.*

Answers: We can in principle apply the inlet correction of the peroxy radicals to the

NOx measurement, since we have ambient measurements of peroxy radicals. However, because the peroxy radicals are highly reactive, they are expected to be easily lost in the inlet. Their contribution to the shift of NO to NO_2 is in general small compared to that of O_3. Therefore, a correction would not significantly change results.

We added a statement in Line 110: 'The effect of changes of the NO to NO_2 ratio by peroxy radicals is negligible due to their small concentrations and their high loss rate in the inlet line.'

Comments: *Table 1. All of the various techniques when multiple instruments were measuring are not given. Suggest making the list complete.*

Answers: We extended Table 1 to include all the techniques (e.g. for NOx, HONO, etc).

Comments: *Line 120. This discussion of HONO measurements is good, but given the potential uncertainties in such observations, it might be good to do a more detailed comparison, perhaps including a figure comparing all six measurements.*

Answers: A detailed comparison of the different HONO measurements is beyond the scope of this publication and will be the topic of a separate publication. Differences in the HONO measurements do not change results of our analysis here and are taken into account as additional uncertainty.

Comments: Line 130. An instrument with higher sensitivity is more sensitive. This is a common confusion. Suggest changing to "are generally better,"

Answers: We revised the text Line 128 – 136: "HONO measurements from the FZJ-LOPAP instrument are used as model constraint, because it showed the best detection limit and temporal coverage during the campaign. Results of model calculations only change less than 10%, if either measurements by the PKU LOPAP or NOAA CEAS are used as constraint. The other CEAS HONO instruments measured only during a few days. The GAC HONO measurement is known to be affected by interferences from ambient NO_2 and was therefore not used here."

Comments: *Line 220. It says that the correction is small compared to ambient OH, but this depends on the conditions. Near sunrise and sunset (or at night), this could be a large correction.*

Answers: We revised the text: 'A correction is applied that is small compared to ambient OH concentrations during daytime:'

Comments: *Line 225. It says that there was no interference from ozonolysis of simple alkenes, but what about larger, more complex alkenes (non-biogenic) that could be present?*

Answers: This statement summarizes results reported in Fuchs et al. (2016). The result was that ozonolysis reactions in general (most likely including also non-biogenic alkenes) are not causing significant interferences in this type of LIF instrument for atmospheric concentrations. GC measurements also suggest that the majority of alkenes were small alkene species (ethene, propene) during this campaign. The effort to investigate interferences in the OH detection will be certainly continued in the future.

Comments: *Line 257. This reviewer does not like the use of "titration" in this context. The authors can do as they choose, but suggest using "removal" or "conversion" efficiency rather than titration. Also suggest removing both commas on this line.*

Answers: We changed this to "removal efficiency".

Comments: *Line 271-272. The issue of mixing reagents into a flow containing HOx radicals at ambient pressure has been solved by others, particularly those make CIMS-based HOx measurements (e.g. Mauldin et al.).*

Answers: As stated in the text, the system was a first attempt to apply this technique in the field and needs technical improvement in the future.

Comments: *Line 277. It states that the titration unit caused a 5% difference in OH sensitivity. Was this applied to the data collected while it was present?*

Answers: Measurements with the titration system were not used as ambient OH measurements, but only to test, if there were interferences in the detection. Therefore, a change of the sensitivity only affects the quantification of a potential interference. As stated in the text, this calculation has a large uncertainty, so that a 5% change in sensitivity would be negligible.

Comments: *Line 307. It states that it is assumed that the contribution of $RO_2^{\#}$ scales with added NO. Is this justified by lab studies? How are the correction factors given in lines 309-310 applied? ($HO_2 = HO_2^*/CF$?)*

Answers: The RO_2 conversion efficiency clearly increases with increasing NO concentration because a reaction of RO_2 with NO is required to form HO_2. This dependence was also shown in laboratory studies (Fuchs et al. 2011.).

We have performed tests on the RO_2 conversion efficiency for simple alkene, e.g. ethene, propene, for this new instrument and observed similar conversion efficiencies as Fuchs et al. (2011) reported for low NO concentrations in the detection cell. The conversion efficiency was about 10%. The other RO_2 conversion efficiencies are then extrapolated as done in Lu et al. (2012).

We revised the text from Line 296 to Line 299 on page 10: "A significant reduction of the relative interference from RO_2 can be achieved by using a smaller amount of added NO. Although less NO will cause a smaller HO_2 conversion efficiency, possible interferences from RO_2 will be even more strongly reduced because RO_2 conversion to OH requires one more reaction step with NO. For this reason, the NO concentration used for the conversion of HO_2 during this campaign was chosen to be significantly smaller ($\leq$ 20 ppmv) than in previous field campaigns (500ppmv) (Lu et al.,2012, 2013). At this low concentration, it is expected that interferences from RO_2 become almost negligible (Fuchs et al., 2011)."

We revised the text from Line 307 to 311 on Page 11: "The HO_2^* ratios were used to

derive correction factors for the determination of interference-free HO_2 concentrations. For small NO concentrations as used in this work, we assume that the interference from $RO_2^{\#}$ is directly proportional to the applied NO concentration. Based on this assumption, we derived HO_2^*/HO_2 ratios of 1.02, 1.05, and 1.2 for the addition of 2.5, 5, and 20ppmv NO, respectively. These ratios were then used as correction factors to generate a consistent data set of interference-free HO_2 concentrations from the $HO2^*$ measurements. After all, the correction was small enough that deviations from this assumption would not significantly affect our results."

Comments: *Lines 334-337. Are the ambient data corrected for the artifacts as described?*

Answers: The background signals from the NO addition are subtracted from the HO_2 and RO_2 measurements. Artifacts caused by NO_3 are not subtracted from ROx measurements since there was no measurement available. The model gives an average concentration of about 10 pptv which only would case an interference that would be equivalent to $1\times10^7 cm^{-3}$ RO_2 which is similar to the detection limit of the ROx measurement.

We added a statement in Line 337: "Measurements were corrected for the NO background signal, but no correction was applied for potential interferences from NO_3, because no NO_3 measurement was available. However, model calculations (see below) suggest that there was no significant interference from NO_3 for conditions of this campaign."

Comments: *Line 358. Based on the discussion, the detection limit at noon is about 1.5×10^6. Is this a systematic or random effect of the solar light leakage? Can the data be corrected for this? Is this included in the overall measurement uncertainties?*

Answers: Sunlight is entering the measurement cell through the orifice through which ambient air is sampled into the fluorescence cell. The signal is subtracted from the total photon count rate as described Line 206-210. The detection limit is higher in the

presence of sunlight because of the higher total count rate, which is only partly due to OH fluorescence in this case. Therefore, the statistical noise (shot noise) of the OH measurement is increased.

Line 363. Do the authors believe that RACM 2 is a suitable mechanism to study detailed HOx radical chemistry? Why not use the explicit MCM mechanism, modified as you did to included updated isoprene chemistry? Perhaps add some discussion as to why the RACM 2 mechanism was selected.

Answers: We applied MCM and RACM in previous, similar studies and found no difference of model results for radicals (Lu et al. 2012). The likely reason for this is that the RACM mechanism is designed for ozone prediction, which is connected to the radical recycling mechanism. An explicit mechanism that includes all VOC intermediates is not required in this case. For the same reason we modified the isoprene mechanism in RACM since this impacts OH recycling.

We added in Line 368: "Previous model studies of radical chemistry showed that predictions of radical concentrations by the RACM are similar to results by explicit mechanisms like the Master Chemical Mechanism (Lu et al. 2012)."

Comments: *Line 389. When saying that the OH reactivity can "be well explained", suggest adding a quantitative value to the degree of agreement (within 22% or whatever).*

Answers: The sentence was changed to "Slightly more than 60% of the OH reactivity can be explained by the measured concentrations of CO, NOx and hydrocarbons during daytime. More than 90% of the OH reactivity can be explained, if also measured oxygenated VOC species are included (Fuchs et al., 2016b)."

Comments: *Line 398. What species are being referred to as "these species"? Suggest a bit more text to make it clear.*

Answers: Namely, most aldehydes are running free in the model. Added a sentence: " In order to avoid unrealistic accumulation of oxygenated VOC species (mostly

aldehydes), …".

Comments: One question: why didn't the peroxy radical concentrations also increase during this time period?

Answers: The peroxy radical concentrations were suppressed by higher NO concentrations on this day.

Comments: *Lines 485-494. It appears to me that the NO_3 interference is sufficient to explain some or all of the nighttime signal observed.*

Answers: Test with a similar design LIF instrument shows that NO_3 could cause an OH interference. In chamber experiment, 1ppbv of NO_3 yielded a signal that is equivalent to an OH concentration of $1\times10^7 cm^{-3}$ (Fuchs et al. 2016). A NO_3 concentration of 10 pptv that is suggested by model calculations for conditions of this campaign would cause an interference that would be equivalent to an OH concentration of $1\times10^5 cm^{-3}$, which is similar to the detection limit.

The statement 'Using NO_3 concentrations from the model (average. 10 pptv), the expected interference would be less than $1\times10^6 cm^{-3}$ for this campaign. ' was changed to: '.., the expected interference would be $1\times10^5 cm^{-3}$ for this campaign, 5 times less than the averaged nighttime OH measurement.'

Comments: *Lines 495-503. Suggest a discussion and perhaps a figure showing the major contributors to the OH reactivity.*

Answers: The OH reactivity contribution is presented in a separate paper by Fuchs et al. The focus for this paper is to analyze the HOx chemistry and thus the OH contribution is discussed in more detail in the accompanying paper.

Comments: *Lines 515-516. Suggest rewording this sentence. One suggestion would be to separate the data into two equal groups rather than have this long discussion about why the two groups are not equal in size.*

Answers: We have divided the data into two groups and analyzed them separately. Though the chemical conditions were slightly different, we found similar results from model-measurement comparison of radicals for the two periods. Therefore, we combined these two periods and present campaign averaged diurnal profiles.

We simplified the sentence and tried to make it more readable: "As described in Section 3.3, chemical conditions were slightly different before and after 20 June. We found similar results of model-measurement comparisons for radicals from the two periods. Therefore, the following interpretation and discussion will focus on campaign averaged diurnal profiles. "

Comments: Line 522. The median measure-model difference discussed is of the order of the various artifacts and interferences. Have the data been corrected for all of them before doing this comparison? If so, suggest stating this somewhere.

Answers: OH data is corrected for the well-known and characterized ozone interferences and no significant interference from NO_3 is expected as described in section 2.3.1.

The interference tests described in 3.1 were only occasionally performed and gave only an upper limit for potential additional interferences that would not change the results of our analysis of daytime OH. No correction of data is justified from these tests. Because reviewer #2 raised the same question, please refer also to the answer there.

Comments: *Line 523. It is not clear what is meant by "At the same time". Suggest rewording to make this clearer.*

Answers: The sentence is changed to "The median diurnal profiles of the measured and modelled OH concentrations agree within their errors of 10% (1σ) and 40%, respectively, from sunrise to midafternoon. When the median NO mixing ratio (cf. Fig. 6) drops gradually from 0.3ppbv to 0.1ppbv in the afternoon, a systematic difference evolves, with measured OH concentrations being approximately $1\times10^6 cm^{-3}$ higher than the model calculations. The discrepancy is of similar magnitude as the averaged unexplained OH determined in the chemical modulation experiments (Table

2)."

Comments: *Line 563. Is there any evidence of organic nitrites contributing to the enhancement of peroxy radicals in the morning? Photolysis of such species, if they exist, could contribute to the difference seen.*

Answers: We have no measurements of organic nitrites during this campaign. We tested including an artificial external source of RO_2, which could be originating from photolytic reactions. To reproduce the observed RO_2, 2 ppb/h of additional RO_2 production is required.

Comments: *Line 592. It states that the production rate of RO_2 could be underestimated, but one should also consider that the loss rate of RO_2 could be overestimated somehow.*

Answers: We also analyzed the destruction of RO_2 in the morning, which is dominated by the reaction with NO. The overestimation of the RO_2 destruction rate could be due to 1) systematic lower NO measurements; 2) segregation between NO and RO_2; 3) an error of lumped reaction rate constants. A sensitivity run testing the effect of this uncertainty shows that the modelled and measured RO_2 would agree if the reaction rate constant of RO_2+NO was smaller by a factor of 4. Such large change cannot be easily explained.

Comments: *Line 594. It states that VOC concentrations are scaled to match measurements. Which measurements? Are they the VOCs or kOH?*

Answers: The VOC concentrations are scaled to match measured OH reactivity. We revised the text: "To fill this gap, the total concentration of the measured VOCs was increased to match the measured k_{OH} in the time window from 06:00 to 09:00. The relative partitioning of the VOCs was not changed. The model run (S1) with the upscaled VOC reactivity resolves part of the RO_2 discrepancy until 09:00 (Fig. 5)."

Comments: *Line 600. Suggest "…concentrations that are used as constraints." A*

thought on nighttime chemistry: if there is NO_3 present, then the NO concentration should be very small unless the NO_3 production rate is very large. This is because of the rapid reaction between NO and NO_3. This could help with the modeling of nighttime chemistry.

Answers: We had no NO_3 measurement in this campaign. The observed NO was usually below detection limit of the instrument (60pptv) during nighttime. In this case, the modelled RO_2 is high and highly variable. We tested another model scenario that forces the NO to be higher than 60pptv to limit accumulation of RO_2, which reduces the observed-to-modelled ratio 1.2 during the night.

Comments: Lines 758-769. Suggest including Ye et al in the discussion of HONO budgets.

Answers: We added a sentence in Line 769. "… and photolysis of particulate nitrate is proposed to be of potential importance for the tropospheric HONO production (Ye et al., 2016). "

Comments: *Line 770. Suggest giving an example of a reaction of OH with VOCs that do not lead to peroxy radicals.*

Answers: We modified the text in line 770: "Further radical terminating OH losses include reactions with unsaturated dicarbonyls (DCB1, DCB2, DCB3) and acetyl nitrate species (PAN, MPAN, etc) in RACM2."

Comments: *Line 832. Yes, the interference would be minor compared to the daytime maximum, but it could be very important at sunrise and sunset.*

Answers: The statement was modified accordingly.

Comments: References. The papers on HOx measurements are very Euro-centric. Suggest adding some papers from US HOx measurement groups.

Answers: More results from the HOx groups outside Europe were added such as

Griffith et al., 2013, 2016; Mauldin et al., 1999; Kim et al., 2014; Brune et al., 2016, Kanaya et al., 2008, 2012.

Comments: *Figure 1. The colors for SN2 and SOH are very similar. Suggest changing one of them to a very different color.*

Answers: Changed accordingly.

Comments: *Figures 3, 4, 5, 6, 8, and 10. Is the gray period meant to signify nighttime? If so, the authors should check this carefully. It appears that there are photolysis processes (such as O_3) that occur after sunset (see Figure 10).*

Answers: The gray area indicates nighttime. For Figure 10 there is a typo error in the data analysis routine, we have now revised this.

Manuscript prepared for Atmos. Chem. Phys.
with version 2015/04/24 7.83 Copernicus papers of the LaTeX class copernicus.cls.
Date: 25 November 2016

Radical chemistry at a rural site (Wangdu) in the North China Plain: Observation and model calculations of OH, HO_2 and RO_2 radicals

Zhaofeng Tan[1], Hendrik Fuchs[2], Keding Lu[1], Andreas Hofzumahaus[2], Birger Bohn[2], Sebastian Broch[2], Huabin Dong[1], Sebastian Gomm[2,a], Rolf Häseler[2], Lingyan He[2], Frank Holland[2], Xin Li[2,b], Ying Liu[1], Sihua Lu[1], Franz Rohrer[2], Min Shao[1], Baolin Wang[1], Ming Wang[4], Yusheng Wu[1], Limin Zeng[1], Yinsong Zhang[1], Andreas Wahner[2], and Yuanhang Zhang[1,5]

[1]State Key Joint Laboratory of Environmental Simulation and Pollution Control, College of Environmental Sciences and Engineering, Peking University, Beijing, China
[2]Institute of Energy and Climate Research, IEK-8: Troposphere, Forschungszentrum Jülich GmbH, Jülich, Germany
[3]Key Laboratory for Urban Habitat Environmental Science and Technology, School of Environment and Energy, Peking University Shenzhen Graduate School, Shenzhen, China
[4]School of Environmental Sciences and Engineering, Nanjing University of Information Science and Technology, Nanjing, China
[5]CAS Center for Excellence in Regional Atmospheric Environment, Chinese Academy of Science, China
[a]now at: d-fine GmbH, Opernplatz 2, 60313 Frankfurt, Germany
[b]now at: College of Environmental Sciences and Engineering, Peking University, Beijing, China

Correspondence to: K. Lu (k.lu@pku.edu.cn), H. Fuchs (h.fuchs@fz-juelich.de)

Abstract. A comprehensive field campaign was carried out in summer 2014 in Wangdu located in the North China Plain. A month of continuous OH, HO_2 and RO_2 measurements ~~were~~ was achieved. Observations of radicals by the laser induced fluorescence (LIF) technique ~~gave~~ revealed daily maximum concentrations between (5-15)$\times10^6$ cm^{-3}, (3-14)$\times10^8$ cm^{-3} and (3-15)$\times10^8$ cm^{-3} for OH, HO_2 and RO_2, respectively. Measured OH reactivities (inverse OH ~~lifetimes~~lifetime) were 10 to 20 s^{-1} during daytime. ~~A~~ The chemical box model ~~constrained by trace-gas observations and based on a state-of-the-art chemical mechanism is~~ RACM 2 including the Leuven Isoprene Mechanism (LIM) was used to interpret the observed radical concentrations. ~~In general, the model can reasonably well reproduce measured radical concentrations during daytime. Like~~ As in previous field campaigns in China, modelled and measured OH concentrations agree for NO mixing ratios higher than 1 ppbv, but systematic discrepancies are observed in the afternoon for NO mixing ratios of less than 300 pptv (the model-measurement ratio is between 1.4 to 2 in this case). If additional OH recycling equivalent to 100 pptv NO is assumed, the model is ~~also~~ capable of reproducing the observed OH, HO_2 and RO_2 concentrations for conditions of high VOC and low NO_x concentrations~~with good agreement in and . Observed~~. For HO_2, good agreement is found between modelled and observed concentrations at day and night. In case of RO_2~~concentrations are underestimated in~~

the morning hours , the agreement between model calculations and measurements is good in the late afternoon when NO concentrations are below 0.3 ppbv. A significant model underprediction of RO_2 by a factor of 3 to 5. This indicates that an additional chemical source of is missing in the model. The reactivity is also underpredicted in the early morning . Increasing VOC concentrations to match measured reactivity helps to reduce the discrepancy between modelled and measured 5 is found in the morning at NO concentrations higher than 1 ppbv, which can be explained by a missing RO_2 . The underprediction of coincides with high concentrations and therefore leads to a significant underestimation of the local ozone production rates determined from the peroxy radical (source of 2 ppbv h^{-1}. As a consequence, the model underpredicts the photochemical net ozone production by 20 ppbv per day, which is a significant portion of the daily integrated ozone production (110 ppbv) derived from the measured HO_2 and RO_2) reactions with . The underestimation corresponds to a daily integral ozone production of about . The additional RO_2 production from the photolysis of $ClNO_2$ and missing reactivity can explain about 10 % and 20 per day.

% of the discrepancy, respectively. The underprediction of the photochemical ozone production at high NO_x found in this study is in consistent with the results from other field campaigns in urban environments, which underlines the need for better understanding of the peroxy radical chemistry for high NO_x conditions.

1 Introduction

Air pollution in Chinese megacity regions has become ~~a problem of high concerns by~~ an issue of great concern for citizens and the government. Ambitious restriction strategies ~~were already~~ have already been implemented for the reduction of the primary air pollutants sulfur dioxide (SO_2), nitrogen oxides (NO_x) and particular matter (PM_{10}) for more than a decade. Significant emission reductions of those primary air pollutants were achieved. However, high concentrations of secondary air pollutants, e.g. ozone (O_3) and small particles ($PM_{2.5}$) still occur and the air quality has ~~even continuously been deteriorated at some places~~ been steadily deteriorating in some locations (Shao et al., 2006). As denoted in the Empirical Kinetics Modelling Approach (Ou et al., 2016), the reduction in primary pollutants may not directly reduce O_3 due to the non-linearity of atmospheric photochemistry. Thus, a critical question is to find an optimized way to control the abundance of secondary air pollutants by the reduction of primary pollutants.

As shown in a large number of studies, hydroxyl radical (OH) chemistry controls the atmospheric oxidation globally (Stone et al., 2012; Ehhalt, 1999). However, also other oxidants can be of importance on a regional scale like NO_3 (Brown and Stutz., 2012), Criegee intermediates (Mauldin et al., 2012) and chlorine radicals (Thornton et al., 2010). In China, studies of atmospheric oxidants are still sparse (Lu et al., 2010; Wang et al., 2015). In summer 2006, we performed two field campaigns (PRIDE-PRD2006 and CareBeijing2006) focussing on hydroxyl and hydroperoxy (HO_2) radical measurements in a rural area in the Pearl River Delta (PRD) and in a suburban area (Yufa) close to Beijing. The major results from these two campaigns were: 1) There were high concentrations of daytime and nighttime HO_x (=OH+HO_2) radicals in the Chinese developed megacity regions indicating a strong atmospheric oxidation capacity. 2) The high daytime OH concentrations at high concentrations of volatile organic compounds (VOC) and low NO_x concentrations could only be explained by introducing an additional OH regeneration process in the model that converts peroxy radicals to OH like NO does. An equivalent of 0.8 ppbv and 0.4 ppbv of NO was required in PRD and Beijing on average, respectively. 3) The high daytime OH concentrations at high VOC and high NO_x conditions could be understood by model calculations (Hofzumahaus et al., 2009; Lu et al., 2012, 2013, 2014). A retrospective analysis (Rohrer et al., 2014) shows that the magnitude of unexplained OH concentrations observed in these two studies in China is similar to other OH observations at high VOC low NO_x conditions (Tan et al., 2001; Lelieveld et al., 2008; Whalley et al., 2011).

Because isoprene was the most important OH reactant during many of these campaigns, theoretical and laboratory investigations were done to investigate its photochemical degradation. Isomerization and decomposition reactions of organic peroxy radicals formed from isoprene were found to be competitive with the reaction of peroxy radicals with NO for conditions of these campaigns (Peeters et al., 2009; Crounse et al., 2011; Fuchs et al., 2013; Peeters et al., 2014). They lead to the direct reformation of radicals and the production of hydroperoxy aldehydes (HPALD), which can

photolyze and produce additional radicals. Isoprene chemistry was less important in our two field campaigns in China 2006 compared to other campaigns that were conducted in forested areas, so that new findings in the degradation of isoprene alone could not close the gap between measured and modelled OH (Lu et al., 2012, 2013).

As a continued effort to explore the hydroxyl radical chemistry in Chinese megacity areas, OH, HO_2, RO_2 radical concentrations and OH reactivity were measured for one month at a rural site (Wangdu) in the North China Plain in summer 2014 as part of a comprehensive field campaign. Several improvements ~~have been~~ were achieved in comparison to the previous campaigns PRIDE-PRD2006 and CareBeijing2006. (1) Interference tests were performed for OH measurements applying a new prototype chemical-modulation device. (2) Unlike before, HO_2 was measured without interferences by RO_2 species that are formed from alkenes and aromatic VOCs. (3) Total RO_2 was measured together with OH and HO_2 in contrast to the two previous campaigns. (4) In addition, the sum of RO_2 species that are formed from alkenes and aromatic VOCs was measured as a separate class of RO_2. (5) Oxygenated VOCs (e.g., ~~formaledehyde~~formaldehyde, acetaldehyde, isoprene oxidation products) were measured, whereas such observations were missing in the previous two campaigns. All improvements provide better constraints for the interpretation of the radical chemistry. The radical measurements were obtained by a newly built, compact instrument that combines resources from Peking University and Forschungszentrum Jülich. In this paper, we report results of radical measurements and model calculations ~~in the context of~~ compared to results from previous campaigns investigating HO_x chemistry in China.

2 Methodology

2.1 Measurement site

The campaign took place between 7 June and 8 July 2014. The measurement site is close to the town Wangdu ~~, which is a small city~~ (population 260000 inhabitants) without major industry. The Taihang Mountains are located 50 km northwest of Wangdu and the Bohai sea 200 km east. The next large city, Baoding, is 35 km northeast of Wangdu. Beijing and Shijiangzhuang, two of the largest cities in the North China Plain, are located 170 km northeast and 90 km southwest of the site, respectively. Times given in this paper are CNST (Chinese national standard time = UTC + 8 h). Sunrise was at 04:30 CNST and sunset at 20:00 CNST.

Instruments were set-up in a ~~botanic~~ botanical garden, which was surrounded by farmland. ~~Weeds~~ Wheat and willows were the dominant ~~tree~~ plant species few of which were growing within 10 m ~~to~~ of the instruments. There was no ~~traffic by cars or trucks in the botanic garden; a nearby~~ car or truck traffic in the botanical garden; the closest road was 2 km away. Most of the instruments were placed in seven sea containers. Two of them were stacked on top of three others and two more containers were placed approximately 5 m away~~from the other containers~~.

2.2 Instrumentation

A large number of trace gases and aerosol properties were measured during this campaign. Most of the instrument inlets were placed 7 m above the ground at the height of the upper containers. Table 1 summarizes the details of the trace gas measurements. OH, HO_2, and RO_2 radicals were measured by laser induced fluorescence described in detail below. The OH reactivity (k_{OH}), which is the inverse chemical lifetime of OH was directly measured by a laser pump and probe technique (Lou et al., 2010; Fuchs et al., 2016b).

Most of the inorganic trace gases (O_3, CO, CO_2, NO, and NO_2) were simultaneously monitored by ~~different instruments.~~ more than one instrument. Measurements of O_3, CO and CO_2 measurements agreed well within ~~their~~ the instrumental accuracies. O_3 measurements were performed by two commercial instruments using ultraviolet (UV) absorption (Environment S.A. model 41M, and Thermo Electron model 49i). Also SO_2, CO, CO_2 concentrations were measured by commercial instruments (Thermo Electron model 43i-TLE, 48i-TLE and 410i). In addition, a cavity ring-down instrument (Picarro model G2401) provided measurements of CO, CO_2, CH_4 and H_2O concentrations.

Chemiluminescence technique was used to detect NO and also NO_2 after conversion to NO. Two commercial instruments were deployed by Peking University (PKU) (Thermo Electron model 42i NO-NO_2-NO_x analyzer), one of which (PKU-PL) was equipped with a home-built photolytic converter for the detection of NO_2 and the other with a catalytic converter (PKU-Mo). The NO_2 data from PKU-Mo were not used here, since catalytic converters can cause interferences from other nitrogen oxygen compounds (e.g., HNO_3, PAN). Another instrument was ~~run~~ operated by Forschungszentrum Jülich (FZJ) (Eco Physics model TR 780, with photolytical converter for NO_2). Instruments were located in the upper two containers to ~~make~~ have inlet lengths as short as possible in order to minimize the correction for shifts in the NO to NO_2 ratio by the reaction of NO with O_3 in the inlet lines. The effect of changes of the NO to NO_2 ratio by peroxy radicals is negligible due to their small concentrations and their high loss rate in the inlet line. The distance between inlets was less than 5 m. Measurements of the two PKU instruments and the FZJ instrument differed overall by $\pm$ 20 %, which cannot be explained by their calibration errors. The reason for this discrepancy is not clear. Calibrations of the FZJ instrument were less reproducible (10 %) ~~as it used to be~~than in previous deployments, while calibration measurements of the PKU instrument varied only by 1 to 2 %. Fortunately, the calibrations did not show a trend over time indicating that there was no accumulation of contaminations in the inlet lines. Because of the ~~better reproducibility of calibration measurements,~~ more stable calibrations of the PKU instruments, the NO and NO_2 ~~measurements from~~ data used as model input (Section 2.4) were taken from the PKU-Mo and PKU-PL instruments~~are used as model constraints in this study~~, respectively. However, the difference between measurements of different instruments is considered ~~in the following as~~ as additional uncertainty in the NO_2 and NO measurements.

Six instruments detected HONO using different techniques. Home-built instruments from FZJ (Li et al., 2014) and from PKU (Liu et al., 2016) utilized long-path absorption photometry (LOPAP). In addition, three instruments applied cavity enhanced absorption spectroscopy (CEAS) for the detection of HONO. They were operated by the US National Oceanic and Atmospheric Administration (NOAA) (Min et al., 2016), by the Anhui Institute of Optics and Fine Mechanics (AIOFM), and by the University of Shanghai for Science and Technology (USST). A gas and aerosol collector (GAC), which is based on the wet denuder/ion chromatography technique, could also detect HONO (Dong et al., 2012). The ~~agreement between measurements of all instruments was generally reasonable and comparison details will be presented in a future publication~~measurements between multiple instruments agreed within 30%. HONO measurements from the FZJ-LOPAP instrument are used as model constraint~~for the following reasons: 1) the sensitivity of instruments using cavity based absorption techniques are generally lower and some of the instruments had instrumental problems due to the degradation of the high reflectivity of the mirrors in the presence of high loads of aerosol during this campaign. 2) The GAC instrument can only be operated at a 30time resolution and the detection limit is only 300. 3) The FZJ-LOPAP instrument has been successfully deployed in various field campaigns. Nevertheless, differences between the two LOPAP instruments of 20~~, because it showed the best detection limit and temporal coverage during the campaign. Results of model calculations only change less than 10%~~cannot be explained by the combined uncertainties and need to be considered as additional uncertainty of the~~ , if either measurements by the PKU-LOPAP or NOAA-CEAS are instead used as constraint. The other CEAS HONO ~~concnetrations~~ instruments measured only during a few days. The GAC HONO measurement is known to be affected by interferences from ambient NO_2 and was therefore not used here.

59 organic species were measured by a gas chromatograph (GC) equipped with a mass spectrometer and a flame ionization detector (FID) (Wang et al., 2014). This instrument provided concentrations of C_2 to C_{11} alkanes, C_2 to C_6 alkenes, and C_6 to C_{10} aromatics. In addition, measurements of volatile organic compounds (VOCs) were performed by a proton transfer reaction - mass spectroscopy system (PTR-MS, Ionicon). These measurements included isoprene, acetaldehyde, the sum of methyl vinyl ketone (MVK) and methacrolein (MACR), benzene, toluene, styrene, C_8-aromatics, C_9-aromatics ~~, the sum of monoterpenes,~~ and acetonitrile. Daytime measurements of the two instruments agreed well for those species which were detected by both instruments. During nighttime, however, PTR-MS measurements gave much larger values compared to measurements by GC for some periods and some species. The reason for that is not clear, but could have been caused by interferences by other species that occur at the same mass in the PTR-MS. Because of this uncertainty mainly measurements by GC are taken as constraints for model calculation here. ~~Only oxygenated species~~ Measurements of acetaldehyde, MVK and MACR ~~that were only measured~~ were only done by PTR-MS~~are used~~. Formaldehyde (HCHO) was measured by a commercial instrument utilizing the Hantzsch method (Aerolaser GmbH model AL4021).

~~15south of the location of the containers, a~~ A 20 m high tower with meteorological instrumentation was set up 15 m south of the containers, where temperature, pressure, relative humidity, wind speed and wind direction were measured at two different heights (10 and 20 m). The height of the planetary boundary layer (PBL) could be estimated by a ceilometer (the minimum detectable PBL height was 200 m). Photolysis frequencies were calculated from the spectral actinic photon flux density measured by a spectroradiometer (Bohn et al., 2008), whose inlet dome was placed on top of the highest container.

More trace gases were detected, but will not be discussed in detail here: Peroxyacyl nitrates (PAN) and peroxypropionyl nitrate (PPN) were measured by gas chromatography with a electron-capture-detector (Wang et al., 2010). H_2O_2 was collected by a scrubbing coil collector and detected by high-performance liquid chromatography (HPLC) coupled with post-column derivatization and fluorescence detection (Hua et al., 2008). Chemical ionization mass spectroscopy (CIMS) was utilized to measure nitryl chloride ($ClNO_2$) and N_2O_5, but measurements were only conducted after 21 June (Tham et al., 2016). A cavity enhanced absorption spectrometry instrument was deployed to detect glyoxal, HONO and NO_2 (Min et al., 2016).

Aerosol properties were characterized in detail during the campaign, but will be discussed elsewhere. Measurements included particle number density and size distribution, and also chemical composition.

2.3 Laser-induced fluorescence instrumentation for the detection of radicals

2.3.1 Instrument description

OH, HO_2 and RO_2 concentrations were measured by laser-induced fluorescence (LIF) technique. LIF is a direct method to detect OH radicals (Heard et al., 2003). In addition, HO_2 and RO_2 radicals can be detected by fluorescence after chemical conversion to OH (Fuchs et al., 2008).

The Peking University laser-induced fluorescence instrument, PKU-LIF, was deployed in this campaign for the first time. It consists of two LIF measurement cells to detect both OH and HO_2. It was built by Forschungzentrum Jülich and is therefore similar to instruments from this organization that have been described earlier (Holland et al., 1995; Hofzumahaus et al., 1996; Holland et al., 2003; Fuchs et al., 2011; Lu et al., 2012). Additionally, a third measurement cell was provided by Forschungzentrum Jülich for the detection of the sum of RO_2 radicals (Fuchs et al., 2008).

The instrument consists of a laser and a measurement module (Fig. 1). The laser radiation for the OH excitation at 308 nm is generated by a pulsed, frequency-doubled, tunable dye-laser system that is pumped by a commercial Nd:YAG laser (Spectra-Physics model Navigator) at 532 nm (repetition rate: 8.5 kHz; pulse duration FWHM 25 ns). The laser light is guided to the measurement cells, to the k_{OH} instrument, and to an OH reference cell by optical fibers. The laser power is divided with a ratio of 0.6:0.32:0.08 resulting in a laser power inside the measurement cells of typically 20 mW.

The signal of the reference cell, in which a large concentration of OH is produced by pyrolysis of water vapor on a hot filament, is used as a wavelength reference and allows for the automatic correction of possible drifts of the laser wavelength.

All components of the measurement module are housed in a weather-proof, air-conditioned box placed on top of the upper container. For the OH and HO_2 detection cells, ambient air is sampled at a flow rate of 1 slpm (standard litre per minute, at standard conditions of 25 °C and 1atm) through conically shaped nozzles (Beam Dynamics, orifice diameter 0.4 mm) into low pressure cells ($p = 4$ hPa). RO_2 is measured by a differentially pumped system consisting of a chemical conversion reactor ($p = 25$ hPa), followed by a fluorescence detection cell ($p = 4$ hPa). 7 slpm ambient air is sampled through a nozzle (orifice diameter 1.0 mm) into the reactor, half of which is sampled through a second orifice into the fluorescence cell. Nitrogen sheath flows of 1 slpm are surrounding the gas expansions of sampled air in all fluorescence cells. Reactive gases for the conversion of peroxy radicals can be injected via ring-shape nozzles in the fluorescence cells and via an injection needle in the RO_2 conversion reactor.

The laser light crosses the three fluorescence cells in a single pass. Microchannel plate photomultiplier detectors (Photek, ~~MCP~~ PMT 325) are used to detect fluorescence photons collected by lens systems. The detection system is mounted perpendicular to the gas beam and laser light axis. The MCPs are gated to switch off the gain for the duration of the laser pulses. The OH fluorescence is recorded by a gated photon-counting system (Becker & Hickl, PMS 300) in a 500 ns time window starting approximately 100 ns after the laser pulse when laser stray light has dropped to an acceptable level.

The total photon count-rate is composed of the OH fluorescence, solar stray light that enters the cell through the orifice, and laser stray light. The solar stray light is detected separately during a second counting window (duration of 25 µs starting 25 µs after the laser pulse), when the OH fluorescence signal has diminished. The long integration time ensures accurate subtraction of the solar background signal, after it has been scaled to the shorter OH fluorescence counting window. The remaining other background signals are separated from the OH fluorescence by wavelength modulation of the laser. Background and fluorescence signals are measured together, when the laser wavelength is tuned on the OH absorption line, and only background signals are detected, when the laser wavelength is tuned ~~away.~~ off the absorption line. During one measurement cycle the laser wavelength is tuned to four different online and two offline positions to make sure that the maximum of the OH absorption line is captured as well as the background signal. A full wavelength cycle gives a time resolution of 32 s~~for one radical measurement~~.

2.3.2 Interferences in the OH ~~detection~~measurement

It is known that O_3 photolysis by 308 nm radiation with subsequent reaction of O^1D with water vapor can produce artificial OH inside the measurement cell. This interference was characterized in

laboratory experiments and parameterized ~~taking~~ using the laser power, and the O_3 ~~,~~and water vapor ~~concentration that were monitored~~concentrations. A correction is applied that is small compared to ambient OH concentrations during daytime: 50 ppbv of O_3 ~~causes~~ could cause an equivalent of 3×10^5 cm^{-3} OH for typical laser power (20 mW) and water concentration (1 %) in this campaign.

Potential interferences from ozonolysis reactions and NO_3 have been investigated for OH and HO_2 detection cells that are similar to the detection cells of the PKU-LIF instrument (Fuchs et al., 2016a). No significant interference was found from the ozonolysis of simple alkenes (e.g., ethene, propene), isoprene and monoterpenes at ozonolysis reaction rates of several ppbv h^{-1}, i.e. at reaction rates that are considerably higher than found in the atmosphere. Therefore, it is not expected that measurements in this campaign are affected by ozonolysis products. Interferences from NO_3 were reported (Fuchs et al., 2016a). The underlying mechanism is still unknown. The magnitude of the interference is 1.1×10^5 cm^{-3} OH in the presence of 10 pptv NO_3. No significant interference is expected at NO_3 concentrations that are predicted by model calculations for the present campaign at nighttime (average 10 pptv).

Wavelength modulation used in this work to distinguish between OH fluorescence and background signals is not capable of discriminating ambient OH signals from signals caused by artificially produced OH in the detection cells. Because interferences from unknown, internal processes have been reported for two other LIF instruments (Mao et al., 2012; Novelli et al., 2014), we have tested a chemical modulation scheme that was proposed and used by these authors. For this purpose, ambient OH is removed by an OH scavenger (propane) that is added to the sampled ambient air just before entering the fluorescence cell, so that any remaining OH signal could be attributed to internally produced OH. The propane concentration has to be chosen such that most of the ambient OH is removed while it is small enough to prevent OH losses inside the fluorescence cell. When the scavenger is replaced by nitrogen, the sum of ambient OH and possible interference OH is measured. By switching between propane and nitrogen addition, ambient OH signals can be discriminated from artifacts.

In the campaign, we applied a prototype device for chemical modulation ~~which~~ that was temporarily attached to the OH detection cell ~~for a few times~~during selected periods (Table 2). The device consisted of a Teflon tube with an inner diameter of 1.0 cm and a length of 10 cm. About 20 slpm of ambient air were drawn through the tube by a blower. 1 slpm of air was sampled into the OH detection cell. At the entrance of the Teflon tube, either propane mixed with ~~a flow of nitrogen or only~~ nitrogen or pure nitrogen was injected into the air flow by a small tube (stainless steel, outer diameter 1/16"). Due to technical problems with the control electronics, the device failed to operate in the first half of the campaign. In the second part of the campaign, it showed ~~still~~ instabilities causing an increased uncertainty in the determination of the OH scavenging efficiency.

The two signals with and without propane have contributions from ambient OH (S_{OH}), from the known ozone interference (S_{O3}) and any potential additional interference signal (S_{int}):

$$S_{\mathrm{N2}} = S_{\mathrm{OH}} + S_{\mathrm{O3}} + S_{\mathrm{int}} \quad (1)$$

$$S_{\mathrm{prop}} = (1-\epsilon)S_{\mathrm{OH}} + S_{\mathrm{O3}} + S_{\mathrm{int}} \quad (2)$$

ϵ is the ~~titration efficiency ,~~ efficiency with which ambient OH is removed ~~,~~ when propane is added.

As long as ambient OH does not change while switching between the two measurement modes, the difference between the two signals can be used to calculate the signal from ambient OH:

$$S_{\mathrm{OH}} = \epsilon^{-1}(S_{\mathrm{N2}} - S_{\mathrm{prop}}) \quad (3)$$

Together with the known ozone interference the signal that is expected to be observed in the absence of an additional interference can be calculated and compared to the total signal that is measured ~~, if~~ with no OH scavenger ~~is~~ added (S_{N2}).

The ~~accurate knowledge of the titration efficiency~~ knowledge of ϵ is essential for an accurate quantification of potential interferences. The ~~titration efficiency was determined before each ambient titration test using~~ removal efficiency was tested and optimized in the field using the OH calibration device as a radical source~~(see below)~~. The value ~~ranged between 80and 97depending on the amount of propane. The titration efficiency depended on both, the flow rate of propane and the flow rate of the additional nitrogenflow. 0.02 to 0.2~~of ϵ was found to depend on the flow rates of the added gases (propane and nitrogen). Propane was added as a 5% ~~propane~~ mixture in nitrogen ~~and an additional flow of pure nitrogen~~ with a flow rate between ~~0.04 and~~ 0.02 and 0.2 lpm (Liter per minute) which was further diluted in a carrier flow of pure nitrogen (0.04 to 0.5 ~~were used~~lpm). The dependence of ~~the titration efficiency~~ ϵ on the flow ~~rate shows~~ rates showed that mixing of the injected ~~flow~~ propane into the high flow of ambient air was inhomogeneous similar to results reported in Novelli et al. (2014). Because of technical ~~problems, the accuracy of~~ difficulties with the flow regulation, the removal efficiency was re-determined before each ambient titration test. The values obtained for ϵ ~~is only~~ ranged between 80% and 97% with an accuracy of 10% ~~at a~~ (1 σ) at fixed nominal propane ~~flow~~and nitrogen flows.

~~The propane concentrations used in the chemical-modulation tests are not expected to influence possible~~ Kinetic calculations show that the added propane removes less than 0.3 % of internally produced OH~~interference signals, because the lifetime with respect to the reaction with propane is~~ . The calculation assumes that the added propane is homogeneously mixed in the sampled air, yielding an expected OH lifetime which is larger than 0.1 s and therefore much longer than the residence time (3 ms) in the low-pressure detection cell. Therefore, the propane concentrations used in the chemical-modulation tests are not expected to influence possible OH interference signals.

Another systematic error could arise from the depletion of ambient OH by wall loss in the attached Teflon tube. Calibrations of OH sensitivities with and without the ~~titration unit~~ chemical-modulation device only differed by 5 %, which indicates that wall loss was not important.

2.3.3 ~~Interferences in the~~ Measurement of HO_2 ~~measurement~~and possible interference

The detection of HO_2 is achieved by chemical conversion to OH in its reaction with NO (Hard et al., 1995). Three types of interferences are known for the current instrument design.

A small OH signal is observed ~~,~~ when NO is injected into the fluorescence cell in the absence of ambient radicals. This background signal was regularly determined during each calibration and was stable over the entire campaign. The equivalent HO_2 concentration of this signal is $3\times10^7\,\mathrm{cm}^{-3}$ for the NO mixing ratios applied in this campaign (see below). ~~On the other hand, the~~ In addition, ambient NO_3 radicals can ~~also introduce~~ cause interferences in HO_2 detection similar to OH ~~cell~~ (see above). The estimated interference is $1\times10^7\,\mathrm{cm}^{-3}$ at 10 pptv of NO_3 (Fuchs et al., 2016a), which is ~~within the range of the~~ comparable to the detection limit.

Specific RO_2 radicals have the potential to be converted to OH on the same time scale as HO_2~~, if the concentration is high enough~~. Therefore, they can contribute to ambient HO_2 measurements (Fuchs et al., 2011). In the following, ~~this class of~~ the class of interfering peroxy radicals is ~~denoted~~ called $RO_2^\#$. It includes, for example, RO_2 species derived from alkenes, isoprene and aromatic compounds. In previous papers ~~,~~ (e.g. Lu et al. (2012)), the quantity $[HO_2^*]$ was defined as the sum of the true HO_2 ~~and interferences from that~~ concentration and the interference from RO_2 species i, which are detected with ~~the conversion efficiency $\alpha^i_{RO_2}$,~~ different relative sensitivities, $\alpha^i_{RO_2}$:

$$[HO_2{}^*] = [HO_2] + \sum\left(\alpha^i_{RO_2}[RO_2]_i\right) = +\alpha_{RO_2} \quad (4)$$

~~is then the sum of interfering~~ RO_2 ~~species that is converted with an averaged conversion efficiency $\alpha^\#_{RO_2}$.~~

~~A low~~ radicals from alkenes, for example, have $\alpha^i_{RO_2}$ values of about 0.8, when NO is sufficiently high to achieve almost complete HO_2 to OH conversion in the detection cell (Fuchs et al., 2011; Lu et al., 2012). A significant reduction of the relative interference from RO_2 can be achieved by using a smaller amount of added NO~~concentration can minimize the potential impact of~~. Although less NO will cause a smaller HO_2 conversion efficiency, possible interferences from RO_2 ~~conversion, will be even more strongly reduced~~ because RO_2 conversion to OH requires one more reaction step with NO. ~~Therefore~~For this reason, the NO concentration used for the conversion of HO_2 during this campaign was chosen to be significantly smaller (≤ 20 ppmv) than in previous field campaigns (500 ppmv) (Lu et al., 2012, 2013). ~~Furthermore, the amount of~~ At this low concentration, it is expected that interferences from RO_2 become almost negligible (Fuchs et al., 2011).

In order to test the importance of the remaining $RO_2^\#$ interference in the HO_2 measurements, the added NO was periodically switched between two ~~concentrations, in order to test, if~~ different concentration values every few minutes. Any $RO_2^\#$ interference is then expected to produce a systematic difference between HO_2 measurements ~~may have still been affected by interferences from . In~~ with smaller and higher NO concentrations. At the beginning of the campaign, NO mixing ratios ~~varied~~ were changed between 5 ppmv and 20 ppmv, yielding HO_2 conversion efficiencies of 11% and 35%,

respectively. On average, HO_2^* was 15% higher when the larger NO value was applied, indicating the influence of $RO_2^\#$. After 14 June, the mixing ratios were switched between values of 2.5 ppmv and 5 ppmv, giving ~~lower~~ HO_2 conversion efficiencies of 6% and 11%, respectively. ~~During operation with alternating concentrations, the application of the higher concentration always yielded higher~~ In this case, HO_2^* ~~concentrations, as expected from the influence of~~ was on average 3% higher when the larger NO value was applied. The ratios of HO_2^* measurements obtained for a pair of alternating NO concentrations showed no temporal trend or diurnal variation ~~. On the assumption that the contribution from scales linearly with the added concentration,~~ in each part of the campaign.

The HO_2^* ratios were used to derive correction factors for the determination of interference-free HO_2 concentrations~~were derived. The factors are~~. For small NO concentrations as used in this work, we assume that the interference from $RO_2^\#$ is directly proportional to the applied NO concentration. Based on this assumption, we derived HO_2^*/HO_2 ratios of 1.02, 1.05, and 1.2 for the addition of 2.5, 5, and 20 ppmv NO, respectively. ~~The correction was then applied~~ These ratios were then used as correction factors to generate a ~~homogenous data set for~~ consistent data set of interference-free HO_2 ~~.~~ concentrations from the HO_2^* measurements. After all, the correction was small enough that deviations from this assumption would not significantly affect our results.

2.3.4 ~~Detection~~ Measurement of RO_2 and possible interference

In the RO_2 detection system, the chemical conversion of RO_2 and of HO_2 to OH is accomplished by a two step process as described in Fuchs et al. (2008). In the first chamber (conversion reactor), the addition of 0.7 ppmv NO and ~~110~~0.11 % CO at a pressure of 25 hPa leads to the conversion of OH and RO_2 to HO_2. The amount of NO in the reactor is optimized for complete conversion of CH_3O_2 to HO_2. Similar conversion efficiencies apply to the majority of other atmospheric RO_2 species, including those resulting from OH reactions with simple alkanes, monoalkenes and isoprene (Fuchs et al., 2008). If these are the ~~dominating~~ dominant RO_2 species, then all sampled RO_X (=OH+HO_2+RO_2) radicals are present as HO_2 at the exit of the conversion reactor. In the second chamber (fluorescence cell at a pressure of 4 hPa), HO_2 is converted to OH by increasing the NO mixing ratio to 0.5 %. In contrast to the pure HO_2 detection described above, there is no need to keep the HO_2 conversion efficiency small to avoid simultaneous RO_2 conversion. Therefore, the NO concentration is much higher compared to the NO concentration in the HO_2 detection system. This measurement mode gives the total RO_2 concentration ~~,~~ when the contributions of OH and HO_2 measured in the other two cells are subtracted.

The RO_x system can be operated in a second mode. CO is still added to the converter causing conversion of OH to HO_2, but NO is switched off, so that RO_2 radicals are not converted to HO_2. In the fluorescence cell, however, $RO_2^\#$ species are converted to OH on the same time scale as HO_2 at the high NO concentration. As a result, this operational mode measures HO_2^* (Eq. 4). ~~Subtraction of the~~ The relative detection sensitivities, $\alpha^i_{RO_2}$, of the RO_x system in the HO_2^* measurement

mode were determined in laboratory experiments for RO_2 radicals derived from small alkenes (e.g., ethene, propene). The values were found to be the same as reported by Fuchs et al. (2011) for an HO_2 ~~concentration measured in~~ detection system with high HO_2-to-OH conversion efficiency. Accordingly, other $\alpha^i_{RO_2}$ values were adopted from Fuchs et al. (2011) and Lu et al. (2012) for these experimental conditions.

The concentration measurements of HO_2 (from the HO_2 cell~~then allows~~) and of HO_2^* (from the RO_x system) allow to estimate the total concentration of $RO_2^\#$ ~~radicals~~ (Whalley et al., 2013). ~~A conversion efficiency of $\alpha^\#_{RO_2} = 0.8 \pm 0.2$~~ :

$[RO_2^\#]$ = ($[HO_2^*]$ - $[HO_2]$) / $\alpha^\#_{RO_2}$

Here $\alpha^\#_{RO_2}$ denotes an average, relative detection sensitivity for $RO_2^\#$ species which contribute to HO_2^*. A value of $\alpha^\#_{RO_2}$ = 0.8 ±0.2 is applied here~~to calculate concentrations . The error of this~~ , representing the range of specific $\alpha^i_{RO_2}$ values for the most relevant RO_2 species from alkenes, isoprene, and aromatics. Any error in this average value adds to the uncertainty of the calculated $RO_2^\#$ ~~concentrations~~concentration.

Like for the HO_2 detection system, the presence of NO alone causes background signals of $5.0 \times 10^7\,cm^{-3}$ and $3.5 \times 10^7\,cm^{-3}$ in the operational modes with and without NO addition in the conversion reactor. In addition, NO_3 causes an interference signal, which is equivalent to $1 \times 10^7\,cm^{-3}$ RO_2 per 10 pptv NO_3 (Fuchs et al., 2016a). Measurements were corrected for the NO background signal, but no correction was applied for potential interferences from NO_3, because no NO_3 measurement was available. Model calculated NO_3 concentrations suggest that there was no significant interference from NO_3 for conditions of this campaign.

A bias in the measurement of RO_2 may be caused in polluted air by peroxy radicals, which are produced in the low-pressure converter of the RO_2 instrument by thermal decomposition of peroxy nitric acid (HO_2NO_2), methyl peroxy nitrate ($CH_3O_2NO_2$) and PAN (Fuchs et al., 2008). In the atmosphere, HO_2NO_2 and $CH_3O_2NO_2$ are in a fast thermal equilibrium with HO_2 and CH_3O_2, respectively, together with NO_2. The possible interference scales with NO_2, which was highest during the Wangdu campaign in the morning (median value of 15 ppbv). For this condition, according to model calculations by Fuchs et al. (2008), HO_2NO_2 and $CH_3O_2NO_2$ are expected to produce interferences of +2.6 % and +9 % for the detected HO_2 and CH_3O_2 radicals, respectively. Since HO_2 and CH_3O_2 contributed about 50 % (measured) and 10 % (modelled) to the total RO_x in the morning, the estimated interference for measured RO_2 is only +2 %. The interference from PAN decomposition in the instrument was calculated by Fuchs et al. (2008) to be 0.1 pptv per ppbv of PAN. Since the modelled PAN concentrations for the Wangdu campaign are less than 1 ppbv, no significant interference is expected from this compound. Another bias could be due to the perturbation of the reactor chemistry from high ambient NO concentrations (Fuchs et al., 2008). For the measurements in the RO_x and HO_2^* mode, the corresponding interferences are estimated to be less than +1 % and +3 %, respectively, at 15 ppbv NO.

2.3.5 Calibration and detection limits

The calibration of the LIF instrument is achieved by a radical source that provides equal concentrations of OH and HO_2 radicals by water vapor photolysis at 185 nm described in detail in Holland et al. (2003). The radical concentrations delivered by the source can be calculated from the measured water vapour concentration, the gas flow, and the intensity of the ~~photolysis lamp~~ 185 nm radiation with a 1 σ accuracy of 10 %. ~~The calibration procedure to determine the sensitivity in the different modes~~ Addition of CO or CH_4 to the calibration gas quantitatively converts the OH into HO_2 or CH_3O_2, respectively. These modes are used for the calibration of the HO_x and RO_x channels~~is achieved by conversion of to and~~ , respectively (Fuchs et al., 2008).

During the campaign, calibrations were done approximately every third day. No ~~trend~~ trends with time for any of the sensitivities ~~was~~ were observed. Thus, averaged sensitivities over the entire campaign were applied to calculate radical concentrations. The variability of the measured sensitivities is considered as an additional calibration uncertainty. The ~~reproducibility~~ reproducibilities (1 σ standard deviation) of the ~~sensitivity for the cell was~~ sensitivities were 5 % ~~, and for the cell 5 and~~ for the OH cell and 5 % or 10 % for the ~~high and low conversion efficiencies~~HO_x cell at high or low NO, respectively. The reproducibilities of the sensitivities of the RO_x system were 7 % for the detection mode without NO in the conversion reactor and 12 % for the mode with NO.

The detection limit depends on the sensitivity, ~~on the~~ the laser power, the value of the background signal, and ~~on~~ the integration time (Holland et al., 1995). For nighttime conditions in the absence of sunlight, the detection limits for a signal-to-noise ratio of ~~two~~ one and a measurement time of 30 s, a laser power of 20 mW during this campaign were 0.32×10^6 cm^{-3}, 0.10×10^8 cm^{-3} and 0.11×10^8 cm^{-3} for OH, HO_2 and RO_2, respectively. During daytime, the detection limits for OH and HO_2 are significantly higher, because higher background signals from solar radiation are present. ~~For example~~The typical solar background was about 40 cts/s which is a factor of 20 higher than the typical background signals obtained at night. Therefore, the detection limit ~~for increased~~ was reduced by a factor of ~~5 for typical solar background signals around noon~~5. A shade-ring was installed during the campaign to shield the cell from direct solar radiation. The detection limit of the RO_x system is not different during day- and nighttime, because no significant solar radiation can enter the fluorescence cell through the conversion reactor.

2.4 Model calculations

~~Measured radical concentrations are compared with results from box model calculations~~A box model is used to simulate the concentrations of OH, HO_2, RO_2 and $RO_2^\#$, and the total OH reactivity. The model is based on the compact Regional Atmospheric Chemical Mechanism version 2 (RACM) described in Goliff et al. (2013). This mechanisms includes 17 stable inorganic species, 4 inorganic intermediates, 55 stable organic compounds and 43 intermediate organic compounds. Compounds

that are not explicitly treated in the RACM are lumped into species with similar functional groups. The assignment of organic compounds that were measured during this campaign to species in the RACM is listed in Table 3.

Some modifications were applied to the RACM. The isoprene mechanism was replaced by the more detailed mechanism listed in Table 4. It is based on the Leuven Isoprene Mechanism (LIM) proposed by (Peeters et al., 2009). Here, we use the updated LIM for bulk RO_2 reactions described in Peeters et al. (2014). In addition, the chemistry of the first generation products of the isoprene oxidation, MVK and MACR, and isoprene hydroperoxides (ISHP) are revised. MACR has been shown to regenerate OH via RO_2 isomerization and decomposition (Crounse et al., 2012; Fuchs et al., 2014). OH is also formed by the reaction of RO_2 from MVK with HO_2 with a significant yield (Praske et al., 2015). The products of the reaction of isoprene hydroperoxides formed in the reaction of isoprene RO_2 with HO_2 have been revised by Paulot et al. (2009) showing that epoxides can be formed in an OH neutral reaction. The modified RACM 2 in this work has been compared to the modified RACM-MIM-GK which was used previously for model studies of the HO_x chemistry in China (Lu et al., 2012). In the present study, modelled HO_x concentrations differ no more than 5% between the old and new modified RACM mechanisms. It is also noteworthy that HO_x results of the modified RACM-MIM-GK agreed well with predictions of the more explicit Master Chemical Mechanism v3.2 (Lu et al., 2012).

Model calculations are constrained to measured trace gases, including inorganic species (H_2O, NO, NO_2, O_3, HONO, CO) and organic species (methane and non-methane organic compounds listed in Table 3). Because only the sum of methyl-vinyl-ketone (MVK) and methacrolein (MACR) were measured, a ratio of 0.6:0.4 (Galloway et al., 2011) was used to divide the sum measurement to individual species. In addition, physical parameters like photolysis frequencies, temperature and pressure are constrained to measured values.

For model calculations, the measured time series are synchronized to ~~equidistant~~ 5 min time intervals. This is done either by averaging or by linear interpolation, if the time resolution of the measurement is shorter or longer than 5 min, respectively. Measurements of the two instruments for ozone and CO are combined, in order to fill data gaps.

~~The total~~ Slightly more than 60% of the measured OH reactivity ~~measured in this campaign can be well explained most of the time~~ can be explained by the measured ~~trace gases listed in Table 3.~~ concentrations of CO, NO_x and hydrocarbons during daytime. More than 90% of the OH reactivity can be explained, if also measured oxygenated VOC species are included (Fuchs et al., 2016b). Consequently, there were no large amounts of other relevant OH reactants in the atmosphere which would otherwise have contributed significantly to the measured reactivity. For this reason, long-lived product species which were not measured are constrained to zero in the model in order to avoid unrealistic build-up of additional reactivity. This constraint is consistent with the assumption that most of the measured pollutants were emitted nearby and were not ~~much~~ photochemically aged.

Only aldehydes (ALD) are not set to zero, because they lead to the formation of reservoir species for organic peroxy radicals (peroxy acyl nitrates, PAN and PPN), which are kept as free parameters. In addition, HPALD that is formed in the new isoprene chemistry is not constrained to zero. In order to avoid unrealistic accumulation of ~~these species~~ oxygenated VOC species (mostly aldehydes), an artificial, constant loss is added, which limits their lifetime to 24 hours.

For comparison with experimental ~~data, calculated~~ data, the modelled concentrations of individual RO_2 ~~concentrations shown here only include those~~ species are summed up in two categories which simulate the measured total RO_2 and $RO_2^\#$ concentrations (cf. Section 2.3.4). Modelled RO_2 contains those species that can be detected by the measurement system. The largest ~~fraction~~ class of RO_2 that ~~are~~ is not included in the calculated RO_2 are NO_3-alkene adducts (RACM name OLND), because their reaction with NO does not produce HO_2. The largest concentration of OLND is predicted in the early evening (approximately $1 \times 10^8\,\mathrm{cm}^{-3}$). In contrast, the majority of modelled RO_2 during daytime consists of species which are detected. In the model, the observable RO_2 species contribute with equal weight to the total RO_2, whereas laboratory calibrations of the RO_2 instrument have shown slightly different (less than $\pm 20\,\%$) detection sensitivities for the measured RO_2 species (Fuchs et al., 2008). Modelled $RO_2^\#$ represents a subclass of RO_2 species which are produced in RACM 2 from alkenes-, aromatics- and long chain (> C4) alkanes.

The relatively large uncertainty of the model calculations is a combination of uncertainties in the measurements used as model constraints and reaction rate constants (for details see Lu et al. (2012)). Differences in the measurements of NO (20 %) and HONO (30 %) from different instruments change modelled OH concentrations by only 7 % and 10 %, if measurements from one or the other instrument is taken as constraint. The uncertainties of measurements and modelling need to be taken into account in the comparison. The uncertainty of radical measurement is mainly determined by the 1 σ measurement accuracies (OH:$\pm$11%, HO_2:$\pm$16%, RO_2:$\pm$18%) . A series of tests based on Monte Carlo simulations show that the uncertainty of the model calculations is approximately 40%.

3 Results and Discussion

3.1 OH chemical modulation tests

Chemical modulation tests as described in Section 2.3.2 were conducted on 29 June (afternoon), 30 June (morning and afternoon), 2 July (afternoon) and 5 July (afternoon and evening). The ~~signal measured when no scavenger is added (S_{N2}) contains contributions from ambient , the interference from ozone, and possibly unknown interferences (Eq. 1).~~ time periods of the tests and the atmospheric chemical conditions are given in Table 2. All test results are shown in Fig. 2~~shows results from all tests performed during this campaign.~~ , where the measured OH signal S_{N2} (without OH scavenger) is compared to the sum of the ~~known ozone interference (S_{O3}) and the concentration of~~ expected signals from ambient OH (S_{OH}) ~~, which is calculated according to Eq. 3 from the measurements with~~

~~(S_{prop})and without (S_{N2}) scavenger. The error bars~~ and the known O_3 interference (S_{O3}). Statistical error bars shown in Fig. 2 are ~~calculated from the measurement precision of the fluorescence signals~~ derived from 1 σ measurement precisions of S_{N2} and S_{prop}. In addition, the sum of S_{OH} and S_{O3} ~~could be affected by~~ has a systematic error (not shown in Fig. 2), which is dominated by the uncertainty ($\pm$ 10%, 1 σ~~uncertainty of the titration efficiency (10)~~ of the removal efficiency (ϵ) needed to calculate S_{OH} ~~. This systematic error would result in a change of 0.3 to 0.5 $\times$ 10^6in S_{OH} (Eq.~~ (see Eq.3).

The ~~total~~ signals S_{N2} (Fig. 2) are on average higher than the corresponding ~~sums~~ sum of S_{OH} and S_{O3}. ~~Although the differences are similar to the combined statistical errors of the measurements, they appear to be systematic. Differences vary between 0.5×10^6 and 1×10^6~~The differences vary within the range between 0.53×10^6 and 1.2×10^6 cm^{-3} (~~average: $(0.85 \pm 0.3) \times 10^6$) , which is on the order of 10of the total~~ Table 2) and could be the result of an unknown OH ~~signal during daytime , when no scavenger is applied~~interference or of the systematic experimental error in the determination of S_{OH}+S_{O3}. The differences are ~~within the the 2σ systematic error~~ subject not only to statistical errors, which shown as the error bars in Fig. 2 but also to the uncertainty arising from the calculation of S_{OH} ~~. Thus, the differences~~ (Eq. 3). Among all, the uncertainty in the removal efficiency (ϵ) has the largest impact on the derived differences. The differences between S_{N2} and S_{OH}+S_{O3} ~~are~~ and their uncertainty are listed in Table 2. No correlation of differences with time of day or with the chemical conditions is observed. The differences fall quantitatively into the 2 σ range of the accuracy of S_{OH}+S_{O3} and are therefore at the limit of detection of the experimental ~~setup~~ set-up used in the campaign. ~~Quantitatively similar differences (up to 1×10^6) were obtained in the chemical modulation tests on other days.~~

~~The observed differences could be the result of a systematic error in the determination of S_{OH} or could be caused by an unknown~~ Because the test results are not sufficiently accurate to draw firm conclusions about an unknown interference, the OH ~~interference.~~ data in this work was not corrected for a potential interference. Instead, the differences found in Fig. 2 are treated as an additional uncertainty of the OH measurements presented in this paper.

In case of an interference, it would be a small fraction of the ~~total~~ measured OH during daytime. The measured nighttime OH, however, would be much stronger affected. Because the existence of an unknown OH interference cannot be ~~ruled out by the test results in this campaign~~strictly ruled out, the interpretation of the radical chemistry will therefore concentrate on daytime conditions. More precise and accurate chemical modulation tests with an improved experimental set-up are needed in future field campaigns.

3.2 Meteorological and chemical conditions

Meteorological conditions were characterized by high temperatures of up to 37 °C and high humidity. The wind velocity was usually below 2 m/s. Back trajectory analysis using the NOAA HYSPLIT

(Hybrid Single Particle Lagrangian Integrated Trajectory Model) model (Stein et al., 2015) showed that air masses were ~~usually~~ often transported from south or east where large city clusters are located. Solar radiation was strong during this campaign with few exceptions of hazy or cloudy days (15 to 19, 25 June and 1 to 4 July, Fig. 3).

Afternoon CO mixing ratios increased during several periods indicating accumulation of anthropogenic emissions on a regional scale. They are separated by sudden drops during rain events on 19 June and 4 July and on 27 and 28 June when clean air was transported from the north.

During the first half of the campaign, burning of agricultural waste after harvesting ~~on~~ in surrounding fields was observed. This was confirmed by high acetonitrile mixing ratios (>1 ppbv) from 12 to 19 June. Biomass burning was accompanied by a reduced visibility and an increase in aerosol mass concentrations ($PM_{2.5}$) with maximum values of 150 $\mu g\,cm^{-3}$ on 16 June (campaign average value: 70 $\mu g\,cm^{-3}$).

Time series of O_3 and NO_2 ~~showed often similar trends like~~ often showed trends similar to CO, but were also strongly influenced by photochemistry. Maximum daily ozone mixing ratios ranged between 100 and 140 ppbv depending on the strength of radiation. Because solar radiation was attenuated between 14 and 19 June during the first pollution episode, O_3 peaked already on 14 June. O_3 was ~~often~~ sometimes completely titrated by ~~nitrogen monoxide~~ nitric oxide during night.

Isoprene mixing ratios exhibited a typical diurnal profile with maximum values between a few hundred pptv and nearly 4 ppbv in the afternoon. These values indicate that chemical conditions were also influenced by presumably local biogenic emissions.

3.3 Time series of measurements and model calculations

The time series of measured and modelled OH, HO_2, RO_2 and k_{OH} are shown in Fig. 4. Distinct diurnal profiles are observed for all radical species. The daily maxima of OH, HO_2 and RO_2 appeared around noontime and concentrations ranged between (5-15)$\times 10^6$ cm^{-3}, (3-14)$\times 10^8$ cm^{-3} and (3-15)$\times 10^8$ cm^{-3}, respectively. On 18, 19 and 25 June and from 1 to 3 July, radical concentrations were ~~small~~ low due to attenuated solar radiation. On 28 June, OH ~~raised~~ increased to exceptionally high concentrations of up to 3×10^7 cm^{-3} for a short period of time, which was accompanied by an increase of the HONO mixing ratio to 2 ppbv, ~~so that~~ leading to enhanced OH production ~~was enhanced by~~ from HONO photolysis. During this time, farmland next to the measurement site was treated with water and artificial nitrogen-containing fertilizer, which may have caused large, local HONO emissions.

In general, the model reproduces well the measured time series of OH, HO_2 and RO_2. Differences between modelled and measured radical concentrations are generally smaller than the combined 1 σ uncertainties of radical measurements (10 %) and model calculations (40 %). ~~The relatively large uncertainty of the model calculations is a combination of uncertainties in the measurements used as model constraints and reaction rate constants (for details see). Differences in the measurements of~~

~~and from different instruments (20for both species) change modelled concentrations by only 7and 5, if measurements from one or the other instrument is taken as constraint.~~

A closer look at the modelled and measured radical concentrations reveals some systematic trends. Modelled OH concentrations tend to be smaller than measurements during afternoon hours and modelled RO_2 concentrations tend to be lower in the early morning and higher in the evening than corresponding RO_2 measurements. In contrast, differences between modelled and measured HO_2 concentrations are small at all times. Because of the similarity of the model-measurement agreement for different days, further analysis of daytime radical concentrations will be done on the basis of median diurnal profiles (Section 3.4).

The OH observed at night are mostly above the limit of detection ($3\times10^5\,\mathrm{cm}^{-3}$) with concentrations around $5\times10^5\,\mathrm{cm}^{-3}$, whereas the model predicts concentrations below the limit of detection. In a few nights, the measured OH is even higher (e.g., 1-3 $\times10^6\,\mathrm{cm}^{-3}$ on 13 June). The reason why the measured OH values are significantly ~~above~~ higher than the model prediction is not clear. It could be caused by missing chemistry in the model or vertical gradients in the nocturnal boundary layer as discussed in Lu et al. (2013). Furthermore, we cannot exclude an unknown interference of the same magnitude. The known interference from NO_3 is probably not sufficient as an explanation (Fuchs et al., 2016a)~~. Using concentrations from the model (average. 10)~~, the expected interference would be ~~less than~~ 1×10^6 $\times10^5\,\mathrm{cm}^{-3}$ for this campaign~~.~~, 5 times less than the averaged nighttime OH measurement. Thus, if interferences played a role, they would probably have a different origin.

The time series of measured OH reactivity shows a change on 20 June (Fig. 4). During the first two weeks, diurnal profiles of k_{OH} are more structured and show higher values with maximum values of up to $40\,\mathrm{s}^{-1}$ compared to values after 20 June, when k_{OH} is only around $10\,\mathrm{s}^{-1}$ in the afternoon and exhibits a less distinct diurnal profile. The first period coincides with the accumulation of pollutants like CO, nitrogen oxides and particles (Fig. 3). In addition, harvesting and biomass burning activities caused local emissions of OH reactants, which may explain the short-term increases in OH reactivity during this period, especially during nighttime, when fresh emissions are released into the shallow nocturnal boundary layer and highest OH reactivity is observed. After 20 June, biomass activities close to the measurement place were less often observed and heavy rainfall cleaned the air.

In the first period of the campaign, the model often underpredicts the measured OH reactivity, especially at night. This is likely caused by unmeasured atmospheric compounds from local emission sources like biomass burning. In the second period, the modelled and measured reactivities agree well at day and night for most of the time.

3.4 Median diurnal profiles

Differences between measurements and model calculations are further analyzed ~~as~~ using median diurnal profiles with a time resolution of one hour (Fig. 5). ~~Only data is included ,~~ Data are only included when measurements of all key species used as model constraints and radical measurements

are available at the same time. Therefore, four days are excluded from the analysis from the entire data set. On 13 June, data gaps are larger than 6 hours for nearly all instruments. No measurements of VOCs are available on 14 June, no measurements of photolysis frequencies on 22 June and no radical measurements on 4 July. ~~The number of data points in the median profiles from the first period of the campaign before 20 June is less than the number of data points from the period~~ As described in Section 3.3, chemical conditions were slightly different before and after 20 June. ~~On the one hand the length of the first period is shorter and on the other hand there are more data gaps in the beginning of the campaign~~We found similar results of model-measurement comparisons for radicals from the two periods for daytime conditions. Therefore, ~~only one third of the data points included in the median diurnal profile originates from days before 20 June~~the following interpretation and discussion will focus on campaign averaged diurnal profiles. Chemical conditions of data included in the median profile are summarized in Table 5 and median diurnal profiles of important photochemical parameters are shown in Fig. 6.

~~Median measured~~ The median diurnal profiles of the measured and modelled OH concentrations ~~are~~ agree within their errors of 10 % (1 σ) and 40 %, respectively, from sunrise to mid afternoon. When the median NO mixing ratio (cf. Fig. 6) drops gradually from 0.3 ppbv to 0.1 ppbv in the afternoon, a systematic difference evolves, with measured OH concentrations being approximately 1×10^6 cm^{-3} ~~larger than model calculations in the afternoon. At the same time, the median~~ higher than the model calculations. The discrepancy is of similar magnitude as the averaged unexplained OH determined in the chemical modulation experiments (Table 2). Thus, the overall agreement for OH would improve, if the unaccounted signal was fully considered as an OH measurement interference. However, the underestimation of OH would persist for low NO ~~mixing ratio drops from 0.3 to 0.1~~conditions if a potential unaccounted signal was subtracted. When NO concentrations are less than 100 ~~(Fig. 6).~~ pptv, the observed-to-modelled OH ratio would be reduced from 1.9 to 1.5, indicating that an OH source would still be missing for low NO conditions. Although newly proposed isoprene mechanisms have the potential to enhance the OH regeneration for low NO_x condition, they only have a small effect on modelled OH concentration ~~in this study due to the moderate (> 0.1~~at the conditions of this study with NO concentrations higher than 0.1 ppbv ~~) and isoprene (typically less than 2~~and isoprene concentrations lower than 2 ppbv~~) concentrations.~~ .

In general, HO_2 concentrations are ~~well~~ reproduced by the model during daytime ~~. The discrepancy~~ within the combined uncertainties of measurements and model calculations. Nevertheless, the model has a tendency to over-predict HO_2 in the afternoon. If we constrain the model to the observed HO_2 concentrations, the observed-to-modelled OH ratio increases from 1.6 to 1.8 for daytime averaged conditions (04:30–20:00). RO_2 and $RO_2^\#$ are significantly underestimated during the morning hours (06:00–10:00) with an observed-to-modelled ratio of 3 to 5, which is larger than the combined uncertainty (a factor of 2). Reasons for discrepancies between measured and modelled RO_2 ~~is analyzed in detail in Section 3.7~~are further analyzed in Section 3.6.

Measured k_{OH} is high during night, peaks in the morning ($22\,s^{-1}$) and decreases to about $11\,s^{-1}$ in the afternoon. Modelled k_{OH} shows a relative flat diurnal profile (average over the day is $14\,s^{-1}$). Whereas good agreement with measurements is achieved during daytime, measured reactivity is higher during nighttime especially during the first part of the campaign. This is likely caused by unmeasured emitted OH reactants. A sensitivity model run, in which product species are not constrained to zero as in this model run, does not give significantly different OH reactivity in the night. A more detailed analysis of the OH reactivity in this campaign ~~will be published in a separate paper~~ is presented in our companion paper by Fuchs et al. (2016b).

3.5 Correlation of OH with $j(O^1D)$

Strong correlation has been found between $j(O^1D)$ and OH radical concentrations for many field campaigns in different environments from marine to continental locations (Ehhalt and Rohrer, 2000; Brauers et al., 2001; Berresheim et al., 2003; Rohrer and Berresheim, 2006; Lu et al., 2012, 2013). A strong linear correlation is also observed for data from this campaign (Fig. 7). A linear fit between measured OH concentrations and measured photolysis frequencies yields a slope of $4.5\times10^{11}\,s\,cm^{-3}$. This value is similar to values that were derived in previous field campaigns in China in 2006 in the Pearl River Delta and Yufa (Lu et al., 2012, 2013).

The intercept of the linear fit for the campaign in Wangdu is $1.0\times10^{6}\,cm^{-3}$, which is smaller than intercepts obtained for the data set from the campaigns in the Pearl River Delta ($2.4\times10^{6}\,cm^{-3}$, Lu et al. (2012)) and Yufa ($1.6\times10^{6}\,cm^{-3}$, Lu et al. (2013)). The intercept gives an estimate of the importance of radical sources when the production of O^1D from ozone is small. This includes non-photolytic sources (e.g. ozonolysis of VOCs) and photolytic processes in the early morning before $j(O^1D)$ starts to rise (Fig. 10).

Modelled OH also shows a strong dependence on $j(O^1D)$ with a slightly smaller intercept compared to the fit result ~~taking~~ using the measurements.

3.6 Model-measurement comparison of RO_2

Figure 8 shows ~~the speciation of~~ median diurnal profiles of measured RO_2 ~~radicals in the model. Measurements give only the total concentration of species that are efficiently converted to by the reaction with on either a very short time scale of milliseconds (~~and $RO_2^\#$ ~~) or on a time scale of one second (~~together with modelled concentrations of speciated RO_2 ~~) in the measurement system. The median diurnal profiles for both classes of measured~~ radicals. The observed profiles of RO_2 ~~are similar, but~~ and $RO_2^\#$ ~~dominates in the early morning hours until 09~~have similar shapes with a maximum around 14:00. ~~Its relative contribution becomes less in the evening. This is also predicted by the model.~~ In the morning ~~, however, the concentrations~~ hours, RO_2 is dominated by $RO_2^\#$, whereas $RO_2^\#$ plays only a minor role in the late afternoon and during night. The model reproduces the general behaviour of RO_2 and $RO_2^\#$ ~~species predicted by the model are 1 to 2×10^{8}~~well,

with very good agreement in the afternoon. However, in the morning the model underestimates RO_2 systematically by a significant amount of (1-2)$\times 10^8$ cm^{-3} ~~smaller than measurements. Good agreement is achieved for total and~~ . This is mainly caused by an underestimation of $RO_2^\#$ ~~in the late afternoon. In the~~ . After sunset in the first half of the night, ~~modelled total~~ the model overestimates RO_2 ~~is larger than measured . This mainly concerns speciesthat are not detected as~~ . This discrepancy is apparently related to organic peroxy radicals, which do not belong to $RO_2^\#$.

In the group of modelled $RO_2^\#$ species, isoprene peroxy radicals (ISOP) make the largest contribution during daytime. Other modelled $RO_2^\#$ include peroxy radicals from alkenes, aromatics, long-chain ($> C_4$) hydrocarbons, and MVK and MACR. Among the RO_2 radicals which do not belong into the $RO_2^\#$ group, peroxy radicals of short-chain ($<C_5$) alkanes are dominating: methyl peroxy radicals (MO_2), ethyl peroxy radicals (ETHP), and peroxy radicals from HC_3P (e.g., propane). Acetyl peroxy radicals (ACO_3+RCO_3) are also a substantial fraction of RO_2.

The strong underprediction of the observed RO_2 by more than a factor of ~~four~~ 4 in the morning cannot be explained by the measurement ~~error of (see Section~~ errors and interferences discussed in Sections 2.3.4 and 2.3.5~~) and points to a model deficiency. Differences between measured and modelled~~ . In order to explore potential reasons for this underprediction, several sensitivity tests were performed. First, the impact of a faster OH to RO_2 ~~in the morning are mainly related to higher measured . This could be a hint that the model does not adequately describe~~ conversion by an increased amount of VOC was tested (model sensitivity run S1). Second, an additional primary source of RO_2 ~~chemistry from alkenes or larger organic compounds, because species are formed from their chemical transformation~~was introduced into the chemical mechanism (S2). Third, the possibility of a slower removal rate of RO_2 was tested (S3).

~~Model sensitivity runs show that a primary~~ The first possibility (S1) is supported by the observation that the modelled OH reactivity in the base run (S0) is smaller than the measured OH reactivity in the morning until about 09:00. If this missing reactivity is caused by unmeasured VOCs, the true RO_2 ~~source of 2~~ production from reactions of VOCs with OH would be larger than the modelled one. To fill this gap, the total concentration of the measured VOCs is increased to match the measured k_{OH} in the time window from 06:00 to ~~4~~09:00. The relative partitioning of the VOCs is not changed. The model run (S1) with the upscaled VOC reactivity resolves part of the RO_2 discrepancy until 09:00 (Fig. 5). The observed-to-modelled RO_2 ratio is improved from 2.8 to 1.7 without affecting the good model-measurement agreement for OH and HO_2. Further sensitivity tests shows that the modelled RO_2 is not sensitive to the speciation of the additional VOC reactivity, since the required change of k_{OH} is relatively small (< 20 ~~would be required, in order to fill the gap in~~ %). Because no missing OH reactivity is found after 09:00, the gap between measured and observed RO_2 ~~in the morning (~~cannot be explained by unmeasured VOCs later.

In sensitivity test S2, an additional primary source of RO_2 (OLTP) from terminal alkenes is introduced into the model. A source strength of 2 ppbv h^{-1} from 06:00 to ~~12:~~12:00 ~~). In this case,~~

however, concentrations would increase to values that are significantly higher than measurements due to the efficient conversion from would be required to achieve a good model-measurement agreement (within 20 %) for both RO_2 to and $RO_2^{\#}$. The modelled OH at high concentrations at this time of the day. Therefore, an unknown primary source alone can be excluded as reason for elevated and HO_2 concentrations also increase and are slightly overpredicted by about 10 % and 20 %, respectively. This can still be considered as agreement within the error of measurements and model calculations. After 12:00 the difference between modelled and measured RO_2 becomes smaller than 15 %, within the range of the accuracy of RO_2 measurements.

One possible A candidate for an additional primary RO_2 source is the would be reactions of VOCs with chlorine atoms, which are produced by photolysis of nitryl chloride ($ClNO_2$) . High concentrations of (Osthoff et al., 2008). $ClNO_2$ were observed in Wangdu from 20 June to 8 July in the early morning. The concentrations reached maximum values of 0.5and decayed after 08:00 . Nitryl chloride is formed from the heterogeneous reactions of Cl^- ions with nitrogen pentoxide (N_2O_5) and accumulates during nighttime. Its photolysis is a source of chlorine atoms in the morning, which After sunrise, $ClNO_2$ is expected to be completely photolysed within a few hours. The resulting Cl atoms can abstract H-atoms from hydrocarbons and directly saturated hydrocarbons or can add to alkenes. The alkyl radicals produce RO_2 . A sensitivity model run including chlorine chemistry described in gives a maximum production rate of 0.2which in case of alkene-derived peroxy radicals carry a chlorine atom. $ClNO_2$ was measured by a CIMS instrument at the Wangdu field site from 20 June to 8 July (Tham et al., 2016). The concentrations increased during night and reached on average high values of 0.5 ppbv at 08:00, followed by a decay to zero until 11:00. In this their study, Tham et al. (2016) investigated the role of $ClNO_2$ photolysis on the photochemical formation of RO_2 and ozone during the Wangdu campaign. They used the MCM v3.3 with an additional chlorine chemistry module by Xue et al. (2015). We repeated the study by adding the same chlorine chemistry to our modified RACM 2 mechanism and found the same additional formation rates of RO_2 and O_3 as reported by Tham et al. (2016). In our model run, a $ClNO_2$ source is assumed that leads to a linear increase of $ClNO_2$ concentrations during nighttime to a maximum value of 0.5 ppbv during nighttime and early morning until at 08:00 on each every day. After 08:00, the modelled source is turned offand all . $ClNO_2$ is photolyzed (photolysis rates are starts to photolyze after 06:00 with a photolysis frequency that was calculated from the measured actinic flux). The fast reaction of . A maximum Cl with VOCs produces production rate of 0.2 ppbv h^{-1} is obtained at 08:00, yielding an additional RO_2 . However, this production with a similar rate. Compared to the additional RO_2 source is not large enough to resolve the discrepancy between measured and modelled production rate required for model run S2, this is an order of magnitude too small. The mechanism is also not capable to sustain the additional RO_2 production during the whole morning, because $ClNO_2$ is photolytically depleted within 2-3 hours. Even if the modelled source strength is increased to match the highest $ClNO_2$ mixing ratios ratio of 2 ppbv observed at 08:00 on 21 June ,

~~additional primary production of from oxidation is only~~ (Tham et al., 2016), the additional primary RO_2 production of 0.5 ppbv h^{-1} ~~on average, an order of magnitude less than required to explain observed~~ is still not sufficient. Thus, although $ClNO_2$ photolysis was a relevant radical source, it alone cannot explain the missing source of RO_2 ~~concentrations.~~ radicals in the morning.

~~The largest relative difference between modelled and measured is observed in the early morningbetween 06:00 and 09:00. This is accompanied by high measured reactivity which is not reproduced by the model. Therefore, also the production~~ A further model test (S3) was performed, in which the rate of RO_2 ~~could be underestimated by the model. In a sensitivity model run, the gap in the reactivity is filled by scaling VOC concentrations to match measurements. In this case, the gap between measured and modelled~~ removal was artificially reduced by decreasing the reaction rate constants between RO_2 ~~concentrations can be partly closed before 09:00 without affecting the good agreement of and indicating that reactants that are oxidized in the early morningare missing in the model.~~ and NO. Such a reduction would be justified, if the rate constant for RO_2+NO would be systematically too large in the model. Another reason could be a systematic measurement error of the NO concentration, or a segregation effect between RO_2 and NO due to inhomogeneous mixing in case of local NO emissions. In order to account for the discrepancy between modelled and measured RO_2 in the morning, the loss rate would have to be changed by a factor of 4, which seems unrealistically high for each of the above mentioned possibilities. Also, there is no plausible reason why a systematically wrong rate constant or NO measurement error would appear only during morning hours.

The overprediction of RO_2 by the model in the evening could be related to the differences in the chemistry of RO_2 during day and night. ~~The~~ Because VOC oxidation by NO_3 is a major contribution to RO_2 production at night, the inability of the model to predict RO_2 ~~in the~~ at night could be ~~partly caused by strong fluctuations around the~~ due to the difficulties to reproduce NO_3 in a box model.One complication is that the NO concentrations are close to the limit of detection of the instrument ~~of~~ (60 pptv~~in the measured~~), which leads to a large variation in NO_3 concentrations in the model because of the fast reaction between NO_3 and NO~~concentrations used as constraint~~. Assuming no RO_2 production from NO_3 chemistry would bring measured and modelled RO_2 into agreement.

3.7 NO dependence of the radical concentrations

NO_x plays a crucial role in RO_x chemistry due to radical propagation via peroxy radical reactions with NO and radical loss by the reaction of OH with NO_2 (Ehhalt, 1999). Because of these two counteracting processes, maximum OH concentrations are expected at NO_x mixing ratios ~~of a few at otherwise constant conditions~~ around 1 ppbv when other conditions controlling OH are constant.

Figure 9 shows ~~measured and model radical concentrations depending~~ the dependence of the measured and modelled radical concentrations on the NO mixing ratio. In order to ~~reduce~~ remove the influence of the OH production strength by photolysis seen in Fig. 7, OH concentrations are

normalized to $j(O^1D)$ measurements. In addition, only daytime values at NO concentrations above the detection limit of the NO instrument are included in this analysis ($j(O^1D) > 0.5 \times 10^5\ s^{-1}$, NO> 60 pptv). Measured OH concentrations appear to be nearly independent on the NO concentration after normalization to $j(O^1D)$. Median values of measurements are almost constant ~~with 7×10^6~~ for NO mixing ratios of up to 5 ppbv. This behavior is only expected for NO mixing ratios between 0.3 and 3 ppbv as indicated by the base model calculations. Median modelled OH concentrations are nearly half of the median measured values ~~(5×10^6)~~ at NO mixing ratios below 100 pptv. This discrepancy is also seen in the median diurnal profile of measured and modelled OH (Fig. 5), but it is less pronounced, because NO mixing ratios only dropped below 0.3 ppbv only for certain times and not on every day.

~~A similar~~ OH behavior ~~as the one~~ similar to that shown in Fig. 9 has been reported for PRD and Yufa (Lu et al., 2012, 2013) and also for other field campaigns selected for conditions with high OH reactivity (> $10\ s^{-1}$) (Rohrer et al., 2014). In contrast, campaigns in relatively clean air have shown a decreasing trend of OH at low NO concentrations as expected from the reduced radical recycling efficiency (Holland et al., 2003).

Measurements and model calculations show similar decreasing trends for both, HO_2 and RO_2, with increasing NO concentrations. This is expected, because the lifetime of these radical species are mainly limited by their reactions with NO. As also seen in the median diurnal profiles (Fig. 5), modelled and measured HO_2 concentrations agree within 20 % over the entire range of NO concentrations, whereas the measured RO_2 decreases less than the modelled RO_2 ~~when~~ as NO increases. At 3 ppbv NO, the modelled RO_2 concentrations ~~become~~ is less than $1 \times 10^8\ cm^{-3}$, whereas the median measured RO_2 ~~concentration remains at~~ is $3.5 \times 10^8\ cm^{-3}$. As a consequence, the measured peroxy radicals yield higher calculated net ozone production rates than predicted by the model (see Section 3.8).

Two sensitivity model runs were done. In the first sensitivity run, the model did not include the updated isoprene mechanism, which is part of the base model run. The overall impact of the new isoprene chemistry is rather small, the maximum increase in the median OH and HO_2 concentrations due to the additional OH recycling is less than $1 \times 10^6\ cm^{-3}$ and $1 \times 10^8\ cm^{-3}$, respectively, at NO mixing ratios ~~smaller~~ lower than 0.1 ppbv. This is ~~smaller~~ lower than the variability of measurements.

In the second sensitivity run, radical recycling was enhanced by introducing an artificial species X that behaves like NO, but does not produce ozone (Fig. 9). This has been successfully applied to describe unexplained high OH concentration in other campaigns (Rohrer et al., 2014) including our previous observations in China (Hofzumahaus et al., 2009; Lu et al., 2012, 2013). Similar to the observations in the previous campaigns, a constant mixing ratio of X would bring modelled and measured OH into agreement for the entire range of NO concentrations (Fig. 9). Here, the

concentration of X needs to be equivalent to 100 pptv NO. Modelled HO_2 and RO_2 concentrations do not change much, if this mechanism is applied.

OH concentrations in this campaign are better predicted by the base model compared to our previous field campaigns that were conducted in China. In all three campaigns, median diurnal profiles of measured and modelled OH agree in the morning, but measured median OH starts to be increasingly higher than modelled OH after noontime. In this campaign, the difference is a factor of 1.4 at 16:00 and a factor of two at sunset (~~18~~20:00). Differences are within the $2\,\sigma$ uncertainty of measurements for most of the time. In contrast, the difference was a factor of 2.6 to 4.5 in previous campaigns for higher OH reactivity conditions. Consequently, also the amount of additional recycling that is required to bring modelled and measured OH into agreement is less in this campaign (100 pptv NO equivalent) compared to Yufa (400 pptv) and PRD (800 pptv) in 2006. The major differences between this campaign and the ~~othres~~ others are: (1) OH concentrations in this campaign are smaller. (2) NO mixing ratios (100 pptv) were lower in previous campaigns, reducing the OH recycling efficiency from the reaction of peroxy radicals with NO. (3) Measured OH reactivity is around $12\,s^{-1}$ in this campaign, but was at least 50 % larger in the other campaigns. ~~This is also larger than the modelled reactivity in this campaign.~~

3.8 Ozone production rate

Peroxy radical measurements allow ~~to calculate~~ the calculation of net ozone production (Mihelcic et al., 2003). The photolysis of NO_2 produces O_3 and NO. Because O_3 can also be consumed in the back-reaction of NO to NO_2, net ozone production is only achieved, if the reformation of NO_2 does not involve O_3. This is the case, if peroxy radicals (HO_2 and RO_2) react with NO. Therefore, net ozone production can be calculated from the reaction rate of peroxy radicals with NO using measured and modelled peroxy radical concentrations (Fig. 5). Production ($P(O_3)_{net}$) is reduced by the loss of NO_2 via its reaction with OH and further losses of ozone ($L(O_3)$) ~~, which includes the loss via~~ by photolysis and reactions with OH, HO_2 and alkenes:

$$\begin{aligned} P(O_3)_{net} &= k_{HO_2+NO}[HO_2][NO] + \sum(k^i_{RO_2+NO}[RO^i_2][NO]) \\ &\quad - k_{OH+NO_2}[OH][NO_2] - L(O_3) \qquad (5) \\ L(O_3) &= \left(\theta\, j(O^1D) + k_{OH+O_3}[OH] + k_{HO_2+O_3}[HO_2]\right)[O_3] \\ &\quad + \left(\sum(k^i_{alkene+O_3}[alkene^i])\right)[O_3] \qquad (6) \end{aligned}$$

θ is the fraction of O^1D from ozone photolysis that reacts with water vapor.

The calculation of the net ozone production from ~~measurements~~ the measured concentration of total RO_2 is complicated by differences in the reaction rate constants of NO with different RO_2 species. An effective rate constant is ~~used for the reaction of the total with . The effective rate constant is~~ determined from the rate constants of the different RO_2 species in RACM ~~and~~ 2 weighted by their relative abundance calculated by the model for each instant of time. The ~~derived~~ effective

rate constant increases in the morning and reaches a maximum $8.5\times10^{-12}\,cm^3\,s^{-1}$ in the afternoon and decreases to a value of $6.5\times10^{-12}\,cm^3\,s^{-1}$ after dusk. For comparison, the rate constant for the reaction of CH_3O_2 with NO is $7.5\times10^{-12}\,cm^3\,s^{-1}$. A systematic underestimation of the calculated ozone production rate may arise from RO_2 species, which react with NO and form NO_2 ~~but no~~ , but do no produce HO_2 ~~as products~~. Such RO_2 species would possibly contribute to the ozone formation, but are not detected in our instrument. As explained in Section 2.4, this behavior is found in the Wangdu campaign for peroxy radicals which are formed by reactions of alkenes with NO_3. However, because NO_3 is easily photolyzed, these particular peroxy radicals ~~play no~~ do not play a role during daytime and do not contribute to photochemical ozone production.

Net ozone production has a distinct diurnal profile that peaks in the morning (Fig. 5). The peak value of ~~17~~19 ppbv h^{-1} (median) derived ~~only~~ from measurements is higher than that calculated in the model (~~11~~14 ppbv h^{-1}) and shifted to earlier times (Fig. 5). The variability of this peak value is much larger than seen in the model with values up to several ten ppbv h^{-1}. ~~Differences in the net ozone production~~

If the diurnal ozone production rates are integrated for daytime (04:30 - 20:00), the model yields about 20 ppbv O_3 less than the experimental value of 110 ppbv derived from the ~~model or radical measurementsstem mainly from~~ radical measurements. The difference between observed and modelled ozone production is mainly caused by the underestimation of the modelled RO_2 ~~radical concentrations~~ concentration in the morning.

~~radical may have been an additional source of~~ As discussed in Section 3.6, two generic mechanisms may partly explain the discrepancy. One possibility are unmeasured VOCs, which would explain the model underestimation of the OH reactivity in the morning and would increase RO_2 ~~. From model sensitivity tests~~ by their reactions with OH. Model run S1 with adjusted VOCs shows a slightly improved agreement of the modelled and measured ozone production rates (Fig. 5), but enhances the daily integrated ozone production only by 4 ppbv. The other possibility is an additional primary RO_2 source of 2 ppbv h^{-1}, which is considered in model run S2. It would enhance the daily integrated ozone production by 30 ppbv, which is on the order of magnitude of the $P(O_3)$ underestimation.

As also mentioned in Section 3.6~~with~~ , one possibility for an additional primary RO_2 source is the reaction of VOCs with chlorine atoms from $ClNO_2$ photolysis, which is not considered in RACM 2. With a maximum $ClNO_2$ concentration of 0.5 ppbv ~~, an integral ozone production rate in the morning,~~ an additional daily integrated ozone production of about 2 ppbv is calculated~~during daytime (06:00–18:00). This additional ozone production is small compared to the discrepancy of 20between the accumulated modelled ozone production and calculations from radical measurements. Although the initiated~~ . It should be noted that RO_2 ~~could have different impacts on the ozone generation than assumed in the model, the additional ozone production from chlorine initiated reactionsis most likely not sufficiently large to explain the difference to calculations using measured peroxy radical concentrations.~~

If the discrepancy between measured and modelled k_{OH} is reduced, the modelled ozone production rate better agrees in the morning. This is seen in a model sensitivity run, for which VOC concentrations are scaled to match observed reactivity. Modelled radical species, which are produced by additional reactions of chlorine atoms with alkenes, may behave kinetically different than RO_2 concentrations increase before 09:00 in this case, but only enhance the daily integral ozone productionby 3radicals from OH reactions. In the chlorine chemistry module that we adopted from Xue et al. (2015), Cl-substituted RO_2 radicals have the same rate constants like OH-substituted RO_2 radicals, because kinetic data are missing for Cl-substituted compounds. It is, however, unlikely that this simplification has a strong influence on the calculated net ozone production.

During the first period of the campaign (8 June to 14 June) daily maximum ozone mixing ratios increased from 50 to 150 ppbv (Fig. 3). However, the connection between the photochemical ozone production rate and ozone concentrations measured over several days at a distinct location is complicated. Additional ozone loss processes need to be taken into account, for example deposition and indirect loss via reactive nitrogen chemistry during the night (NO_3 and N_2O_5) that are not included in Eq. 5 and 6. Furthermore, the effect of high ozone production in the morning on midday ozone mixing ratios is reduced due to the dilution by the rise increase of the boundary layer height. Also regional transportation of ozone can be of importance, if the spatial distribution of ozone production and/or loss processes is inhomogeneous. The cumulative ozone production observed during the first period of the campaign is approximately 700 ppbv. This high total ozone production indicates that most of the locally produced ozone could be transported to downwind regionswas removed by transport or deposition.

Previous Other HO_x field studies have also found that models underpredict the underpredicted the observed ozone production rate . Calculations from in urban atmospheres (Martinez et al., 2003; Ren et al., 2003; Kanaya et al., 2008; Mao et al., 2010; Kanaya et al., 2012; Ren et al., 2013; Brune et al., 2016; Griffith et al., 2016). In these studies, the observed production rates were determined from measured HO_2 radical measurements resulted in higher ozone production rates (up to a factor of ten) in the early morning concentrations only, without the contribution of RO_2 for which measurements were not available. In general, the ozone production from HO_2 was underpredicted by chemical models at NO concentrations higher than a few mixing ratios greater than 1 ppbvin campaigns in urban and forested environments . The high , reaching a factor of about 10 between 10 ppbv and 100 ppbv NO. In campaigns before 2011, unrecognized interferences from $RO_2^\#$ species may have contributed to the deviation between measurement and model results. The interference, however, is expected to account for less than a factor of 2, because HO_2 in previous campaigns may be partly explained by and RO_2 that caused unrecognized interferences in detection . The shape of the diurnal profile with the high unexplained ozone production rate in the morning, however, is not expected to change much , if also concentrations are approximately equal (Cantrell et al., 2003; Mihelcic et al., 2003) and $RO_2^\#$ is only a fraction of the total RO_2 is taken into account , because a good

~~correlation between~~ (e.g., Fig. 5). This expectation has been confirmed in recent studies, where the interference was taken into account and the significant underprediction of the ozone production from HO_2 still persists (Ren et al., 2013; Brune et al., 2016; Griffith et al., 2016). During the CalNex-LA 2010 campaign in Pasadena (California), part of the discrepancy could be explained by unmeasured VOCs, which were recognized as missing OH reactivity (Griffith et al., 2016). Another major reason for the HO_2 underprediction could be an incomplete understanding of the HO_2 chemistry at high NO_x concentrations (Ren et al., 2013; Brune et al., 2016; Griffith et al., 2016). Similar arguments as for the underprediction of HO_2 apply to RO_2. Whalley et al. (2016) have pointed out that modelled RO_2 and the associated ozone production could be severely underestimated (60 %) in the London atmosphere due to the presence of larger VOCs (mainly monoterpenes). In the Wangdu campaign, missing reactivity from unmeasured VOCs is much smaller. As shown above, unmeasured VOCs caused an underprediction of the daily ozone production of less than 5 %.

Total photochemical ozone production rates were directly measured in a sunlit environmental chamber during the SHARP campaign in Houston (Texas) 2009 (Cazorla et al., 2012; Ren et al., 2013). The comparison with ozone production rates determined from measured HO_2 and from modelled HO_2 and RO_2 ~~is expected for conditions of high concentrations. This was also confirmed by the direct measurement of the total photochemical ozone production rate in one of the studies~~ suggests that the model underestimated both HO_2 and RO_2 at high NO_x in the morning. The underprediction of the daily ozone production was a factor of 1.4. At Wangdu, we find an underprediction of the daily ozone production by a factor of 1.2, which is mainly caused by an underprediction of RO_2. In conclusion, all field studies indicate that the photochemical formation of ozone in a polluted urban atmosphere is not well understood either due to incomplete chemical characterization of the air composition, or incomplete understanding of the peroxy radical chemistry at high NO_x.

3.9 Budget analysis based on model results

The budget analysis for OH, HO_2 and RO_2 radicals is based on the results of model calculations. There are two classes of radical reactions. On the one hand, RO_x radicals are produced or destroyed by reactions, in which RO_x radical species are not reactants and products at the same time. On the other hand, RO_x species are converted into each other by radical recycling reactions. In polluted air ~~,~~during daytime, the conversion reactions are fast, so that the RO_X species are in an equilibrium. Under these conditions, the impact of primary production and destruction is similar on all radical species~~regardless which radical species is formed.~~. The partitioning of RO_X, however, depends on the relative rates of the conversion reactions.

3.9.1 Primary radical production and destruction

~~Mean~~ Median diurnal profiles of primary radical production and destruction rates of RO_x radicals are shown in Fig. 10. Highest turnover rates occur after noontime reaching maximum values around

5 ppbv h^{-1}. HONO, O_3 and HCHO photolysis account for approximately two third of the daytime radical production. HONO, O_3 and HCHO concentrations as well as their photolysis frequencies are well constrained by measurements. HONO photolysis alone is the most important single primary source with maximum values of nearly 2 ppbv h^{-1} at 13:~~00.~~ 00, 38 % of the total radical production. O_3 photolysis contributes 15 % to the total radical production rate. Formaldehyde photolysis is a major source for HO_2 accounting for 18 % of total daytime primary production.

Other production processes of OH includes alkene ozonolysis, which also produces HO_2 and RO_2. The remaining part of the daytime production can be attributed to the photolysis of carbonyl compounds.

Recent findings in the understanding of the oxidation of isoprene found that photo-labile hydroxperoxy aldehydes (HPALD) can be formed in environments where radical recycling via NO is not efficient (Peeters et al., 2014). HPALD photolysis can be a significant radical source in this case. In this campaign, this reaction is almost negligible (Fig. 10), because modelled HPALD concentrations are only around 100 pptv.

In the morning (till 10:00), the major loss of RO_x is the reaction of OH with NO_2. At later times, radical destruction is dominated by the loss via peroxy radical self-reactions, HO_2+HO_2, HO_2+RO_2 and RO_2+RO_2. HO_2 and RO_2 concentration values and their diurnal profiles are similar. Because the ~~reaction~~ reactions of HO_2 with RO_2 have the largest reaction rate constant of the three types of peroxy radical self-reactions, these reactions make the largest contribution. The effect of radical destruction by RO_2 self-reactions could be underestimated in the model, because only reactions of RO_2 with methyl-peroxy radicals and acetyl peroxy radicals are included in the RACM mechanism.

The reaction of OH with NO is the only known gas phase production of HONO, which can compensate the OH production by HONO photolysis. During this campaign, however, HONO formation in the gas phase is always much smaller compared to HONO photolysis making HONO a net source of OH. This also means that the high HONO concentrations during the day cannot be explained by production from the reaction of OH with NO. The importance of HONO photolysis to HO_x chemistry has been reported from urban to forest environments (Dusanter et al., 2009; Mao et al., 2010; Griffith et al., 2013; Kim et al., 2014). The observation of an unusual high HONO concentration of 2 ppbv at noon of 28 June (Fig. 3), when the nearby agricultural field was treated with artificial nitrogen fertilizer, suggests that HONO emissions from surrounding farmland may have played an important role at the measurement site in Wangdu. An imbalance of the two gas-phase reactions of HONO has also been found in many other field campaigns, for example in previous field campaigns in China in 2006 (Li et al., 2012). Heterogeneous formation of HONO is thought to explain part of the missing daytime source (VandenBoer et al., 2014, and ref. therein) ~~, but also unaccounted gas-phase sources might be of importance .~~and photolysis of particulate nitrate is proposed to be of potential importance for tropospheric HONO production (Ye et al., 2016).

Further radical terminating OH losses include reactions ~~of with hydrocarbons that do not lead to radical propagating peroxy radicals.~~ with unsaturated dicarbonyls (DCB1, DCB2, DCB3) and acetyl nitrate species (PAN, MPAN, etc) in RACM 2.

Compared to our previous campaign in Yufa in 2006, the primary radical production in this campaign is significantly less in the morning mainly because of smaller OH production from HONO photolysis. In the afternoon, however, radical production was mainly due to ozone and formaldehyde photolysis in Yufa. The relative contributions of radical destruction processes are similar in this campaign compared to Yufa, but radical loss due to reactions with nitrogen oxides is less important in the morning and slightly enhanced in the afternoon in this campaign.

3.9.2 Radical propagation reactions

Figure 11 shows the distribution of turnover rates of radical recycling reactions. These conversion reactions establish the partitioning of total RO_x species into OH, HO_2 and RO_2.

The conversion of OH to HO_2 (43 % of the total OH destruction rate) is dominated by the reaction of OH with CO and HCHO contributing 25 % and 13 % to the total OH destruction during daytime. Isoprene and its oxidation products (MVK and MACR) are the dominant organic OH reactants in the afternoon. In contrast, alkenes and aldehydes reactions with OH dominate the conversion from OH to RO_2 in the morning.

The radical recycling from RO_2 to HO_2 and also from HO_2 to OH is mainly driven by NO reactions. NO reactions with methyl peroxy radicals (MO_2) and isoprene derived radicals (ISOP) each account for 26 % of the total conversion rate of RO_2 to HO_2 during daytime. Alkane (ALKAP) and alkene (ALKEP) derived peroxy radicals contribute another 20 % and 13 %, respectively. Their relative importance is largest in the morning.

Acyl peroxy radicals (ACO_3 and RCO_3) do not directly convert to HO_2, but form other RO_2 species (MO_2 and ETHP in RACM). A second reaction step with NO is required to form HO_2. Therefore, they are not included in the budget in Fig. 11. However, this conversion reaction contributes to ozone production as discussed above. The daytime average turnover rate of this type of conversion reaction is $0.9\,\mathrm{ppbv\,h^{-1}}$.

Direct conversion of RO_2 radicals to HO_2 and OH by isomerization reactions with subsequent decomposition has been found to be competitive with radical recycling via reactions with NO in the isoprene oxidation mechanism (Peeters et al., 2014; Crounse et al., 2012). The effective isomerization rate of isoprene derived RO_2 is $0.01\,\mathrm{s^{-1}}$ for conditions of this campaign in the afternoon hours (temperature: 303 K). This loss rate is small compared to the loss of isoprene derived RO_2 via the reaction with NO. The average NO mixing ratio is 0.19 ppbv (for the subset of days shown in Fig. 11) giving a loss rate of $0.04\,\mathrm{s^{-1}}$. Therefore, only 20 % of RO_2 from isoprene (ISOP) undergoes isomerization, so that radical recycling from ISOP to HO_2 via isomerization is small. This also explains, why HPALD photolysis as primary RO_x source is not important in this campaign. In

contrast to RO_2 from isoprene, one RO_2 species from MACR (MACP) nearly exclusively isomerizes for afternoon conditions of the campaign. However, the overall impact of this radical recycling reaction is also small, because the median production rate of MACP is only $0.14\,\mathrm{ppbv\,h^{-1}}$ in the afternoon.

The maximum turnover rate of recycling reactions is slightly shifted to earlier times compared to the maximum turnover rate of primary radical production. This is mainly due to the dominance of conversion reactions of RO_2 and HO_2 with NO. This can be best seen in the ~~mean~~ median diurnal profile of the HO_2 conversion to OH, which peaks earlier than the OH conversion to HO_2 and RO_2 (Fig. 11, lower panel). Because the total OH production and destruction rates equal in the model calculation, this imbalance is compensated by the larger primary OH production (Fig. 10).

Compared to the turnover rates in Yufa 2006, radical conversion is less strong in the morning in this campaign, mainly due to smaller peak NO concentrations leading to a reduced reformation of OH from HO_2. This is accompanied by lower HO_2 production in the reaction of OH with formaldehyde. In the afternoon, the strength of radical conversion reaction is similar in both campaigns.

4 Summary and conclusions

A comprehensive set of measurements was ~~collected~~ achieved to characterize the photochemistry at the rural site Wangdu in the North China Plain in 2014. Air pollution was likely transported from surrounding industrial areas and farmland in the North China Plain and few days were influenced by clean air coming from the North.

A new LIF instrument was used to measure concentrations of OH, HO_2 and RO_2~~radicals were~~, and a special group of organic peroxy radicals ($RO_2^{\#}$) which are produced from alkenes and aromatics. Furthermore, total OH reactivity was measured by a ~~new instrument applying laser induced fluorescence technique. In contrast to most previous studies, and were measured separately, and could be determined without interferences from . In~~ laser pump-and-probe instrument. In order to test, if OH measurements included artifacts from OH production inside the measurement cell, chemical modulation tests were performed. These tests identified unexplained OH signals equivalent to (0.5~~to 1~~-1) $\times 10^6\,\mathrm{cm^{-3}}$ with a systematic experimental $1\,\sigma$ uncertainty of $0.5\times10^6\,\mathrm{cm^{-3}}$. Given this uncertainty, the unexplained OH signal may have been caused by an experimental bias of the chemical modulation setup, but also an unknown OH interference cannot be excluded. In case of an interference, ~~it would have contributed about 10of the maximum daytime~~ its contribution to the maximum OH concentration would have been only 10%, so that it would have a minor impact on the interpretation of daytime OH measurements. However, it cannot be excluded that nighttime OH measurements were significantly affected by interferences. An improved ~~set-up~~ setup of this system will be used in future field campaigns.

Daily maximum concentrations of OH, HO_2 and RO_2 ranged from 5×10^6 to 15×10^6 cm^{-3}, 3×10^8 to $14\times10^8\,cm^{-3}$ and 3×10^8 to $15\times10^8\,cm^{-3}$, respectively. Model calculations ~~applying the chemical mechanism RACM~~ using a modified RACM 2 mechanism reproduce the measured radical concentrations generally well in this campaign. The ~~RACM is extended by~~ modified RACM 2 contains an extension based on recent findings in the isoprene chemistry (Peeters et al., 2014; Crounse et al., 2012), ~~but radical concentrations are only slightly enhanced by the additional radical recycling in this mechanism~~ which leads to a small increase of the modelled OH for the conditions of this campaign.

~~Like in other field campaigns, measured~~ The model-measurement comparison for OH ~~concentrations are larger than model predictions at~~ shows a tendency to less good agreement at low NO ~~mixing ratios below~~ concentrations. At concentrations above 0.3 ppbv ~~in the afternoon . However,~~ NO, OH is well described by the model, but is increasingly underpredicted at lower NO in the ~~measure-to-model ratio is only 1.4 to 2.0 and therefore smaller than in previous campaigns in the Pearl River Delta and North China Plain. In these campaigns, model-measurements ratios were~~ afternoon by up to a factor ~~4.5 . Like in previous campaigns, introduction~~ of 2. The unexplained OH signals from the chemical modulation test cannot explain this trend. Introduction of an additional radical recycling process ~~that~~ which has the same effect as 100 pptv NO can close the gap between modelled and measured OH~~. In this campaign, an equivalent of 100~~, but the nature of the process remains unknown. This behaviour is qualitatively in agreement with previous results from two field campaigns in China, in the Pearl River Delta and in the North China Plain, where the required equivalent NO is 800 pptv ~~would be needed~~and 400 pptv (Lu et al., 2012, 2013).

~~Measured~~ An opposite trend is found for RO_2 ~~concentrations are significantly larger than the model predicts~~ radicals. At higher NO concentrations in the morning~~. At the same time measured~~ , the model shows an underprediction of the measured RO_2, which reaches a factor of 10 at about 4 ppbv NO. The underprediction is mainly related to $RO_2^\#$ species, whose concentrations were half of the total RO_2 concentrations. The reaction of OH ~~reactivity is smaller than modelled~~ with unknown VOCs, estimated from missing OH ~~reactivity, which suggests missing~~ reactivity, can explain part of the RO_2 ~~production from unmeasured reactants in the model.~~

~~To our knowledge, there are not many published studies where measured~~ discrepancy until 9:00, but not later in the morning. Good agreement between measured and modelled RO_2 ~~data were available in addition to measured . Therefore, this study provides the opportunity to calculate the~~ and $RO_2^\#$ can be achieved by assuming an additional primary source of 2 ppbv h^{-1} of RO_2 (from alkenes) until noon. Reactions of VOCs with chlorine atoms from the photolysis of $ClNO_2$ were a likely source of additional RO_2 after sunrise, but the measured $ClNO_2$ concentrations (< 2 ppbv) reported by Tham et al. (2016) can explain only (10-20)% of the required additional RO_2 source early in the morning. Another source which sustains additional RO_2 production until noon is therefore needed.

As a consequence of the model underprediction of RO_2, the total net ozone production ~~rate from measurements of all peroxy radicals including~~ from HO_2 and RO_2 ~~. Local net ozone production can then be compared to model results. In the afternoon, both rates agree well, but the model underpredicts the ozone production rate by about 6~~radicals is also underestimated by the model. The median measured concentrations of HO_2 and RO_2 yield a daily integrated ozone production of 110 ppbv, which is 20 ppbv more than predicted by the modified RACM 2. About 10 % of the discrepancy can be explained by $ClNO_2$ chemistry during the Wangdu campaign. The underprediction of the photochemical ozone production at high NO_x in the morning ~~. This underestimation is caused by underpredicted in the model, whereas the modelled concentrations agree well with measurements. This result is different from the findings in~~ is in general agreement with other studies in urban ~~and forested environments, where the ozone production rate was also underestimated, but caused by too low values of the modelled~~ environments, underlining the need for better understanding of the peroxy radical chemistry in polluted air.

Radicals are primarily produced by photolysis reactions and radical loss is dominated by reactions with nitrogen oxides in the morning and peroxy radical self-reactions in the afternoon. This is similar to our previous campaign 2006 in Yufa that is also located in the North China Plain (Lu et al., 2013). OH production from HONO photolysis in the afternoon was the largest primary radical source in this campaign. Because NO concentrations are lower than in 2006 in the morning, radical conversion rates are smaller. Higher OH concentrations and OH reactivity measured in 2006 and smaller OH recycling from the reaction of HO_2 with NO in the afternoon led to the need of a larger enhancement of the radical recycling efficiency for the campaign in 2006 compared to results from this campaign.

Acknowledgements. We thank the science teams of Wangdu-2014 Campaign. This work was supported by the Strategic Priority Research Program of the Chinese Academy of Sciences (grant no. XDB05010500), the National Natural Science Foundation of China (Major Program: 21190052 and Innovative Research Group: 41121004), the ~~Strategic Priority Research Program of the Chinese Academy of Sciences (grant no. XDB05010500), the~~ Collaborative Innovation Center for Regional Environmental Quality, the EU-project AMIS (Fate and Impact of Atmospheric Pollutants, PIRSES-GA-2011-295132). The authors gratefully acknowledge the NOAA Air Resources Laboratory (ARL) for the provision of the HYSPLIT transport and dispersion model and/or READY website (http://www.ready.noaa.gov) used in this publication.

References

Berresheim, H., Plass-Dülmer, C., Elste, T., Mihalopoulos, N., and Rohrer, F.: OH in the coastal boundary layer of Crete during MINOS: measurements and relationship with ozone photolysis, Atmos. Chem. Phys., 3, 639–649, doi:10.5194/acp-03-639-2003, 2003.

Bohn, B., Corlett, G. K., Gillmann, M., Sanghavi, S., Stange, G., Tensing, E., Vrekoussis, M., Bloss, W. J., Clapp, L. J., Kortner, M., Dorn, H.-P., Monks, P. S., Platt, U., Plass-Dülmer, C., Mihalopoulos, N., Heard, D. E., Clemitshaw, K. C., Meixner, F. X., Prevot, A. S. H., and Schmitt, R.: Photolysis frequency measurement techniques: results of a comparison within the ACCENT project, Atmos. Chem. Phys., 8, 5373–5391, doi:10.5194/acp-08-5373-2008, 2008.

Brauers, T., Hausmann, M., Bister, A., Kraus, A., and Dorn, H.-P.: OH radicals in the boundary layer of the Atlantic Ocean 1. Measurements by long-path laser absorption spectroscopy, J. Geophys. Res., 106, 7399–7414, doi:10.1029/2000jd900679, 2001.

Brown, S. S., and Stutz, J.: Nighttime radical observations and chemistry, Chem. Soc. Rev., 41, 6405–6447, doi:10.1039/c2cs35181a, 2012.

Brune, W. H. and Baier, B. C., Thomas, J., Ren, X., Cohen, R. C., Pusede, S. E., Browne, E. C., Goldstein, A. H., Gentner, D. R., Keutsch, F. N., Thornton, J. A., Harrold, S., Lopez-Hilfiker, F. D. and Wennberg, P. O.: Ozone production chemistry in the presence of urban plumes, Faraday Discuss., 189, 169, doi:10.1039/C5FD00204D, 2016.

Cantrell, C. A., Edwards, G. D., Stephens, S., Mauldin, R. L., Zondlo, M. A., Kosciuch, E., Eisele, F. L., Shetter, R. E., Lefer, B. L., Hall, S., Flocke, F., Weinheimer, A., Fried, A., Apel, E., Kondo, Y., Blake, D. R., Blake, N. J., Simpson, I. J., Bandy, A. R., Thornton, D. C., Heikes, B. G., Singh, H. B., Brune, W. H., Harder, H., Martinez, M., Jacob, D. J., Avery, M. A., Barrick, J. D., Sachse, G. W., Olson, J. R., Crawford, J. H., and Clarke, A. D.: Peroxy radical behavior during the Transport and Chemical Evolution over the Pacific (TRACE-P) campaign as measured aboard the NASA P-3B aircraft, J. Geophys. Res., 108, 1801–1821, doi:10.1029/2003jd003674, 2003.

Cazorla, M., Brune, W. H., Ren, X., and Lefer, B.: Direct measurement of ozone production rates in Houston in 2009 and comparison with two estimation methods, Atmos. Chem. Phys., 12, 1203–1212, doi:10.5194/acp-12-1203-2012, 2012.

Crounse, J. D., Paulot, F., Kjaergaard, H. G., and Wennberg, P. O.: Peroxy radical isomerization in the oxidation of isoprene, Phys. Chem. Chem. Phys., 13, 13 607–13 613, doi:10.1039/C1CP21330J, 2011.

Crounse, J. D., Knap, H. C., Ornso, K. B., Jorgensen, S., Paulot, F., Kjaergaard, H. G., and Wennberg, P. O.: On the atmospheric fate of methacrolein: 1. Peroxy radical isomerization following addition of OH and O_2, J. Phys. Chem. A, 116, 5756–5762, doi:10.1021/jp211560u, 2012.

Dong, H. B., Zeng, L. M., Hu, M., Wu, Y. S., Zhang, Y. H., Slanina, J., Zheng, M., Wang, Z. F., and Jansen, R.: Technical Note: The application of an improved gas and aerosol collector for ambient air pollutants in China, Atmos. Chem. Phys., 12, 10 519–10 533, doi:10.5194/acp-12-10519-2012, 2012.

Dusanter, S., Vimal, D., Stevens, P. S., Volkamer, R., Molina, L. T., Baker, A., Meinardi, S., Blake, D., Sheehy, P., Merten, A., Zhang, R., Zheng, J., Fortner, E. C., Junkermann, W., Dubey, M., Rahn, T., Eichinger, B., Lewandowski, P., Prueger, J., and Holder, H.: Measurements of OH and HO_2 concentrations during

the MCMA-2006 field campaign - Part 2: Model comparison and radical budget, Atmos. Chem. Phys., 9, 6655-6675, doi:10.5194/acp-9-6655-2009, 2009.

Ehhalt, D. H.: Photooxidation of trace gases in the troposphere, Phys. Chem. Chem. Phys., 1, 5401–5408, doi:10.1039/a905097c, 1999.

Ehhalt, D. H. and Rohrer, F.: Dependence of the OH concentration on solar UV, J. Geophys. Res., 105, 3565–3571, doi:10.1029/1999JD901070, 2000.

Fuchs, H., Hofzumahaus, A., and Holland, F.: Measurement of tropospheric RO_2 and HO_2 radicals by a laser-induced fluorescence instrument, Rev. Sci. Instrum., 79, 084 104, doi:10.1063/1.2968712, 2008.

Fuchs, H., Bohn, B., Hofzumahaus, A., Holland, F., Lu, K. D., Nehr, S., Rohrer, F., and Wahner, A.: Detection of HO_2 by laser-induced fluorescence: calibration and interferences from RO_2 radicals, Atmos. Meas. Tech., 4, 1209–1255, doi:10.5194/amt-4-1209-2011, 2011.

Fuchs, H., Hofzumahaus, A., Rohrer, F., Bohn, B., Brauers, T., Dorn, H.-P., Häseler, R., Holland, F., Kaminski, M., Li, X., Lu, K., Nehr, S., Tillmann, R., Wegener, R., and Wahner, A.: Experimental evidence for efficient hydroxyl radical regeneration in isoprene oxidation, Nature Geosci., 6, 1023–1026, doi:10.1038/NGEO1964, 2013.

Fuchs, H., Acir, I. H., Bohn, B., Brauers, T., Dorn, H. P., Häseler, R., Hofzumahaus, A., Holland, F., Kaminski, M., Li, X., Lu, K., Lutz, A., Nehr, S., Rohrer, F., Tillmann, R., Wegener, R., and Wahner, A.: OH regeneration from methacrolein oxidation investigated in the atmosphere simulation chamber SAPHIR, Atmos. Chem. Phys., 14, 7895–7908, doi:10.5194/acp-14-7895-2014, 2014.

Fuchs, H., Tan, Z., Hofzumahaus, A., Broch, S., Dorn, H. P., Holland, F., Künstler, C., Gomm, S., Rohrer, F., Schrade, S., Tillmann, R. and Wahner, A., : Investigation of potential interferences in the detection of atmospheric ROx radicals by laser-induced fluorescence under dark conditions, Atmos. Meas. Tech., 9, 1431-1447, doi:10.5194/amt-9-1431-2016, 2016.

Fuchs, H., Tan, Z., Lu, K., Bohn, B., Broch, S., Brown, S. S., Dong, H., Gomm, S., Häseler, R., He, L., Hofzumahaus, A., Holland, F., Li, X., Liu, Y., Lu, S., Min, K. E., Rohrer, F., Shao, M., Wang, B., Wang, M., Wu, Y., Zeng, L., Zhang, Y., Wahner, A., and Zhang, Y.: OH reactivity at a rural site (Wangdu) in the North China Plain: Contributions from OH reactants and experimental OH budget, Atmos. Chem. Phys. Discuss., 2016, 1-30, doi:10.5194/acp-2016-716, 2016.

Galloway, M. M., Huisman, A. J., Yee, L. D., Chan, A. W. H., Loza, C. L., Seinfeld, J. H., and Keutsch, F. N.: Yields of oxidized volatile organic compounds during the OH radical initiated oxidation of isoprene, methyl vinyl ketone, and methacrolein under high-NO_x conditions, Atmos. Chem. Phys., 11, 10779–10790, doi:10.5194/acp-11-10779-2011, 2011.

Goliff, W. S., Stockwell, W. R., and Lawson, C. V.: The regional atmospheric chemistry mechanism, version 2, Atmos. Environ., 68, 174–185, doi:10.1016/j.atmosenv.2012.11.038, 2013.

Griffith, S. M., Hansen, R. F., Dusanter, S., Stevens, P. S., Alaghmand, M., Bertman, S. B., Carroll, M. A., Erickson, M., Galloway, M., Grossberg, N., Hottle, J., Hou, J., Jobson, B. T., Kammrath, A., Keutsch, F. N., Lefer, B. L., Mielke, L. H., O'Brien, A., Shepson, P. B., Thurlow, M., Wallace, W., Zhang, N., and Zhou, X. L.: OH and HO_2 radical chemistry during PROPHET 2008 and CABINEX 2009-Part 1: Measurements and model comparison, Atmos. Chem. Phys., 13, 5403-5423, doi:10.5194/acp-13-5403-2013, 2013.

Griffith, S. M., Hansen, R. F., Dusanter, S., Michoud, V., Gilman, J. B., Kuster, W. C., Veres, P. R., Graus, M., de Gouw, J. A., Roberts, J., Young, C., Washenfelder, R., Brown, S. S., Thalman, R., Waxman, E., Volkamer, R., Tsai, C., Stutz, J., Flynn, J. H., Grossberg, N., Lefer, B., Alvarez, S. L., Rappenglueck, B., Mielke, L. H., Osthoff, H. D., and Stevens, P. S.: Measurements of Hydroxyl and Hydroperoxy Radicals during CalNex-LA: Model Comparisons and Radical Budgets, J. Geophys. Res. Atmos., 121, doi:10.1002/2015JD024358, 2016.

Hard, T. M., George, L. A., and O'Brian, R. J.: FAGE determination of tropospheric OH and HO_2, J. Atmos. Sci., 52, 3354–3372, 1995.

Heard, D. E. and Pilling, M. J.: Measurement of OH and HO_2 in the troposphere, Chem. Rev., 103, 5163-5198, doi:10.1021/cr020522s, 2003.

Hofzumahaus, A., Aschmutat, U., Heßling, M., Holland, F., and Ehhalt, D. H.: The measurement of tropospheric OH radicals by laser-induced fluorescence spectroscopy during POPCORN field campaign, Geophys. Res. Lett., 23, 2541–2544, doi:10.1029/96GL02205, 1996.

Hofzumahaus, A., Rohrer, F., Lu, K., Bohn, B., Brauers, T., Chang, C.-C., Fuchs, H., Holland, F., Kita, K., Kondo, Y., Li, X., Lou, S., Shao, M., Zeng, L., Wahner, A., and Zhang, Y.: Amplified trace gas removal in the troposphere, Science, 324, 1702–1704, doi:10.1126/science.1164566, 2009.

Holland, F., Heßling, M., and Hofzumahaus, A.: In situ measurement of tropospheric OH radicals by laser-induced fluorescence - a description of the KFA instrument, J. Atmos. Sci., 52, 3393–3401, doi:10.1175/1520-0469(1995)052<3393:ISMOTO>2.0.CO;2, 1995.

Holland, F., Hofzumahaus, A., Schäfer, J., Kraus, A., and Pätz, H. W.: Measurements of OH and HO_2 radical concentrations and photolysis frequencies during BERLIOZ, J. Geophys. Res., 108, 8246, doi:10.1029/2001JD001393, 2003.

Hua, W., Chen, Z. M., Jie, C. Y., Kondo, Y., Hofzumahaus, A., Takegawa, N., Chang, C. C., Lu, K. D., Miyazaki, Y., Kita, K., Wang, H. L., Zhang, Y. H., and Hu, M.: Atmospheric hydrogen peroxide and organic hydroperoxides during PRIDE-PRD'06, China: their concentration, formation mechanism and contribution to secondary aerosols, Atmos. Chem. Phys., 8, 6755–6773, doi:10.5194/acp-8-6755-2008, 2008.

Kanaya, Y., Fukuda, M., Akimoto, H., Takegawa, N., Komazaki, Y., Yokouchi, Y., Koike, M., and Kondo, Y.: Urban photochemistry in central Tokyo: 2. Rates and regimes of oxidant ($O_3 + NO_2$) production, J. Geophys. Res., 113, D06301, doi:10.1029/2007JD008671, 2008.

Kanaya, Y., Hofzumahaus, A., Dorn, H. P., Brauers, T., Fuchs, H., Holland, F., Rohrer, F., Bohn, B., Tillmann, R., Wegener, R., Wahner, A., Kajii, Y., Miyamoto, K., Nishida, S., Watanabe, K., Yoshino, A., Kubistin, D., Martinez, M., Rudolf, M., Harder, H., Berresheim, H., Elste, T., Plass-Duelmer, C., Stange, G., Kleffmann, J., Elshorbany, Y., and Schurath, U.: Comparisons of observed and modeled OH and HO_2 concentrations during the ambient measurement period of the HO_xComp field campaign, Atmos. Chem. Phys., 12, 2567-2585, doi:10.5194/acp-12-2567-2012, 2012.

Kim, S., VandenBoer, T. C., Young, C. J., Riedel, T. P., Thornton, J. A., Swarthout, B., Sive, B., Lerner, B., Gilman, J. B., Warneke, C., Roberts, J. M., Guenther, A., Wagner, N. L., Dube, W. P., Williams, E., and Brown, S. S.: The primary and recycling sources of OH during the NACHTT-2011 campaign: HONO as an important OH primary source in the wintertime, Geophys. Res. Atmos., 119, 6886-6896, doi:10.1002/2013jd019784, 2014.

Kleffmann, J., Gavriloaiei, T., Hofzumahaus, A., Holland, F., Koppmann, R., Rupp, L., Schlosser, E., Siese, M., and Wahner, A.: Daytime formation of nitrous acid: A major source of OH radicals in a forest, Geophys. Res. Lett., 32, L05 818, doi:10.1029/2005GL022524, 2005.

Lelieveld, J., Butler, T. M., Crowley, J. N., Dillon, T. J., Fischer, H., Ganzeveld, L., Harder, H., Lawrence, M. G., Martinez, M., Taraborrelli, D., and Williams, J.: Atmospheric oxidation capacity sustained by a tropical forest, Nature, 452, 737–740, doi:10.1038/nature06870, 2008.

Li, X., Brauers, T., Häseler, R., Bohn, B., Fuchs, H., Hofzumahaus, A., Holland, F., Lou, S., Lu, K. D., Rohrer, F., Hu, M., Zeng, L. M., Zhang, Y. H., Garland, R. M., Su, H., Nowak, A., Wiedensohler, A., Takegawa, N., Shao, M., and Wahner, A.: Exploring the atmospheric chemistry of nitrous acid (HONO) at a rural site in Southern China, Atmos. Chem. Phys., 12, 1497–1513, doi:10.5194/acp-12-1497-2012, 2012.

Li, X., Rohrer, F., Hofzumahaus, A., Brauers, T., Hšeler, R., Bohn, B., Broch, S., Fuchs, H., Gomm, S., Holland, F., Jäger, J., Kaiser, J., Keutsch, F. N., Lohse, I., Lu, K., Tillmann, R., Wegener, R., Wolfe, G. M., Mentel, T. F., Kiendler-Scharr, A., and Wahner, A.: Missing gas-phase source of HONO inferred from Zeppelin measurements in the troposphere, Science, 344, 292–296, doi:10.1126/science.1248999, 2014.

Liu, Y., Lu, K., Dong, H., Li, X., Cheng, P., Zou, Q., Wu, Y., Liu, X., and Zhang, Y.: In situ monitoring of atmospheric nitrous acid based on multi-pumping flow system and liquid waveguide capillary cell, ~~Journal of Environmental Sciences-China,~~J. Environ. Sci., 43, 273-284, doi:10.1016/j.jes.2015.11.034, 2016.

Lou, S., Holland, F., Rohrer, F., Lu, K., Bohn, B., Brauers, T., Chang, C. C., Fuchs, H., Häseler, R., Kita, K., Kondo, Y., Li, X., Shao, M., Zeng, L., Wahner, A., Zhang, Y., Wang, W., and Hofzumahaus, A.: Atmospheric OH reactivities in the Pearl River Delta - China in summer 2006: measurement and model results, Atmos. Chem. Phys., 10, 11 243–11 260, doi:10.5194/acp-10-11243-2010, 2010.

Lu, K. D., Zhang, Y., Su, H., Brauers, T., Chou, C. C., Hofzumahaus, A., Liu, S. C., Kita, K., Kondo, Y., Shao, M., Wahner, A., Wang, J., Wang, X., and Zhu, T.: Oxidant (O_3 + NO_2) production processes and formation regimes in Beijing, J. Geophys. Res., 1115, D7303, doi:10.1029/2009JD012714, 2010.

Lu, K. D., Rohrer, F., Holland, F., Fuchs, H., Bohn, B., Brauers, T., Chang, C. C., Häseler, R., Hu, M., Kita, K., Kondo, Y., Li, X., Lou, S. R., Nehr, S., Shao, M., Zeng, L. M., Wahner, A., Zhang, Y. H., and Hofzumahaus, A.: Observation and modelling of OH and HO_2 concentrations in the Pearl River Delta 2006: a missing OH source in a VOC rich atmosphere, Atmos. Chem. Phys., 12, 1541–1569, doi:10.5194/acp-12-1541-2012, 2012.

Lu, K. D., Hofzumahaus, A., Holland, F., Bohn, B., Brauers, T., Fuchs, H., Hu, M., Häseler, R., Kita, K., Kondo, Y., Li, X., Lou, S. R., Oebel, A., Shao, M., Zeng, L. M., Wahner, A., Zhu, T., Zhang, Y. H., and Rohrer, F.: Missing OH source in a suburban environment near Beijing: observed and modelled OH and HO_2 concentrations in summer 2006, Atmos. Chem. Phys., 13, 1057–1080, doi:10.5194/acp-13-1057-2013, 2013.

Lu, K. D., Rohrer, F., Holland, F., Fuchs, H., Brauers, T., Oebel, A., Dlugi, R., Hu, M., Li, X., Lou, S. R., Shao, M., Zhu, T., Wahner, A., Zhang, Y. H., and Hofzumahaus, A.: Nighttime observation and chemistry of HO_X in the Pearl River Delta and Beijing in summer 2006, Atmos. Chem. Phys., 14, 4979–4999, doi:10.5194/acp-14-4979-2014, 2014.

Mao, J., Jacob, D. J., Evans, M. J., Olson, J. R., Ren, X., Brune, W. H., Clair, J. M. S., Crounse, J. D., Spencer, K. M., Beaver, M. R., Wennberg, P. O., Cubison, M. J., Jimenez, J. L., Fried, A., Weibring, P., Walega,

J. G., Hall, S. R., Weinheimer, A. J., Cohen, R. C., Chen, G., Crawford, J. H., McNaughton, C., Clarke, A. D., Jaegle, L., Fisher, J. A., Yantosca, R. M., Le Sager, P., and Carouge, C.: Chemistry of hydrogen oxide radicals (HO_X) in the Arctic troposphere in spring, Atmos. Chem. Phys., 10, 5823–5838, doi:10.5194/acp-10-5823-2010, 2010.

Mao, J., Ren, X., Brune, W. H., Van Duin, D. M., Cohen, R. C., Park, J. H., Goldstein, A. H., Paulot, F., Beaver, M. R., Crounse, J. D., Wennberg, P. O., DiGangi, J. P., Henry, S. B., Keutsch, F. N., Park, C., Schade, G. W., Wolfe, G. M., and Thornton, J. A.: Insights into hydroxyl measurements and atmospheric oxidation in a California forest, Atmos. Chem. Phys., 12, 8009–8020, doi:10.5194/acp-12-8009-2012, 2012.

Martinez, M., Harder, H., Kovacs, T. A., Simpas, J. B., Bassis, J., Lesher, R., Brune, W. H., Frost, G. J., Williams, E. J., Stroud, C. A., Jobson, B. T., Roberts, J. M., Hall, S. R., Shetter, R. E., Wert, B., Fried, A., Alicke, B., Stutz, J., Young, V. L., White, A. B., and Zamora, R. J.: OH and HO_2 concentrations, sources, and loss rates during the Southern Oxidants Study in Nashville, Tennessee, summer 1999, J. Geophys. Res., 108, 4617, doi:10.1029/2003JD003551, 2003.

Mauldin, R. L., Tanner, D. J., and Eisele, F. L.: Measurements of OH during PEM-Tropics A, J. Geophys. Res., 104, 5817-5827, doi:10.1029/98jd02305, 1999.

Mauldin III, R. L., Berndth, T., Sipila, M., Paasonen, P., Petaja, T., Kim, S., Kurten, T., Stratmann, F., Kerminen, V. M., and Kulmala, M.: A new atmospherically relevant oxidant of sulphur dioxide, Nature., 488, 193–196, doi:10.1038/nature11278, 2012.

Mihelcic, D., Holland, F., Hofzumahaus, A., Hoppe, L., Konrad, S., Müsgen, P., Pätz, H.-W., Schäfer, H.-J., Schmitz, T., Volz-Thomas, A., Bächmann, K., Schlomski, S., Platt, U., Geyer, A., Alicke, B. and Moortga, G. K.: Peroxy radicals during BERLIOZ at Pabstthum: Measurements, radical budgets and ozone production, J. Geophys. Res., 108, 8254, doi:10.1029/2001JD001014, 2003.

Min, K. E., Washenfelder, R. A., Dube, W. P., Langford, A. O., Edwards, P. M., Zarzana, K. J., Stutz, J., Lu, K., Rohrer, F., Zhang, Y., and Brown, S. S.: A broadband cavity enhanced absorption spectrometer for aircraft measurements of glyoxal, methylglyoxal, nitrous acid, nitrogen dioxide, and water vapor, Atmos. Meas. Tech.~~Discuss., 8, 11209–11254, , 2015.~~ , 9, 423–440, doi:10.5194/amt-9-423-2016, 2016.

Novelli, A., Hens, K., Tatum Ernest, C., Kubistin, D., Regelin, E., Elste, T., Plass-Dülmer, C., Martinez, M., Lelieveld, J., and Harder, H.: Characterisation of an inlet pre-injector laser-induced fluorescence instrument for the measurement of atmospheric hydroxyl radicals, Atmos. Meas. Tech., 7, 3413–3430, doi:10.5194/amt-7-3413-2014, 2014.

Osthoff, H., Roberts, J. M., Ravishankara, A. R., Williams, E. J., Lerner, B. M., Sommariva, R., Bates, T. S., Coffman, D., Quinn, P. K., Dibb, J. E., Stark, H., Burkholder, J. B., Talukdar, R. K., J. Meagher, Fehsenfeld, F. C. and Brown, S. S.: High levels of nitryl chloride in the polluted subtropical marine boundary layer, Nature Geosci., 1, 324–328, doi:10.1038/ngeo177, 2008.

Ou, J., Yuan, Z., Zheng, J., Huang, Z., Shao, M., Li, Z., Huang, X., Guo, H., Louie, P. K. K.: Ambient ozone control in a photochemically active region: Short-term despiking or long-term attainment?, Environ. Sci. Technol., ~~in press,~~ 50 (11), 5720–5728, doi:10.1021/acs.est.6b00345, 2016.

Paulot, F., Crounse, J. D., Kjaergaard, H. G., Kurten, A., St. Clair, J. M., Seinfeld, J. H., and Wennberg, P. O.: Unexpected epoxide formation in the gas-phase photooxidation of isoprene, Science, 325, 730–733, doi:10.1126/science.1172910, 2009.

Peeters, J. and Müller, J.-F.: HO_X radical regeneration in isoprene oxidation via peroxy radical isomerisations. II: experimental evidence and global impact, Phys. Chem. Chem. Phys., 12, 14 227–14 235, doi:10.1039/C0CP00811G, 2010.

Peeters, J., Nguyen, T. L., and Vereecken, L.: HO_X radical regeneration in the oxidation of isoprene, Phys. Chem. Chem. Phys., 11, 5935–5939, doi:10.1039/b908511d, 2009.

Peeters, J., Müller, J.-F., Stavrakou, T., and Nguyen, V. S.: Hydroxyl radical recycling in isoprene oxidation driven by hydrogen bonding and hydrogen tunneling: The upgraded LIM1 mechanism, J. Phys. Chem. A, 118, 8625–8643, doi:10.1021/jp5033146, 2014.

Praske, E., Crounse, J. D., Bates, K. H., Kurten, T., Kjaergaard, H. G., and Wennberg, P. O.: Atmospheric fate of methyl vinyl ketone: Peroxy radical reactions with NO and HO_2, J. Phys. Chem. A, 119, 4562–4572, doi:10.1021/jp5107058, 2015.

Ren, X., Harder, H., Martinez, M., Lesher, R. L., Oliger, A., Shirley, T., Adams, J., Simpas, J. B., and Brune, W. H.: HO_X concentrations and OH reactivity observations in New York City during PMTACS-NY2001, Atmos. Environ., 37, 3627–3637, 2003.

Ren, X. R., Brune, W. H., Cantrell, C. A., Edwards, G. D., Shirley, T., Metcalf, A. R. and Lesher, R. L.: Hydroxyl and peroxy radical chemistry in a rural area of Central Pennsylvania: Observations and model comparisons, J. Atmos. Chem., 52, 231-257, doi:10.1007/s10874-005-3651-7, 2005.

Ren, X., van Duin, D., Cazorla, M., Chen, S., Mao, J., Zhang, L., Brune, W. H., Flynn, J. H., Grossberg, N., Lefer, B. L., Rappenglück, B., Wong, K. W., Tsai, C., Stutz, J., Dibb, J. E., Thomas Jobson, B., Luke, W. T., and Kelley, P.: Atmospheric oxidation chemistry and ozone production: Results from SHARP 2009 in Houston, Texas, J. Geophys. Res., 118, 5770–5780, doi:10.1002/jgrd.50342, 2013.

Rohrer, F. and Berresheim, H.: Strong correlation between levels of tropospheric hydroxyl radicals and solar ultraviolet radiation, Nature, 442, 184–187, doi:10.1038/nature04924, 2006.

Rohrer, F., Lu, K., Hofzumahaus, A., Bohn, B., Brauers, T., Chang, C.-C., Fuchs, H., Häseler, R., Holland, F., Hu, M., Kita, K., Kondo, Y., Li, X., Lou, S., Oebel, A., Shao, M., Zeng, L., Zhu, T., Zhang, Y., and Wahner, A.: Maximum efficiency in the hydroxyl-radical-based self-cleansing of the troposphere, Nature Geosci., 7, 559–563, doi:10.1038/ngeo2199, 2014.

Shao, M., Tang, X. Y., Zhang, Y. H. and Li, W. J.: City clusters in China: air and surface water pollution, ~~Chem. Soc. Rev~~Front. Ecol. Environ., 4, 353-361, doi:10.1890/1540-9295(2006)004[0353:ccicaa]2.0.co;2, 2006.

Stein, A.F., Draxler, R.R, Rolph, G.D., Stunder, B.J.B., Cohen, M.D., and Ngan, F.,: NOAA's HYSPLIT atmospheric transport and dispersion modeling system, Bull. Amer. Meteor. Soc., 96, 2059-2077, doi:http://dx.doi.org/10.1175/BAMS-D-14-00110.1, 2015.

Stone, D., Whalley, L. K., and Heard, D. E.: Tropospheric OH and HO_2 radicals: field measurements and model comparisons, ~~Front. Ecol. Environ~~Chem. Soc. Rev., 41, 6348–6404, doi:10.1039/C2CS35140D, 2012.

Tan, D., Faloona, I., Simpas, J. B., Brune, W., Shepson, P. B., Couch, T. L., Summer, A. L., Carroll, M. A., Thornberry, T., Apel, E., Riemer, D., and Stockwell, W.: HO_X budget in a deciduous forest: results from the ~~PROPHET~~ PROPHET summer 1998 campaign, J. Geophys. Res., 106, 24 407–24 427, doi:10.1029/2001JD900016, 2001.

Tham, Y. J., Wang, Z., Li, Q., Yun, H., Wang, W., Wang, X., Xue, L., Lu, K., Ma, N., Bohn, B., Li, X., Kecorius, S., Grösss, J., Shao, M., Wiedensohler, A., Zhang, Y. and Wang, T.: Significant concentrations of

nitryl chloride sustained in the morning: Investigations of the causes and impacts on ozone production in a polluted region of northern China, Atmos. Chem. Phys. Discuss., 2016, 1-34, doi:10.5194/acp-2016-439, 2016.

Thornton, J. A., Kercher, J. P., Riedel, T. P., Wagner, N. L., Cozic, J., Holloway, J. S., Dube, W. P., Wolfe, G. M., Quinn, P. K., Middlebrook, A. M., Alexander, B., and Brown, S. S.: A large atomic chlorine source inferred from mid-continental reactive nitrogen chemistry, Nature, 464, 271-274, doi:10.1038/Nature08905, 2010.

VandenBoer, T. C., Markovic, M. Z., Sanders, J. E., Ren, X., Pusede, S. E., Browne, E. C., Cohen, R. C., Zhang, L., Thomas, J., Brune, W. H., and Murphy, J. G.: Evidence for a nitrous acid (HONO) reservoir at the ground surface in Bakersfield, CA, during CalNex 2010, J. Geophys. Res., 119, 9093–9106, doi:10.1002/2013JD020971, 2014.

Wang, B., Shao, M., Roberts, J. M., Yang, G., Yang, F., Hu, M., Zeng, L., Zhang, Y., and Zhang, J.: Ground-based on-line measurements of peroxyacetyl nitrate (PAN) and peroxypropionyl nitrate (PPN) in the Pearl River Delta, China, Int. J. Environ. Anal. Chem., 90, 548–559, doi:10.1080/03067310903194972, 2010.

Wang, M., Zeng, L., Lu, S., Shao, M., Liu, X., Yu, X., Chen, W., Yuan, B., Zhang, Q., Hu, M., and Zhang, Z.: Development and validation of a cryogen-free automatic gas chromatograph system (GC-MS/FID) for online measurements of volatile organic compounds, ~~Analytical~~ Anal. Methods, 6, 9424–9434, doi:10.1039/C4AY01855A, 2014.

Wang, Q., Shao, M., Liu, Y., William, K., Paul, G., Li, X., Liu, Y., and Lu, S.: Impact of biomass burning on urban air quality estimated by organic tracers: Guangzhou and Beijing as cases, Atmos. Environ., 41, 8380–8390, doi:10.1016/j.atmosenv.2007.06.048, 2007.

Wang, H. C., Chen, T., and Lu, K. D.: Measurement of NO_3 and N_2O_5 in the ~~Troposphere~~troposphere, Prog. Chem., 27, 963-976, doi:10.7536/PC141230, 2015.

Whalley, L. K., Edwards, P. M., Furneaux, K. L., Goddard, A., Ingham, T., Evans, M. J., Stone, D., Hopkins, J. R., Jones, C. E., Karunaharan, A., Lee, J. D., Lewis, A. C., Monks, P. S., Moller, S. J., and Heard, D. E.: Quantifying the magnitude of a missing hydroxyl radical source in a tropical rainforest, Atmos. Chem. Phys., 11, 7223–7233, doi:10.5194/acp-11-7223-2011, 2011.

Whalley, L. K., Blitz, M. A., Desservettaz, M., Seakins, P. W., and Heard, D. E.: Reporting the sensitivity of laser-induced fluorescence instruments used for HO_2 detection to an interference from RO_2 radicals and introducing a novel approach that enables HO_2 and certain RO_2 types to be selectively measured, Atmos. Meas. Tech., 6, 3425–3440, doi:10.5194/amt-6-3425-2013, 2013.

Whalley, L. K., Stone, D., Bandy, B., Dunmore, R., Hamilton, J. F., Hopkins, J., Lee, J. D., Lewis, A. C., and Heard, D. E.: Atmospheric OH reactivity in central London: observations, model predictions and estimates of in situ ozone production, Atmos. Chem. Phys., 16, 2109-2122, doi:10.5194/acp-16-2109-2016, 2016.

Xue, L. K., Saunders, S. M., Wang, T., Gao, R., Wang, X. F., Zhang, Q. Z., and Wang, W. X.: Development of a chlorine chemistry module for the Master Chemical Mechanism, Geosci. Model Dev., 8, 3151-3162, doi:10.5194/gmd-8-3151-2015, 2015.

Table 1. ~~Instruments deployed in the campaign and~~ Measured quantities used for data analysis and model calculations.

Parameters	Measurement technique	Time resolution	Detection limit [a]	~~Accuracy~~ [b] 1 σ Accuracy
OH	LIF [c,b]	32 s	0.32×10^6 cm^{-3}	$\pm$11 %
HO_2	LIF [b,c,d]	32 s	0.10×10^8 cm^{-3}	$\pm$16 %
RO_2	LIF [b,c,d]	32 s	0.05×10^8 cm^{-3}	$\pm$18 %
k_{OH}	LP-LIF [e,d]	180 s	0.3 s^{-1}	$\pm$10 % $\pm$0.7 s^{-1}
photolysis frequency	spectroradiometer	20 s	[f,e]	$\pm$10 %
O_3 [f]	UV photometry	60 s	0.5 ppbv	$\pm$5 %
NO [g]	chemiluminescence	180 s	60 pptv	$\pm$20 %
NO_2 [g]	chemiluminescence [g,h]	60s	300 pptv	$\pm$20 %
HONO [i]	LOPAP [h,j], CEAS [k]	30s	7 pptv	$\pm$20 %
CO, CH_4, CO_2, H_2O	cavity ring down	60 s	[i,l]	[j,m]
SO_2	pulsed UV fluorescence	60 s	0.1 ppbv	$\pm$5 %
HCHO	Hantzsch fluorimetry	60 s	25 pptv	$\pm$5 %
volatile organic compounds [k,n]	GC-FID/MS [l,o]	1 h	20 to 300 pptv	$\pm$15 to 20 %
volatile organic compounds [m,p]	PTR-MS	20 s	0.2 ppbv	$\pm$15 %

[a] signal to noise ratio = 1

[b] laser induced fluorescence

[c] chemical conversion via NO reaction before detection

[d] laser photolysis - laser induced fluorescence

[e] process specific, 5 order of magnitudes lower than maximum in noon time

[f] O_3 was measured by two photometers (Environment S.A. (41M) and Thermo (49i)); data were taken from the Thermo (49i) instrument, which agreed well with the data from the Environment S.A. instrument (see text).

[g] NO and NO_2 were measured by three chemiluminescence instruments (Eco Physics CLD TR780, and two Thermo (42i-TL)); data were taken from the Thermo (42i-TL) instruments which agreed well with each other; the data accuracy represents the unexplained difference between the data from the Thermo and Eco Physics instruments (see text).

[h] photolytical conversion to NO before detection, home built converter

[i] HONO was measured by two different, home-built (FZJ, PKU) LOPAP instruments and one CEAS instrument (NOAA); data were taken from the FZJ-LOPAP instrument; the data accuracy represents the unexplained differences between the data of the three instruments (see text).

[j] long-path absorption photometry

[k] cavity enhanced absorption spectrometer

[l] species specific, for CO: 1 ppbv; CH_4:1 ppbv; CO_2: 25 ppbv; H_2O: 0.1 % (absolute water vapor content)

[m] species specific, for CO: 1 ppbv; CH_4:$\pm$1 ppbv; CO_2: $\pm$25 ppbv; H_2O: $\pm$5 %

[n] VOCs including C_2-C_{11} alkanes, C_2-C_6 alkenes, C_6-C_{10} aromatics

[o] gas chromatography equipped with mass spectrometer and a flame ionization detector

[p] OVOCs including acetaldehyde, methyl-vinyl ketone and methacrolein

Table 2. ~~Assignment~~ Unexplained OH signal and chemical conditions during the OH interference tests. The mean value and the 1 σ standard deviation of ~~measured VOCs to species in~~ the ~~RACM~~unexplained OH signal are calculated from the differences between S_{N2} and S_{OH}+S_{O3} shown in Fig. 2 for each test. The differences are expressed as equivalent ambient OH concentrations (see text).

#	Date	Time / CNST	OH /10^6cm^{-3}	k_{OH}/s^{-1}	NO/ppbv	ISO/ppbv	O_3/ppbv	T/°C	Unexplained Signal/10^6 cm^{-3}
1	06.29	13:00-15:00	7.0	15.2	0.16±0.11	2.8	126	34	0.65(±0.34)
2	06.30	09:50-11:00	10.4	15.4	1.39±0.51	2.1	81	31	0.97(±0.14)
3	06.30	14:40-16:10	8.5	8.8	0.14±0.05	2.0	110	34	1.15(±0.21)
4	07.02	10:50-11:30	4.6	10.0	1.19±0.27	n/a[a]	52	26	0.74(±0.24)
5	07.05	16:30-17:40	3.3	9.2	0.08±0.02	1.6	94	32	0.99(±0.04)
6	07.05	18:00-21:00	1.5	16.7	0.02±0.03	1.4	77	31	0.53(±0.30)

[a] No VOC measurement during the chemical modulation experiment

Table 3. Assignment of measured VOCs to species in the RACM 2 (Goliff et al., 2013).

RACM	Measured hydrocarbons
CH4	methane
ETH	ethane
HC3	propane, i-butane, n-butane, 2,2-dimethybutane
HC5	i-pentane, n-pentane, cyclopentane, n-hexane, 2,3-dimethylbutane, 2-methylpentane, 3-methylpentane, n-heptane, 2,4-dimethylpentane, 2,3-dimethypentane, methylcyclopentane, 2-methylhexane, MTBE
HC8	cyclohexane, 3-methylhexane,2,2,4-trimethylpentane, 2,3,4-trimethylpentane, n-heptane, methylcyclohexane, 2-methylheptane, 3-methylheptane, n-octane, n-nonane, n-decane
ETE	ethene
DIEN	1,3-butadiene
OLI	trans-2-butene, cis-butene, trans-2-pentene, cis-2-pentene
OLT	propene,1-butene, i-butene, 1-pentene, 1-hexene, styrene
ACE	ethyne
ISO	isoprene
BEN	benzene
TOL	toluene, ethylbenzene, i-propylbenzene, n-propylbenzene
XYM	m-ethyltoluene, 1,3,5-trimethylbenzene, 1,2,4-trimethylbenzene, 1,2,3-trimethylbenzene, m-diethylbenzene
XYO	o-xylene, o-ethyltoluene
XYP	m-p-xylene, p-ethyltoluene, p-diethylbenzene
HCHO	formaldehyde
ACD	acetaldehyde
MVK/MACR	methyl vinyl ketone and methacrolein

Table 4. ~~Median values of measured species for morning and afternoon hours.~~Isoprene oxidation mechanism replacing the isoprene chemistry in RACM 2.

~~06:00–10:00 12:00–16:00 / 10^{-5}0.63 1.3 / 10^{-3}3.5 4.9 / 10^{6}3.8 6.9 / 10^{8}1.9 7.4 / 10^{8}3.2 8.8 k_{OH}/20 11 /2.5 0.25 /12 3.3 /0.78 0.51 /39 93 /0.70 0.54 /2.2 2.0 ISO / 0.59 0.84 ETH / 4.1 2.7 HC3 / 4.0 2.0 HC5 / 2.5 1.0 HC8 / 0.57 0.22 ETE / 3.3 0.93 OLI / 0.25 0.20 OLT / 0.83 0.21 BEN / 1.3 0.71 TOL / 1.6 0.69 HCHO / 8.4 7.5 ACD / 2.6 1.9 MACR / 0.36 0.28 MVK / 0.54 0.43~

~~Modifications in the isoprene oxidation mechanism applied to the model (RACM).~~

reaction	reaction rate constant / $\mathrm{cm^3 s^{-1}}$	reference
ISOP–>MACR+HCHO+OH	$0.31\times1.8\times10^{11}\times\exp(-9752/T)$ ~~)~~	a
ISOP–>MVK+HCHO+OH	$0.62\times1.04\times10^{11}\times\exp(-9746/T)$ ~~)~~	a
ISOP–> HPALD1+HO2+HPCARPO2	$0.5\times0.62\times(9.5\times10^{7}\exp(-7009/T)+1.79\times10^{-7}\exp(3722.5/T)\times k_{tr}$ [f])	a
ISOP–> HPALD2+HO2+HPCARPO2	$0.5\times0.31\times(3.8\times10^{13}\exp(-10745/T)+5.82\times10^{-2}\exp(476.3/T)\times k_{tr}$ [f])	a
HPALD1+HV–>OH+HO2+0.5×HKET +0.5×MGLY+0.5×ALD+HCHO	100×~~jmacr~~ jMACR	b
HPALD2+HV–>OH+HO2+0.5×HKET +0.5×GLY+0.5×ALD+HCHO	100×~~jmacr~~ jMACR	b
HPALD1+OH–>OH	4.6×10^{-11}	b
HPALD2+OH–>OH	4.6×10^{-11}	b
HPCARPO2–>CO+OH+OP2	0.1	a
HPCARPO2+NO–>NO2+MGLY+OH+OP2	$2.9\times10^{-12}\exp(-300/T)$	a
HPCARPO2+HO2–> OP2	$7.5\times10^{-13}\exp(-700/T)$	a
ISHP+OH–>IEPOX+OH	$1.9\times10^{-11}\exp(-390/T)$	c
ISHP+OH–>0.7×ISOP+0.3×MACR+0.3×OH	$0.38\times10^{-11}\exp(-200/T)$	c
IEPOX+OH–>IEPOXO2	$5.78\times10^{-11}\exp(-400/T)$	c
IEPOXO2+NO–>IEPOXO+NO2	$2.54\times10^{-12}\exp(-360/T)$	
IEPOXO2+HO2–>IEPOXO+OH+O2	$0.074\times10^{-11}\exp(-700/T)$	c
IEPOXO–>0.125×OH+0.825×HO2+0.251×CO +0.725×HKET+0.275×GLY+0.275×ALD +0.074×ORA1+0.275×MGLY+0.375×HCHO	1×10^{6}	c
MCP–>HKET+OH+CO	$2.9\times10^{7}\exp(-5297/T)$	d
MACP+NO–>0.65×MO2+0.65×CO +0.35×ACO3+NO2+HCHO	$2.54\times10^{-12}\exp(-360/T)$	d
MCP+NO–>NO2+HO2+HKET+CO	$2.54\times10^{-12}\exp(-360/T)$	d
MVKP+HO2–>OP2	$0.34\times2.91\times10^{-13}\exp(-1300/T)$	e
MVKP+HO2–>ACO3+OH+ALD	$0.48\times2.91\times10^{-13}\exp(-1300/T)$	e
MVKP+HO2–>HO2+OH+ORA2	$0.18\times2.91\times10^{-13}\exp(-1300/T)$	e

[a] Peeters et al. (2014)

[b] Peeters and Müller (2010)

[c] Paulot et al. (2009)

[d] Crounse et al. (2012)

[e] Praske et al. (2015)

[f] k_{tr} = NO×2.43×10^{-12} exp(-360/T)+HO2×2.05×10^{-13} exp(1300./T)+ACO3×8.4×10^{-14} exp(-221/T)+MO2×3.4×10^{-14} exp(-221/T)

Table 5. Median values of measured species for morning and afternoon hours.

	06:00–10:00	12:00–16:00
$j(O^1D)$ / 10^{-5} s^{-1}	0.63	1.3
$j(NO_2)$ / 10^{-3} s^{-1}	3.5	4.9
OH / 10^6 cm^{-3}	3.8	6.9
HO_2 / 10^8 cm^{-3}	1.9	7.4
RO_2 / 10^8 cm^{-3}	3.2	8.8
k_{OH} / s^{-1}	20	11
NO /ppbv	2.5	0.25
NO_2 /ppbv	12	3.3
HONO /ppbv	0.78	0.51
O_3 /ppbv	39	93
CO /ppmv	0.70	0.54
CH_4 /ppmv	2.2	2.0
ISO / ppbv	0.59	0.84
ETH / ppbv	4.1	2.7
HC3 / ppbv	4.0	2.0
HC5 / ppbv	2.5	1.0
HC8 / ppbv	0.57	0.22
ETE / ppbv	3.3	0.93
OLI / ppbv	0.25	0.20
OLT / ppbv	0.83	0.21
BEN / ppbv	1.3	0.71
TOL / ppbv	1.6	0.69
HCHO / ppbv	8.4	7.5
ACD / ppbv	2.6	1.9
MACR / pbv	0.36	0.28
MVK / ppbv	0.54	0.43

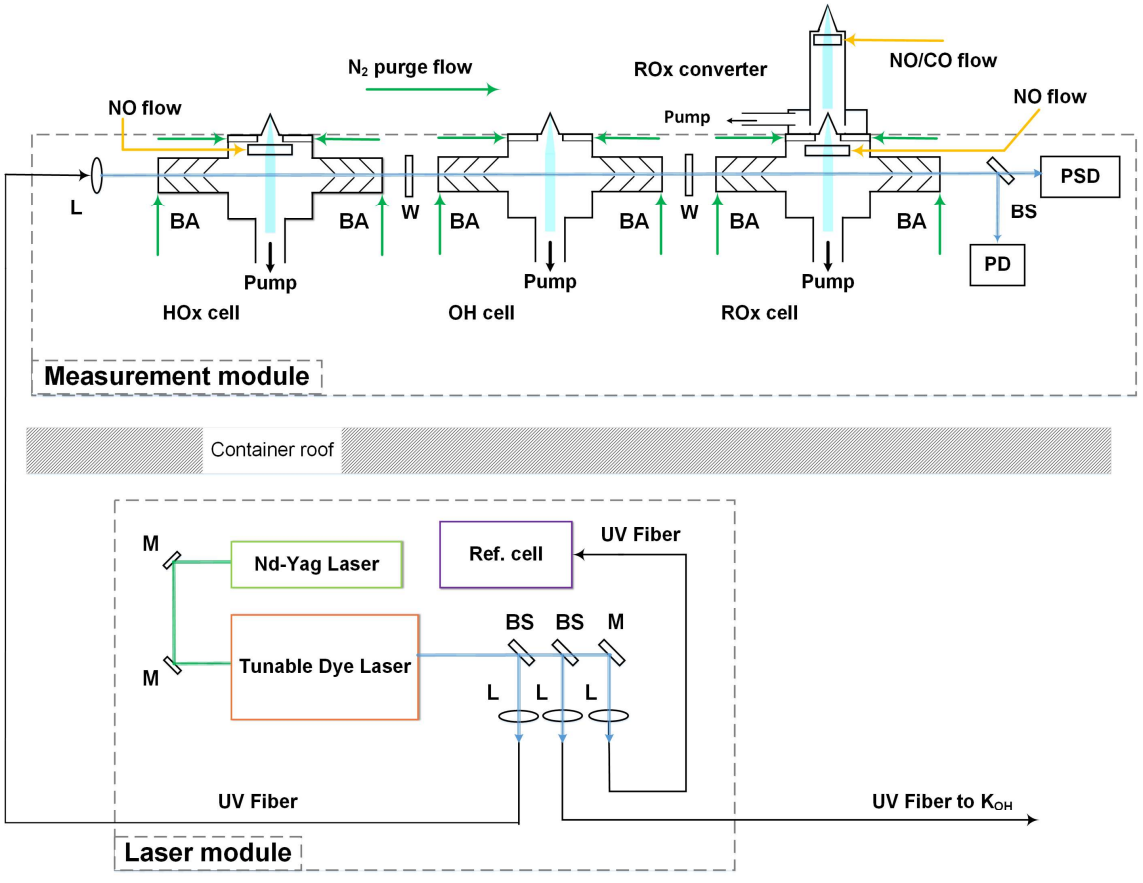

Figure 1. Schematic drawing of the LIF instrument for the detection of OH, HO_2 and RO_2. The laser module and the measurement module were installed inside and on top of a sea container, respectively. 308 nm laser-light is split into three parts (BS: beam splitter, L: lens) and guided by optical fibers to the measurement cells, the k_{OH} instrument and the reference cell. Ambient air is sampled into low pressure fluorescence cells that are separated by windows (W). Reactive gases (NO, CO) are added into the HO_x- and RO_x- cells and the RO_x converter. Baffle arms (BA) and fluorescence cells are continuously purged with N_2. The position and the power of the laser beam are monitored by a photodiode (PD) and a position-sensitive diode (PSD).

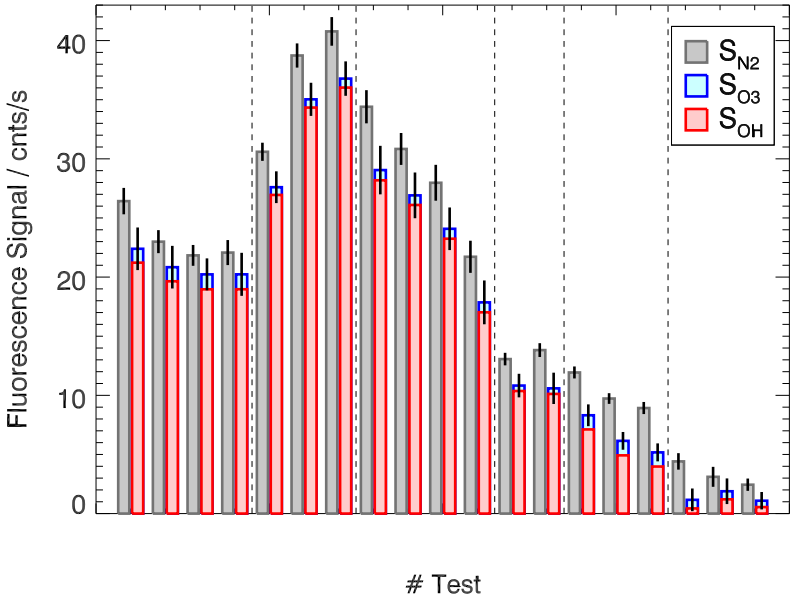

Figure 2. Results of chemical OH modulation tests performed during the campaign. In each test, the total measured OH signal without OH scavenger (S_{N2}~~, red column~~) is compared to the sum of the known contributions from ambient OH (S_{OH}~~, purple column~~) and the ~~small, known~~ interference from O_3 (S_{O3}~~, blue column~~). The error bars denote the 1σ statistical error. A fluorescence signal of ~~100 cts~~ 30 cnts/s (counts per s) corresponds to an OH concentration of ~~6.8×10^{6}~~ 1.0×10^{7} cm^{-3}.

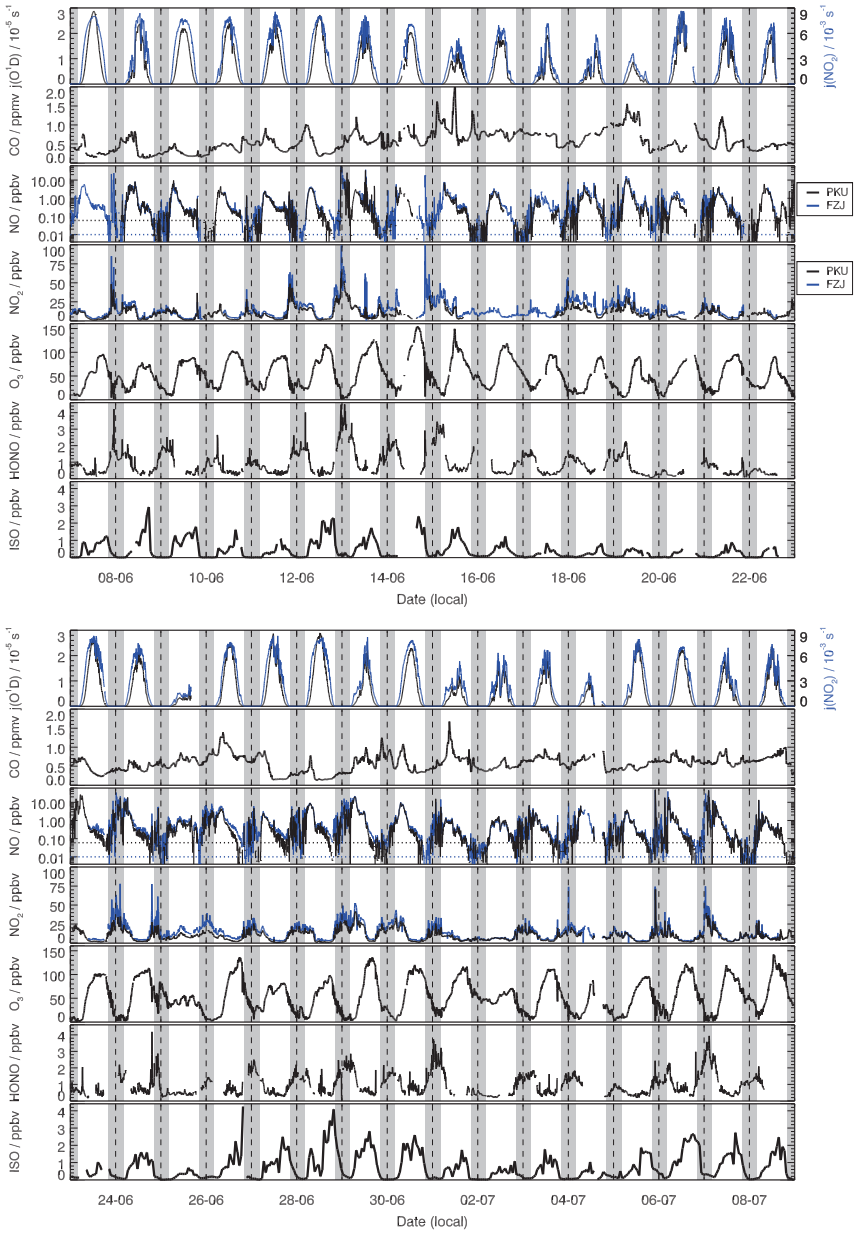

Figure 3. Time series (5-minute data) of measurements during this campaign for $j(O^1D)$, $j(NO_2)$, CO, NO, NO_2, HONO, O_3 and isoprene (ISO) used as constraints for model calculations. Vertical, dashed lines denote midnight. Grey areas indicate nighttime. Several species were measured by two instruments provided by PKU and FZJ. Measurements of both instruments for O_3 and CO well agreed, so that data sets were combined to close data gaps. Only the combined data set is shown here, but different colors indicate the origin of data. NO_2 and NO mixing ratios measured by the PKU instruments were generally 20 % smaller than those measured by the FZJ instrument. The horizontal lines denote the limit of detection for two NO instruments (10 pptv for FZJ; 60 pptv for PKU;). Both time series are shown, but measurements from the PKU instruments were used as model constraints.

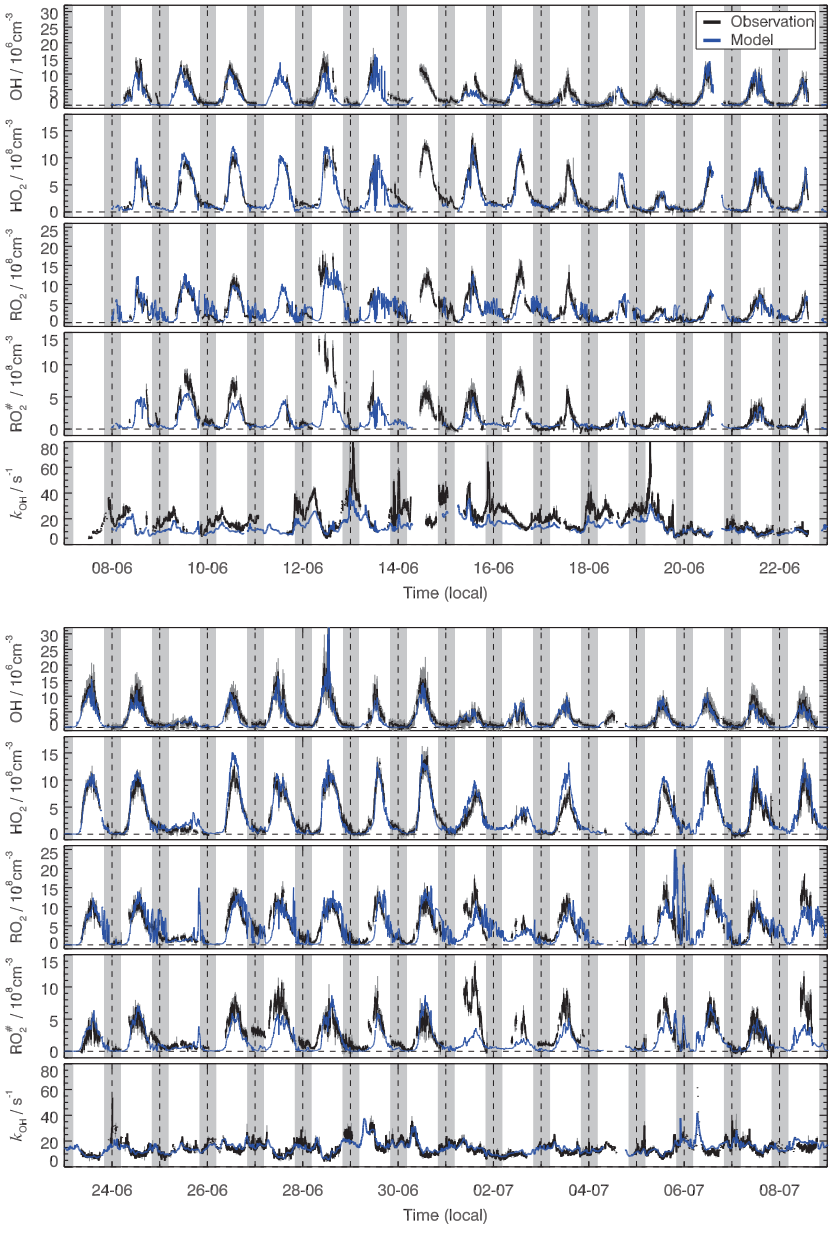

Figure 4. Time series of measured and modelled OH, HO_2, $RO_2^{\#}$, total RO_2 concentrations and k_{OH}. Vertical, dashed lines denote midnight. See text for details of the definition of $RO_2^{\#}$ and total RO_2. Grey vertical lines denote 1 σ standard deviation for measured radicals concentration with respect to 5 min variability. Grey areas indicate nighttime.

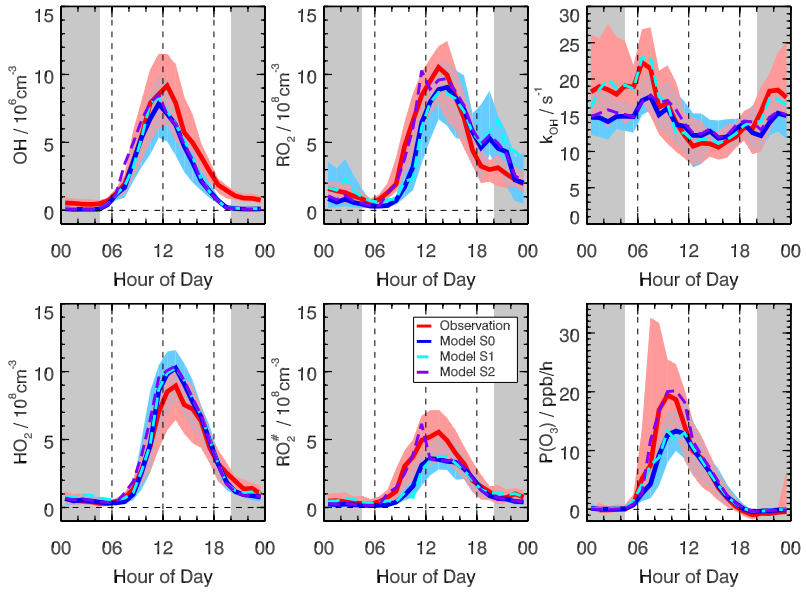

Figure 5. Comparison of hourly median diurnal profiles of OH, HO_2, RO_2, $RO_2^{\#}$ concentrations and k_{OH} and the ozone production rate $P(O_3)$ (thick lines give median values, colored areas give 25 % and 75 % percentiles). S0 denotes results from the base model run. S1 shows results, when the VOC concentrations in the model are increased to match the observed OH reactivity. S2 shows results, when an additional primary RO_2 source (2 ppbv h^{-1}) is added in the model for the time between 6:00 and 12:00. Grey areas indicate nighttime.

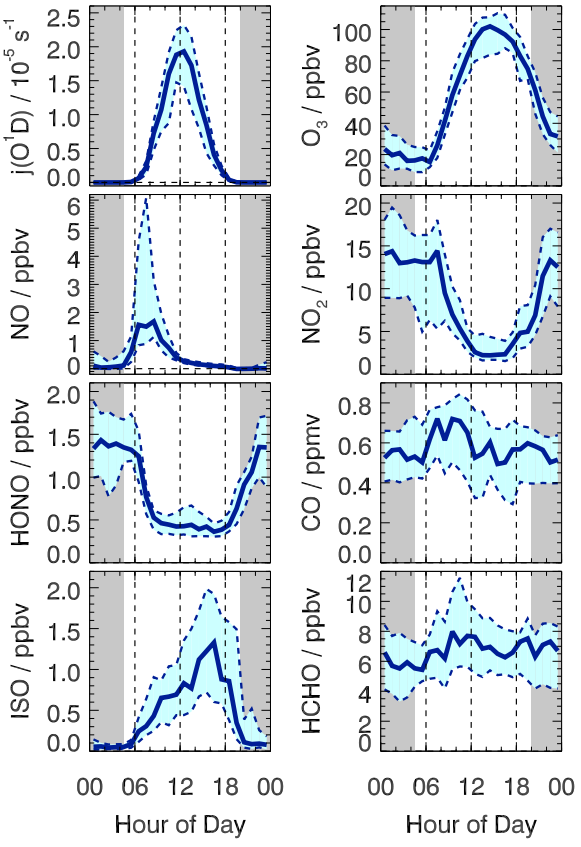

Figure 6. Hourly median diurnal profiles of measured j(O^1D), O_3, NO, NO_2, HONO, CO, isoprene (ISO) and HCHO (thick lines give median values, colored areas give 25 % and 75 % percentiles). Grey areas indicate nighttime.

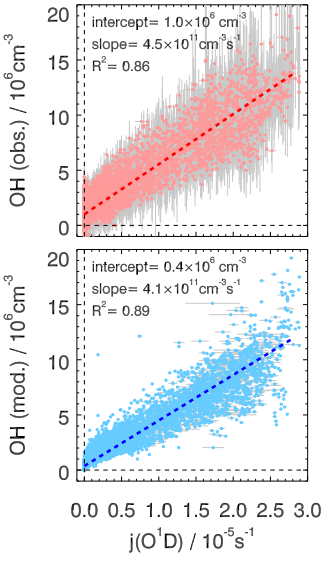

Figure 7. Correlation between $j(O^1D)$ and measured (upper panel) and modelled OH (lower panel). A linear fit is applied, which takes errors in both measurements into account.

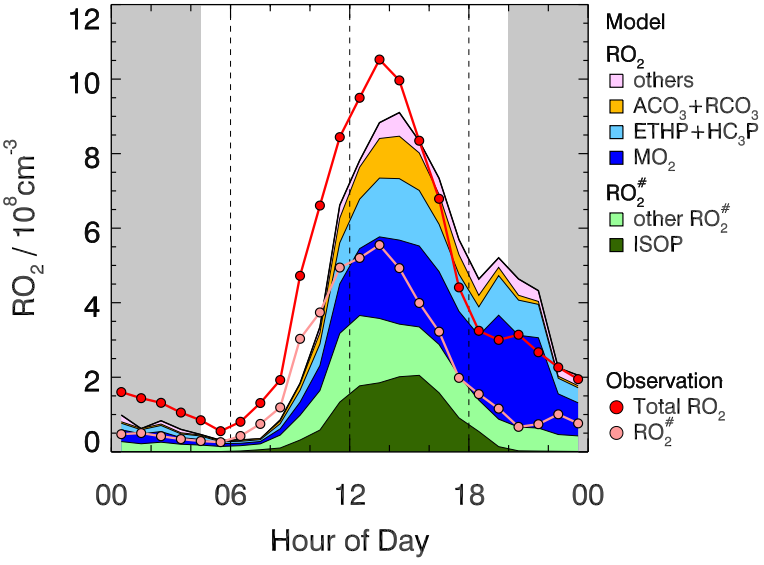

Figure 8. Hourly median diurnal profiles of measured and modelled RO_2 concentrations. Measurements can distinguish between total RO_2 concentrations and the subclass of $RO_2^{\#}$. Modelled RO_2 species are shown as colored areas. ~~Other~~ MO_2 are methyl peroxy radicals~~in~~. ETHP are ethyl peroxy radicals. HC_3P are alkyl peroxy radical (carbon number = 3 or 4). ACO_3 + RCO_3 are acetyl peroxy radicals. In the evening, "other" RO_2 radicals are mainly RO_2 species produced by the reaction of ~~organic compounds~~ VOCs with NO_3. ISOP are isoprene peroxy radicals. "other" $RO_2^{\#}$ include peroxy radicals from long alkanes, alkenes, aromatics, and isoprene oxidation products (MVK and MACR). Grey areas indicate nighttime.

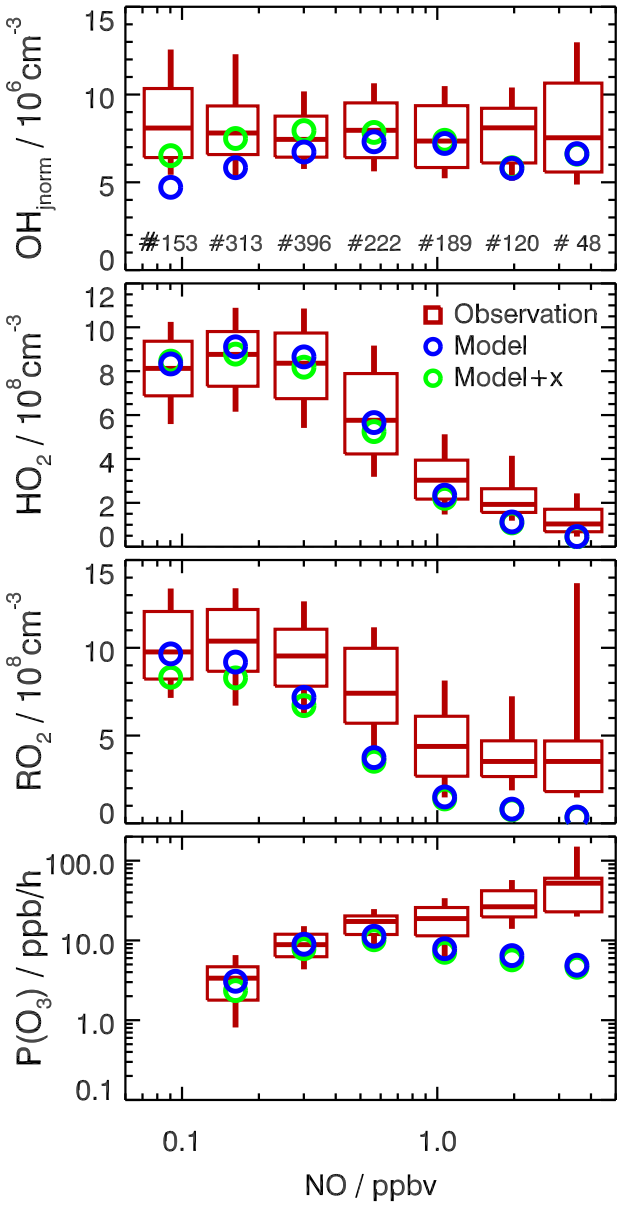

Figure 9. NO dependence of OH, HO_2 and RO_2 concentrations and instantaneous ozone production rate ($P(O_3)_{net}$) for daytime conditions ($j(O^1D)$ ~~$> 0.5 \times 10^5$~~ $> 0.5 \times 10^{-5}$ s^{-1}). OH concentrations are normalized to the average of $j(O^1D)$ (1.5×10^{-5} s^{-1}). Boxes give 75 % and 25 % percentiles, the center lines the median, and vertical lines 90 % and 10 % percentiles for NO intervals of Δln(NO)/ppbv=0.57. Numbers in the upper panel give the number of data points included in the analysis of each NO interval. Only median values are shown for model results. Results from the base model and with additional radical recycling by a species X (equivalent to 100 pptv NO) are plotted.

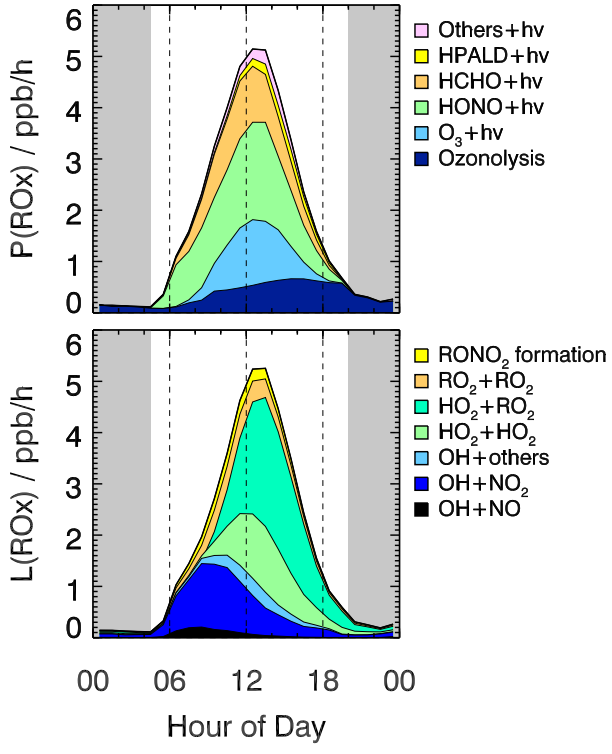

Figure 10. Hourly median diurnal profiles of modelled rates of primary RO_x production and termination reactions. Grey areas indicate nighttime.

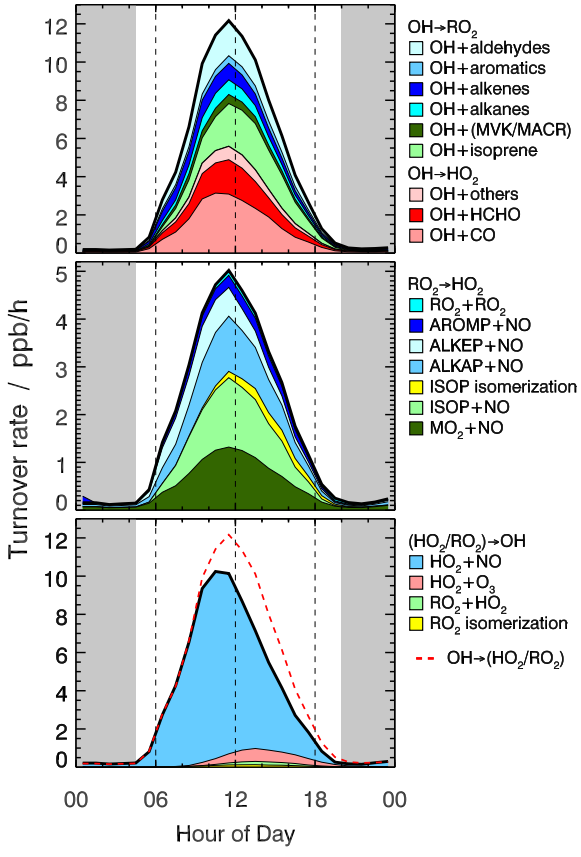

Figure 11. Hourly median diurnal profiles of turnover rates (model results) of radical propagation reactions between OH, HO_2 and RO_2 radicals. ALKAP: alkanes derived peroxi radicals; ALKEP: alkenes derived peroxi radicals; AROMP: aromatics derived peroxi radicals. Grey areas indicate nighttime.